α-Diimine complexes of transition metals for the polymerisation of lower α-olefins

By

Phillip V. Fullaway

A thesis presented in fulfillment of the requirements for the degree of

Master

In the

Natural Sciences

At the

University of Stellenbosch

Supervisor: *Prof. H.G. Raubenheimer*

Co-supervisor: *Dr. V. Grumel* December 2005

Declaration

I, the undersigned, hereby declare that the work contained in this thesis is my own original work and I have not previously in its entirety or in part submitted it at any other university for a degree.

Signature: ……..
P.V. Fullaway

Date: ……..

Abstract

In this study several potential polymerisation catalysts were synthesised. This was accomplished by coordinating α-diimine ligands such as N,N'-diferrocenyl-diazabutadiene (DFDAB), N,N'-dimesityldiazabutadiene (DMDAB) as well as the bidentate amine N,N,N',N'-tetramethylethylenediamine (TMEDA), to several transition metals.

The multi-step synthesis of N,N'-diferrocenyldiazabutadiene (DFDAB) from ferrocene involved the use of lithiated ferrocene, iodoferrocene, N-ferrocenylphthalimide and aminoferrocene; the latter three were characterised. This ligand was coordinated to the transition metal ions iron(II) and zinc(II) to form $Fe(DFDAB)Cl_2$ and $Zn(DFDAB)Cl_2$ respectively. ^{1}H and ^{13}C NMR, FT-IR and mass spectrometry revealed that the expected product had been synthesised in a useful form.

2,4,6-Trimethylaniline reacted with glyoxal to form N,N'-dimesityldiazabutadiene (DMDAB). The DMDAB ligand was coordinated to the transition metal ions zinc(II) and silver(I) to form $Zn(DMDAB)Cl_2$ and $Ag(DMDAB)_2$ respectively. Characterisation now also include molecular and crystallographic structural determinations by means of X-ray diffractometry.

Another N-donor complex, $Cr(CO)_4(TMEDA)$, was also prepared by coordinating N,N,N',N'-tetramethyl ethylenediamine (TMEDA) to $Cr(CO)_5(THF)$. This was done to give an indication of the activity of low oxidation state complexes in the catalysis of olefin polymerisation.

The metal-α-diimine complexes mentioned above were employed in the polymerisation of the monomers ethylene and 1-pentene probably according to a cationic mechanism. High density, high molar mass polyethylene products with narrow polydispersities were obtained. The chromium(TMEDA) complex produced polyethylene exhibiting ultra-high molar mass (> 10 000 kg/mol). The polymerisation of 1-pentene, using the $Fe(DFDAB)Cl_2$ complex, afforded oligo-pentene with a molar mass of ~800 g/mol.

After an unsuccessful attempt to prepare the $(CO)_5Cr{=}C(OZrCp_2Cl)$(ferrocenyl) modified Fischer-type carbene complex, the $(CO)_5Cr{=}C(OMe)$(ferrocene) complex was eventually insolated. Elucidation of its molecular structure was accomplished by X-ray diffractometry.

Finally, the DFDAB-ligand was coordinated to $Fe_2(CO)_9$ to generate $Fe(CO)_3$(DFDAB) in another attempt to investigate the role of carbonyl groups and also low oxidation state metals in polymerisation reactions [compare to $Cr(CO)_4$(TMEDA) unit above]. The sensitivity of this complex towards moisture and air prevented such action.

Pectora roborant cultus recti

Opsomming

Verskeie moontlike katalisatore vir die polimerisasie van laer orde α-olefiene is gedurende hierdie studie gesintetiseer deur α-di-imienligande en ‘n bidentate amien aan verskeie oorgangsmetale te koördineer. Die α-di-imineligande, N,N'-diferrosenieldiasabutadieën (DFDAB) en N,N'-dimesitieldiasabutadieën (DMDAB) asook die amien N,N,N',N'-tetrametiel etileendiamien (TMEDA) is gebruik.

Die sintese van die N,N'-diferrosenieldiasabutadieën (DFDAB) ligand is vermag in ‘n reeks stappe vanaf ferroseen en tussenprodukte sluit gelitieerde ferroseen, jodoferroseen, N-ferrosenielfatalimied en aminoferroseen. Karakterisering van die laaste drie produkte is gedoen. Die ligand is aan yster(II) en sink(II) gekoördineer om $Fe(DFDAB)Cl_2$ en $Zn(DFDAB)Cl_2$ onderskeidelik te vorm. Bevestiging dat die verlangde produk verkry is, is gedoen met behulp van ^{1}H-, ^{13}C-KMR, FT-IR-spektrometrie en massaspektrometrie.

Die N,N'-dimesitieldiasabutadieën (DMDAB) ligand is uit ‘n een-stap sintese verkry deur 2,4,6-trimetielanilien met glyoksal in *n*-propanol te reageer. DMDAB is aan die oorgangsmetale sink(II) en silwer(I) gekoördineer om $Zn(DMDAB)Cl_2$ en $Ag(DMDAB)_2$ te lewer. Karakterisering van hierdie twee komplekse sluit molekulêre- en kristalstruktuur bepalings met behulp van X-straal diffraktometrie in.

‘n Addisionele N-donor kompleks, $Cr(CO)_4(TMEDA)$, is berei ten einde vas te stel hoe metale in lae oksidasie toestande as katalisatore in olefienpolimerisasie optree. Die kompleks is gesintetiseër deur N,N,N',N'-tetrametieletileendiamien (TMEDA) aan $Cr(CO)_5(THF)$ te koördineer, ‘n reaksie wat gepaardgaan met THF substitusie.

Bo-genoemde N-donor komplekse is ingespan as pre-katalisatore vir die polimerisasie van die olefien monomere etileen en 1-penteen, heelwaarskynlik volgens ‘n kationiese meganisme. Polietileen produkte van hoë digtheid, hoë molekulêre massa en lae polidisperiteite is verkry. Ultra-hoë molekulêre massa polietileen (> 10 000 kg/mol) is geïsoleer uit die polimerisasie-studie waar die chroom(TMEDA) kompleks as katalisator

gebruik is. $Fe(DFDAB)Cl_2$ is ook gebruik as katalisator vir die polimerisasie van 1-penteen. Oligopenteen met ‘n molekulêre massa van ~800 g/mol is as produk verkry.

Die poging om $(CO)_5Cr{=}C(OZrCp_2Cl)$(ferroseniel), ‘n gemodifiseerde Fischer-tipe karbeenkompleks, te berei was onsuksesvol, maar kon nietemin uiteindelik $(CO)_5Cr{=}C(OMe)$(ferrosiel) as produk geïsoleer. Die molekulêre struktuur van hierdie kompleks is bepaal met behulp van X-straaldiffraksie metodes.

In ‘n verdere poging om die rol van karbonielgroepe asook dié van metale in lae oksidasie toestande in polimerisasie te ondersoek, is die DFDAB ligand aan $Fe_2(CO)_9$ gekoördineer om $Fe(CO)_3$(DFDAB) te vorm [vergelyk met die bogenoemde $Cr(CO)_4$(TMEDA) eenheid]. Hierdie ondersoek is gekniehalter weens die kompleks se sensititwiteit ten opsigte van suurstof en vogtigheid.

Pectora roborant cultus recti

Dedicated to J.M.M Adendorff
(3/1912 – 08/2005)

Acknowledgements

Allow me the opportunity to thank the following institutions and persons who made invaluable contributions to my study:

The National Research Foundation (NRF) for the financial support.
Prof. Helgard Raubenheimer for exceptional leadership, vision and support.
Dr. Valérie Grumel for her invaluable input, assistance and support. In addition, I would like to thank her with the collection and interpretation of the SEC data.
Dr. Stephanie Cronje I would like to acknowledge for her advice and assistance.
Prof. Len Barbour for his assistance with the crystallographic study.
Dr. Jean Mackenzie and Ms. Elsa Malherbe for the NMR data collection.
Mr. Bertie Barnard for the collection of MS and X-ray crystallographic data.
Mr. Marius Pretorius for his assistance with the collection of DSC data.
Mr. Nyambeni Luruli for his input in the polymerisation study.
My parents for their undying support and belief in me.
Ms. Elana de Goede for her love and support.
My laboratory colleagues at Inorganic Chemistry as well as Polymer Chemistry for their support and advice.

Pectora roborant cultus recti

List of symbols

%I	Relative Intensity to Base Peak
δ	Chemical shift in ppm
Λ	Superfluidity or lambda point
SHOP	Shell Higher Olefin Process
°C	Temperature in degrees Celsius
Å	Ångström (10^{-10} m)
acac	acetyl acetonate
Ar'	3,5-bis(trifluoromethyl)phenyl
BAF	tetrakis[3,5-bis(trifluoromethyl)phenyl]borate
bipy	Bipyridyl
Bu	Butyl
COD	1,5 – Cyclooctadiene
Cp	Cyclopentadienyl
DAB	α-diimine or 1,4-diazabutadiene
DFDAB	Diferrocenyl diazabutadiene
DMDAB	Dimesityl diazabutadiene
dme	1,2-dimethoxy ethane
EIMS	Electron Impact Mass Spectrometry
ESMS	Electron Spray Mass Spectrometry
Et	Ethyl
GPC	Gel Permeation Chromatography
HDPE	High density polyethylene
IR	Infra Red
K	Temperature in Kelvin
L	Ligand
LDPE	Low density polyethylene
LLDPE	Linear low density polyethylene
m	Medium
M	Metal
m	Multiplet (NMR)

M^+	Molecular Ion
MALDI	Matrix Assisted Laser Desorption Ionisation
MAO	Methyl aluminoxane
Mes	Mesityl or 2,4,6-Trimethylaniline
MMAO	Modified methyl aluminoxane
M_n	Number-average molecular weight
MS	Mass spectrometry
MS	Mass Spectroscopy
M_w	Weight-average molecular weight
NMR	Nuclear Magnetic Resonance Spectrophotometry
NMR	Nuclear Magnetic Resonance Spectroscopy
PDI	Polydispersity index
	per mole of metal in catalyst
Ph	Phenyl
PPh_3	Triphenylphosphine
ppm	Parts per million
py	Pyridine
RT	Room temperature
s	Singlet (NMR)
s	Strong (IR)
SEC	Size Exclusion Chromatography
sh	Shoulder (IR)
SHOP	Shell Higher Olefin Process
T_g	Glass-transition temperature
THF	Tetrahydrofuran
TOF	Turnovers, the number of moles of monomer polymerised
vs	Very strong (IR)
w	Weak (IR)

Pectora roborant cultus recti

List of Figures

Chapter 1

Fig. 1.1:	Grubbs first generation ROMP catalyst	3
Fig. 1.2:	Grubbs second generation ROMP catalyst	3
Fig. 1.3:	α-Diimine-Cu(II) complex	5
Fig. 1.4:	Tridentate bis(imido)pyridyl ligand coordinated to $FeCl_2$	10
Fig. 1.5:	Constrained-geometry Ti complex	14
Fig. 1.6:	Zwitterionic metallocenes	14
Fig. 1.7:	Complex of complexes involving anionic carbene complexes (bidentate carbene ligand)	14
Fig. 1.8:	Complex of complexes involving anionic carbene complexes (monodentate carbene ligand)	15
Fig. 1.9:	Covalently bridged metallocene pre-catalyst	15
Fig. 1.10:	Half-sandwich amide or constrained-geometry catalysts	16
Fig. 1.11:	Unbridged sandwich compound	16
Fig. 1.12:	α-olefin polymerisation pre-catalysts bearing the ferrocene	17

Chapter 2

Fig. 1.1.1:	Molecular illustration of dicyclopentadienyl iron(II)	23
Fig. 1.1.2:	The MO-diagram of the cyclopentadienyl anion	24
Fig. 1.2.1:	Molecular structure of N-ferrocenylphthalimide	30
Fig. 1.2.2:	Packing of N-ferrocenylphthalimide	33
Fig. 1.2.3:	Hydrogen bonds in N-ferrocenylphthalimide	34
Fig. 2.1:	The 1,3-bis-(2,4,6-trimethylphenyl)imidazolin-2-ylidene ligand	39
Fig. 2.2:	The molecular structure of N,N'-dimesityl diazabutadiene	42
Fig. 2.3:	Crystal packing of the dimesityldiazabutadiene ligand	44
Fig. 2.4:	Hydrogen bonds in the dimesityldiazabutadiene ligand	45

Chapter 3

Fig. 3.1:	Compounds discussed in Chapter 3	49
Fig. 3.1.1:	Molecular structure of bis(DMDAB)silver(I) tetrafluoroborate	53
Fig. 3.1.2:	Crystal packing of bis(DMDAB)silver(I) tetrafluoroborate	55
Fig. 3.2.1:	The molecular structure of tetracarbonyl chromium(0(TMEDA)	59
Fig. 3.2.2:	Crystal packing of $Cr(CO)_4$[TMEDA]	61
Fig. 3.5.1:	Molecular structure of $ZnCl_2$(DMDAB)	70
Fig. 3.5.2:	Simplified diagram of $ZnCl_2$(DMDAB)	72
Fig. 3.5.3:	Crystal packing of $ZnCl_2$(DMDAB)	73
Fig. 3.5.4:	Hydrogen bonds in $ZnCl_2$(DMDAB)	74
Fig. 3.7.1:	Illustration of two-electron donor effect of the carbene ligand	79
Fig. 3.7.2:	General formula of Fischer-type carbene complexes	79
Fig. 3.7.3:	Illustration of the overlap of molecular orbitals	79
Fig. 3.7.4:	Molecular structure of the $(CO)_5Cr{=}C(OMe)(C_{10}H_9Fe)$	83
Fig. 3.7.5:	Ferrocenyl Fischer carbene complexes by Hursthouse and Jayaprakash	84
Fig. 3.7.6:	Crystal packing of $(CO)_5Cr{=}C(OMe)(C_{10}H_9Fe)$	86

Chapter 4:

Fig. 4.1:	Crystallisation temperature (T_c) of polymers using DSC	91
Fig. 4.2:	Melting temperature (T_m) of polymers using DSC	91

List of Schemes

Chapter 1

Scheme 1:	Complexes of Sc and Y	3
Scheme 1.1:	Chain transfer via associative displacement or β-hydride transfer	7
Scheme 1.2:	Mechanism for the formation of linear α-olefins	8
Scheme 1.3:	Polymer growth utilising olefin monomers	13

Chapter 2

Scheme 1.1:	α-Diimine ligand intermediates	22
Scheme 1.2:	Synthesis of ferrocene utilising Grignard and iron(III)chloride	25
Scheme 2.2:	Fragmentation of aniline	46

Chapter 4

Scheme 4.1:	Pre-catalysts utilised for the polymerisation of ethylene and 1-pentene	89
Scheme 4.2:	Polymerisation mechanism of ethylene *via* the cationic pathway	93

Pectora roborant cultus recti

List of Tables

Chapter 2

Table 1.1.1: ^{1}H and ^{13}C NMR data for iodoferrocene 27

Table 1.2.1: ^{1}H and ^{13}C NMR data for N-ferrocene phthalimide 29

Table 1.2.2: Experimental and crystallographic data for N-ferrocene phthalimide 31

Table 1.2.3: Bond lengths for N-ferrocenylphthalimide 32

Table 1.2.4: Bond angles for N-ferrocenylphthalimide 32

Table 1.3.1: ^{1}H and ^{13}C NMR data for aminoferrocene 35

Table 1.4.1: ^{1}H and ^{13}C NMR data for N,N'-diferrocenyldiazabutadiene 37

Table 1.4.2: Spectrophotometric data for N,N'-diferrocenyldiazabutadiene 38

Table 1.4.3: Mass spectral data for N,N'-diferrocenyldiazabutadiene 38

Table 2.1: ^{1}H and ^{13}C NMR data for N,N'-dimesityldiazabutadiene 40

Table 2.2: Spectrophotometric data for N,N'-dimesityldiazabutadiene 41

Table 2.3: Experimental and crystallographic data for N,N'-dimesityldiazabutadiene 43

Table 2.4: Bond lengths for N,N'-dimesityldiazabutadiene 43

Table 2.5: Bond angles for N,N'-dimesityldiazabutadiene 44

Table 2.6: Mass spectral data for N,N'-dimesityldiazabutadiene 46

Table 2.7: Infrared stretching frequencies for N,N'-dimesityldiazabutadiene 46

Chapter 3

Table 3.1.1: ^{1}H and ^{13}C NMR data of bis(DMDAB)Ag(I) tetrafluoroborate 51

Table 3.1.2: Experimental and crystallographic data of bis(DMDAB)Ag(I)BF_4 52

Table 3.1.3: Bond lengths of bis(DMDAB)Ag(I)BF_4 54

Table 3.1.4: Bond angles of bis(DMDAB)Ag(I)BF_4 54

Table 3.1.5: The infrared stretching frequencies for bis(DMDAB)Ag(I)BF_4 56

Table 3.1.6: MALDI-TOF Mass Spectra data for bis(DMDAB)Ag(I)BF_4 56

Table 3.2.1: Experimental and crystal data for $(CO)_4Cr$(TMEDA) 59

Table 3.2.2: Bond lengths for $(CO)_4Cr$(TMEDA) 60

Table 3.2.3: Bond angles for $(CO)_4Cr(TMEDA)$ 61
Table 3.2.4: Stretching frequencies for the carbonyl groups for $(CO)_4Cr(TMEDA)$ 62
Table 3.3.1: ^1H and ^{13}C NMR data for $FeCl_2(DFDAB)$ 64
Table 3.3.2: Electron Impact MS data for $FeCl_2(DFDAB)$ 64
Table 3.4.1: ^1H NMR data for $ZnCl_2(DFDAB)$ 66
Table 3.4.2: Electron Impact MS data $ZnCl_2(DFDAB)$ 66
Table 3.5.1: MALDI-TOF MS data for $ZnCl_2(DMDAB)$ 68
Table 3.5.2: Conditions and crystallographic data for $ZnCl_2(DMDAB)$ 69
Table 3.5.3: Bond lengths in $ZnCl_2(DMDAB)$ 71
Table 3.5.4: Bond angles in $ZnCl_2(DMDAB)$ 72
Table 3.5.5: Infrared stretching frequencies for $ZnCl_2(DMDAB)$ 74
Table 3.6.1: ^1H and ^{13}C NMR data for $Cr(CO)_3(DFDAB)$ 77
Table 3.6.2: Electron Spray Ionisation MS data for $Cr(CO)_3(DFDAB)$ 77
Table 3.6.3: FT-IR stretching frequencies for $Cr(CO)_3(DFDAB)$ 78
Table 3.7.1: ^1H and ^{13}C NMR data for $(CO)_5Cr{=}C(OMe)(Fc)$ 81
Table 3.7.2: MS data for $(CO)_5Cr{=}C(OMe)(Fc)$ 81
Table 3.7.3: Experimental and crystallographic data for $(CO)_5Cr{=}C(OMe)(Fc)$ 82
Table 3.7.4: Bond lengths of $(CO)_5Cr{=}C(OMe)(Fc)$ 84
Table 3.7.5: Bond angles of $(CO)_5Cr{=}C(OMe)(Fc)$ 85
Table 3.7.6: Ifrared vibration frequencies, $\nu(CO)$, for $(CO)_5Cr{=}C(OMe)(Fc)$ 86

Chapter 4

Table 4.1: Analytical data of polyethylene 93
Table 4.2: Comparative polymerisation data from literature 96
Table 4.3: ^{13}C NMR and SEC data for oligopentene 97

Table of contents

Declaration i

Abstract ii

Opsomming iv

Acknowledgements vii

List of symbols and abbreviations viii

List of figures x

List of schemes xii

List of tables xiii

Chapter 1

Introduction 1

The choice of metal for catalyst design 2

Ligands 8

Physical conditions to consider during catalyst design 10

Metallocene-based ethylene and α - olefin polymerisation catalysts 11

Aim of the study 17

Chapter 2

Introduction 22

1. Introduction to N,N'-diferrocenyldiazabutadiene 22

1.1 Iodoferrocene 26

1.2 N-ferrocene phthalimide 28

1.3 Aminoferrocene 34

1.4 N, N'-Diferrocenyldiazabutadiene (DFDAB) 36

2. N,N'-dimesityldiazabutadiene (DMDAB) 39

Conclusions 47

Chapter 3

Introduction 49

3.1 Bis(dimesityldiazabutadiene)silver(I) tetrafluoroborate 50

3.2 Tetracarbonylchromium(0)(N,N,N',N'-tetramethylethylenediamine) 57

3.3 Dichloro[N,N'-diferrocenyldiazabutadiene]iron(II) 62

3.4 Dichloro[N,N'-diferrocenyldiazabutadiene]zinc(II) 65

3.5 Dichloro[N,N'-dimesityldiazabutadiene]zinc(II) 67

Conclusions 75

3.6 Tricarbonyliron(N,N'-diferrocenyldiazabutadiene) 76

3.7 {Ferrocenyl(methoxy)-carbene}pentacarbonylchromium(0) 78

Chapter 4

Introduction 89

Differential Scanning Calorimetry 90

Size Exclusion Chromatography 91

4.1 Polymerisation of ethylene 92

Characterisation of polyethylene 93

4.2 Polymerisation of 1-pentene 97

Conclusions and future work 98

Chapter 5

General procedures 100

Lithiated ferrocene 101

Iodoferrocene 102

N-ferrocene phthalimide 102

Aminoferrocene 102

N,N'-Diferrocenyldiazabutadiene 103

N,N'-dimesityldiazabutadiene 103

Bis(dimesityldiazabutadiene)silver(I) tetrafluoroborate 103

Tetracarbonylchromium(0)(N,N,N',N'-tetramethylethylenediamine) 103

Dichloro(N,N'-diferrocenyldiazabutadiene)iron(II) 104
Dichloro(N,N'-diferrocenyldiazabutadiene)zinc(II) 104
Dichloro[N,N'-dimesityldiazabutadiene]zinc(II) 105
Tricarbonyl(N,N'-diferrocenyldiazabutadiene)iron 105
Ferrocenyl(methoxy)-carbene}pentacarbonylchromium(0) 105
Polymerisation of ethylene 106
Polymerisation of 1-pentene 107

Pectora roborant cultus recti

Chapter 1: Introduction and historical overview

Transition metal complexes as catalysts for the polymerisation of lower olefins:

1.1 Introduction

The discovery of ethylene polymerisation with the $TiCl_4$-$AlClEt_2$ catalyst by Karl Ziegler[1] in the 1950's, the stereoselective polymerisation of propene by Giulio Natta[2] and the polymerisation of α-olefins created a multibillion dollar industry which still grows at an exceptional rate. The production of polyolefins is in excess of 160 billion kilograms annually, 75% of that figure being polyethylene, making polyolefins the fastest growing sector in the polymer business to date. With an internal structure comprised solely of carbon and hydrogen, polyolefins are relatively easy to recycle. Being thermoplastics; it can be combusted for a gain in energy with carbon dioxide and water being the only products. Research done by Arno Behr[3] showed that by applying the appropriate metal catalysts, CO_2 can be used as a C_1 synthon in the formation of C-C bonds. Although some industrial applications already lead to the production of fertilisers, resins, solvents and hydroxy compounds, much more work is necessary in future.

Pectora roborant cultus recti

Three types of polyethylene are manufactured for industry, each with its unique properties and applications.

High-density polyethylene (HDPE) is a linear, semi-crystalline ethylene homopolymer (T_m ~ 135 ^oC) prepared by Ziegler-Natta-type and chromium-based catalysts. HDPE is used for the production of grocery bags and shampoo bottles amongst others. Linear polyethylene is normally produced with molar mass in the range of 200,000 to 500,000, but it can be made even higher. Polyethylene with molar mass of three to six million is referred to as ultra-high molar mass polyethylene and can be used to make fibers which are so strong that they have replaced Kevlar® for use in bullet-proof vests.

Linear low-density polyethylene (LLDPE) is a random co-polymer of ethylene and α-olefin (e.g. 1-hexene etc.) catalysed by Ziegler-Natta-type, chromium-based or metallocene catalysts. These co-polymers are used for the production of light-weight transparent and semi-transparent plastic bags.

The last type of polyethylene, low-density polyethylene (LDPE), is prepared in a high-temperature, high pressure free-radical process. These polymers are branched homopolymers and the extreme conditions of production, makes it a non-economically viable commodity with very few industrial uses.

A number of aspects have to be considered when designing a new catalyst for polymerisation of α-olefins. The productivity (which includes the cost of catalyst manufacture, cost of raw materials, sensitivity towards air and moisture of these raw materials, the possibility of large scale production and the impact of the synthesis of these materials on the environment) of the desired catalyst must be such as to make its production viable. Productivity, catalytic activity, lifespan, initiation and decay functions are intimately linked to ligand structure, type of co-catalyst, and olefin concentration, not to mention the desired product characteristics such as polymer molar mass, weight distribution and degree of branching. In short, catalyst design is performed to optimise polymerisation as well as application functions and entails: a) choice of metal, b) choice of ligand (cationic or anionic) and c) physical conditions under which polymerisation takes place.

1.2 The choice of metal for catalyst design

The choice of metal is clearly related to where it resides in the periodic table.

Neutral Group 3 alkyl complexes of Sc and Y are isoelectronic with Group 4 cationic complexes. A potential advantage of Group 3 catalysts is that they are single-component catalysts, thus no co-catalyst is needed. Most of the ligand systems used in this group flow from successful ligand systems employed in Group 4. Generally, low olefin polymerisation activity is found in Sc and Y catalysts, but detailed mechanistic studies have been conducted with complexes Scheme 1.*(i)* to *(iii)* below [M = Sc, Y]. [4,5]

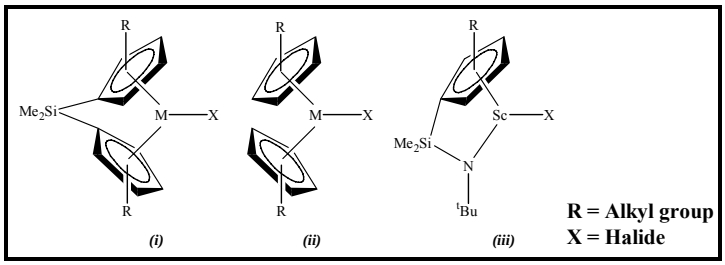

Scheme 1

Mono(pentamethylcyclopentadienyl)alkoxy scandium compounds have not shown any polymerisation activity probably due to the formation of oxygen-bridged complexes.

Transition metal complexes have been thoroughly investigated and defined as polymerisation catalysts, so emphasis will be placed on transition metals from here on.

Early transition metal complexes are known to be highly oxophilic. This characteristic causes them to be incompatible with most functionalised olefins, particularly commercial polar monomers. However, there are reported cases of protection of the polar functionality by incorporating special substrates[6,7] or high levels of Lewis acids[8] into the polymer system. Metathesis of cyclic olefins and metathesis of polar cycloolefins followed by hydrogenation to remove the resultant unsaturation, are alternative routes to polar co-polymers.[9] The Grubbs 1st generation[10,11] (Fig. 1.1) and 2nd generation[12] (Fig. 1.2) ruthenium carbene catalysts used for the 'Ring-opening Metathesis Polymerisation' (ROMP) of strained cyclic olefins such as norbornene and cyclooctadiene are examples of these types of catalysts. However, none of these routes are economically viable, thus copolymers of functionalised olefins with ethylene are still produced commercially *via* a free-radical process.[13]

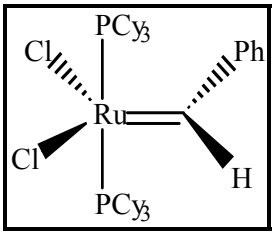

Fig. 1.1: Grubbs 1st gen. ROMP catalyst

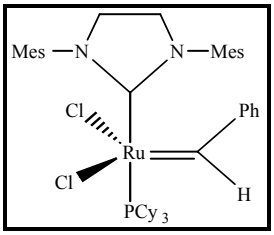

Fig. 1.2: Example of Grubbs 2nd gen. ROMP catalyst

Middle to late transition metals exhibit lower oxophilicity as well as greater functional-group tolerance relative to the lower-transition metals. Copolymerisation of ethylene and polar co-monomers under mild conditions are successfully achieved.[14] The lack of late transition metal catalysts in the past was due to the fact that late transition metal catalysts generally exhibited reduced activity for olefin insertion. In fact, β-hydride elimination that competes with chain growth is favoured, resulting in low-molar mass polymers or oligomers. This phenomenon formed the basis of the Shell Higher Olefin Process (SHOP). This process will be discussed later in this chapter.

Brookhart and co-workers have demonstrated that cationic Ni(II) and Pd(II) diimine complexes are highly active catalysts for the polymerisation of ethylene.[15,16] It is worth noting that these catalysts are not suitable for higher α-olefin polymerisation where 1,ω-rearrangements occur. Similar results have been reported by Gibson with cationic Co(II) and Fe(II) complexes[17,18], by Small and Brookhart, with a cationic Fe-pyridine-bis(imine) complex[19,20], by Bart and co-workers with a four-coordinated dihalide Fe(II)-complex[21] and by Walther and co-workers with di-, tri-, and tetranuclear complexes of Ni, Pd and Zn.[22] Molar masses vary from oligomers ($M_w \sim 800$) to polymers ($M_w > 300\ 000$), and the products from highly crystalline to totally amorphous just by a variation in catalyst structure, *i.e.* metal and ligand system. Under a given set of conditions, Ni(II) α-diimine catalysts yield generally less branched, larger polymers than that of their Pd(II) analogues. Products from the polymerisation of the Pd(II) catalyst are amorphous, highly branched polyethylenes with densities as low as 0.85 with glass transition temperatures of -30 to -70 ^{o}C, which give rise to unique polymer properties.

"Late" transition metal catalysts include Pt, Fe, Co, Rh and Cu. The catalytic activity of Pt complexes can not be compared with that found for Ni and Pd, but its chemical lability makes Pt a useful model for more active catalysts.[23] Baar and co-workers have emphasized the conclusion by Brookhart and co-workers[15] that the activity of Pd(II) and Ni(II) complex catalysts of α-olefins depend critically on the steric properties of the supporting diimine ligands.[24] They came to the conclusion that a) bulky substituents are needed to block associative olefin substitution leading to chain transfer, while b)

asymmetry in the diimine ligands can induce high tacticity in polymers. Yang and co-workers have coordinated an α-diimine ligand to Pt(II), but the activity for polymerisation of α-olefins has not been investigated.[23] Iron α-diimine complexes polymerise ethylene, but the results were not even comparable to that of Ni(II) and Pd(II).[25] The low activity of the Fe-system repeats itself with the metals Co, Rh and Cu. Although Rh α-diimine complexes exhibit favourable polydispersity indexes (~ 1.6), low molar masses (M_w ~ 5100) and slow turnover rates make these complexes poor catalysts for the polymerisation of ethylene.[26] Cu-ethylene chemistry is well defined, but reports of polymerisation of ethylene with copper catalysts are very rare and the yield of polyethylene almost negligible. Gibson and co-workers[27] report a Cu(II) α-diimine (Fig. 1.3) complex to have moderate polymerisation activity towards ethylene, although still not even comparable to the Ni and Pd systems.

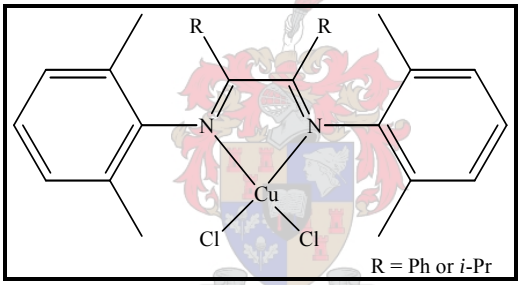

Fig. 1.3: α-Diimine-Cu(II) complex

As stated earlier, nickel, palladium, iron, copper and zinc have been utilised as metal (M) centres in recent years. These metal chlorides are the simplest catalyst precursors and form the most stable complexes as well. Halides (particularly chloride) are utilised as the anion groups and play a vital role in the activation of the pre-catalyst by the co-catalyst to form the cationic species. The polymerisation mechanism will be discussed in detail later in this chapter. (Equation 1.1)

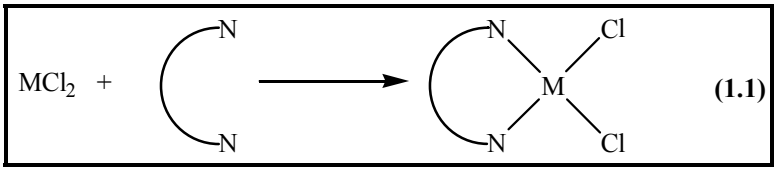

(1.1)

Solubility of the complexes is always a problem, not for polymerisation, but for analytical purposes. The cationic species is of interest for polymerisation and the use of methyl aluminoxane species (e.g. MAO), as co-catalyst usually forms the soluble alkyl complex. Methyl aluminoxane and its role in the polymerisation process will be discussed below. Diazabutadiene (DAB) complexes can react with non-coordinating anions to yield cationic organometallic species (Equation 1.2).[16,29,30] These complexes are stabilised by weak donor ligands such as acetonitrile, which makes them easy to handle and useful as precursors in polymerisation reactions.

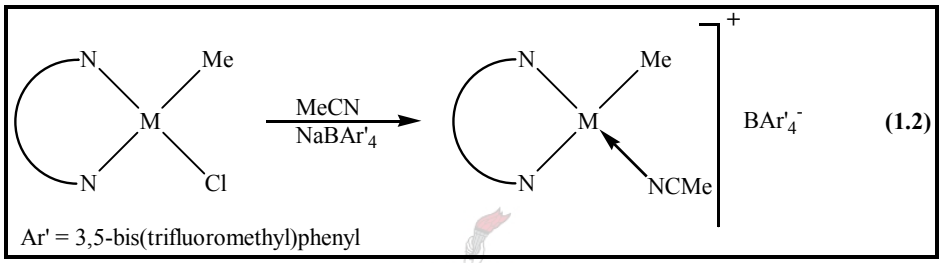

The key features of diimine pre-catalysts are highly electrophilic metal centers (especially Ni and Pd), the use of sterically bulky diimine ligands and the use of non-coordinating counter ions. Introduction of steric bulk at the axial sites of the square plane has an inhibitory effect on the monomer incorporation rate as well as an inhibitory effect on chain transfer.[30] This inhibitory effect by the bulky ligands favors insertion over chain transfer, which means that longer chains and higher molar mass polymers will be produced rather than many shorter chains. A more accessible coordination site for incoming olefins is created and then filled by non-coordinated olefins (the encircled olefin in Scheme 1.1). Chain transfer is thought to proceed *via* an associative displacement of the unsaturated polymer chain from the olefin hydride intermediate by an incoming monomer (Scheme 1.1**A**). These hypotheses have been proven to be correct when the rate of exchange was dramatically retarded by bulky diimine ligands. The aryl rings lie roughly perpendicular to the square plane and the ortho substituents block axial approach of olefins. The tempo of chain propagation becomes much greater than the tempo of chain transfer and thus permits the formation of high molar mass polymers.[31]

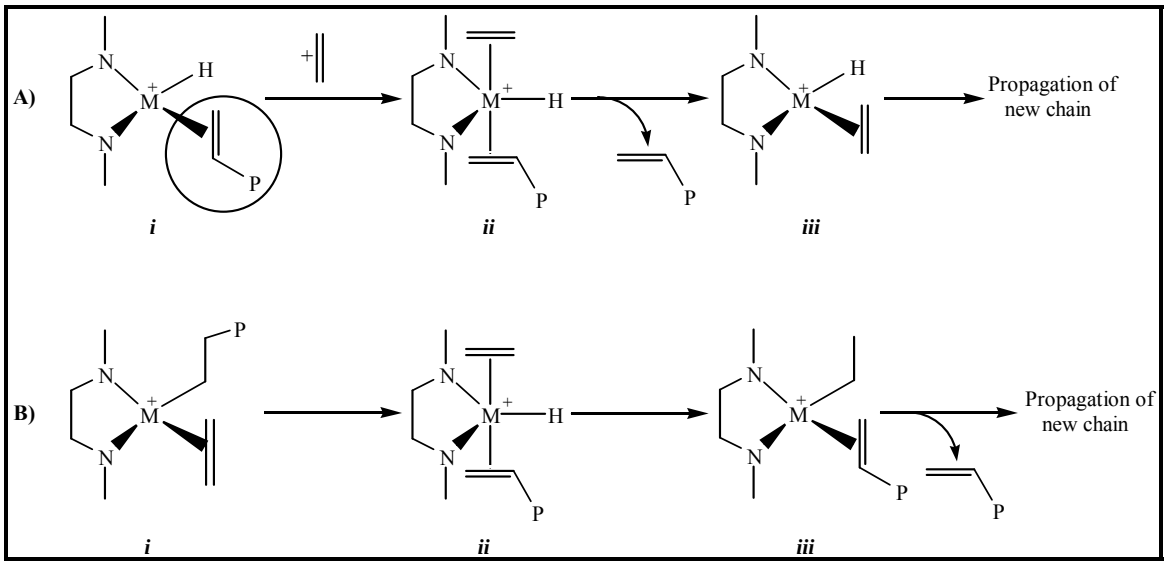

Scheme 1.1

The Ni system follows a different mechanism for chain transfer. Direct β-hydrogen transfer from the resting state (**B*i***) to the monomer (Scheme 1.1**B**) causes chain transfer. In the transition state, the olefin units occur in the axial coordination positions of the complex. By increasing the bulk of the axial site substituents of the diimine ring, the barrier towards chain transfer is increased. The four coordinated ethylene alkyl adduct becomes more stable than this state and chain transfer is retarded even more.[32]

Ni(II) complexes bearing anionic ligands for the oligomerisation of ethylene, form the basis of the Shell's Higher Olefin Process. Linear α-olefins (C_6 – C_{20}) are formed from ethylene due to the selectivity of these catalysts for the insertion of ethylene and β-hydride elimination. The Ni catalyst oligomerises ethylene at a rate of ~3000 TO/h to form linear α-olefins with a purity of > 98%. The term TO/h is the Turn-Over frequency and is measured in grams polymer produced per mol catalyst consumed per hour. The distribution of olefin molar mass is essentially of the Schulz-Flory type.[33] The mechanism for the formation of linear α-olefins is shown in Scheme 1.2.

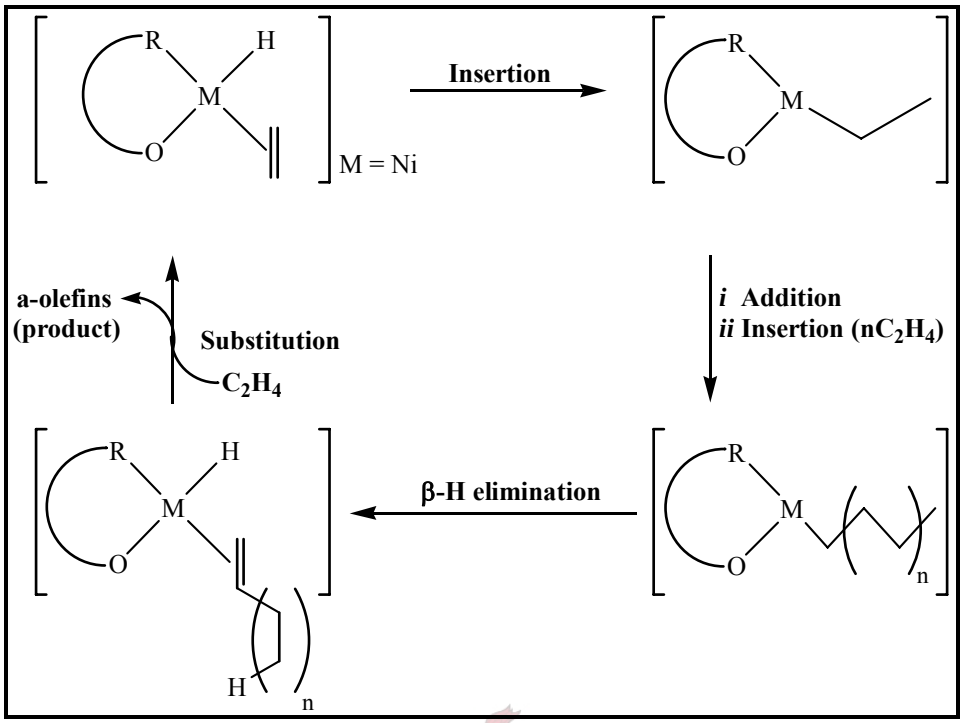

Scheme 1.2

The initiating ethyl complex is generated by the insertion of ethylene into the Ni-hydride bond. Ni-alkyls of various lengths are formed by the additional insertions of ethylene. Subsequent β-hydride elimination produces an α-olefin hydride complex. Regeneration of the starting Ni-hydride ethylene complex occurs by an associative olefin exchange between a free ethylene unit and the Ni-ligated α-olefin by the chain-transfer in these systems (release of the produced α-olefin). The formation of branched species by reinsertion of the α-olefin product is minimal due to its selectivity for ethylene insertion.[34]

1.3 Ligands

As indicated earlier, ligands play a very important role in the catalysis of polymerisation reactions. In polymerisation-active metal complexes, the ligands play four important roles: a) control the metal coordination number, b) control the metal coordination geometry, c) control the formal oxidation number of the metal and d) sterically protect the active site.

Bulky ligands have an inhibitory effect on monomer insertion as well as chain transfer at the axial sites on the metal centre of the catalyst. This inhibitory effect favors monomer insertion over chain transfer resulting in higher molar mass polymers. A few examples of these bulky ligands will be discussed shortly.

The oxidative addition of phosphorus ylides to zerovalent Ni, such as in the Ni-cyclooctadiene complex, in the presence of PPh_3 or other ligands yields P-O chelated catalysts as illustrated in Equation 1.3. These catalysts can produce higher molar mass oligomers and polymers of ethylene.[35]

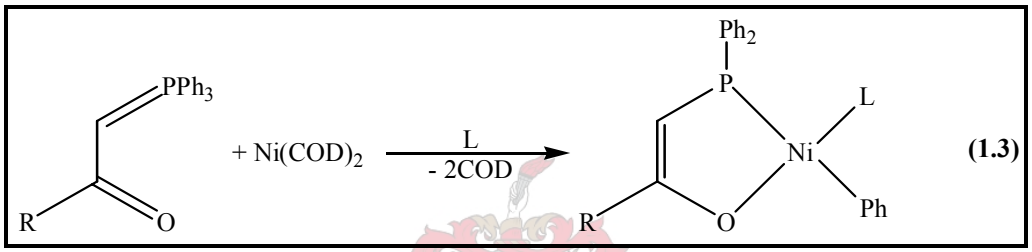

(1.3)

The synthesis of well defined Fe(II) cationic alkyl complexes was made difficult by the instability of the Fe(II) dialkyl precursor species. This is emphasised by the very few reports of stable Fe(II) dialkyl species in literature. The six coordinate $(dmdpm)_2FeMe_2$ and $(bipy)_2FeEt_2$ [bipy = bipyridyl] and the 5-coordinate $(PPh_3)_3FeMe_2$[36] being the only structurally well characterised complexes. To illustrate the ligand effect on stability of complexes and polymerisation, consider the following complex prepared by Britovsek and co-workers using a tridentate bis(imido)pyridyl ligand coordinated to Fe and Co.[37] Although the Co analogue still shows hardly any catalytic activity, the Fe exhibits similar catalytic activity as its Ni and Pd counterparts as well as the metallocene-based polymerisation catalysts. In addition, polymer products that form when using the iron catalysts have similar properties (M_w, M_n and PDI) as those from the aforementioned catalysts. This is in direct contrast to the earlier findings of Brookhart and others. Thus, although certain metals (e.g. Fe) exhibit low catalytic activity with a specific type of ligand, by adjusting the substituents on these ligands, the activity of the complex can be increased exponentially. These results open a new field of research for Fe-based catalysts.

Its low cost, relatively low toxicity, natural abundance and ease of handling make iron an attractive metal centre for modern catalysts.

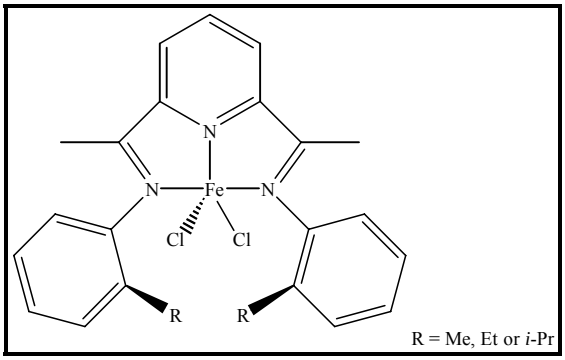

Fig. 1.4: Tridentate bis(imido)pyridyl ligand coordinated to $FeCl_2$

1.4 Physical conditions to consider during catalyst design

A kinetic study by Small and Brookhart[19] with the tridentate bis(imido)pyridyl ligand coordinated to $FeCl_2$ (Fig. 1.4) in the oligomerisation of ethylene to linear α-olefins, shows that the reaction rate constant (K_{obs}) and the selectivity for α-olefin formation is exceptionally high and exceeds those of the commercial systems. These studies have been extended to include the polymerisation of propylene. Yet again, the steric bulk of the ligand system plays a significant role in determining the molar mass of polymer product. These systems also showed that Fe-based catalysts are extremely active and selective for the oligomerisation of α-olefins.

Physical factors (e.g. temperature, pressure i.e. monomer and catalyst concentration, reaction time) can influence polymerisation results significantly. Raising the temperature during the polymerisation, generally results in a decrease in molar mass. This is certainly true for ethylene polymerisation. It has been reported that rates of chain growth and chain transfer are both first-order in the monomer,[19,38] so assuming similar entropies of activation, an increase in temperature will result in a decrease in the propagation/transfer rate and ultimately a decrease in M_n. An increase in pressure, especially for ethylene polymerisation, will increase the monomer concentration in solution; this will increase the rate of propagation and ultimately increase M_n. The effect of increasing the reaction

time depends solely on the lifespan of the catalyst. Some catalysts are very resilient towards harsh conditions of the polymerisation process. In cases like this, reaction time will not influence the M_n, but only the yield.

1.5 Metallocene-based ethylene and α - olefin polymerisation catalysts

Metallocenes have been known as catalysts for the polymerisation of ethylene and other olefins for a number of years now.[39] Polymerisation with Group 4 metallocenes started soon after its discovery in 1953 by Wilkinson and co-workers.[40] Mixtures of $TiCp_2Cl_2$ and $AlClEt_2$ polymerise ethylene at moderate rates, but are too inactive to polymerise any higher olefins. Unfortunately, useful complexes of Ti are readily reduced to the inactive Ti(III) species and do not compete with the highly active and stereoselective heterogeneous catalysts of the time and consequently have not found industrial applications. The observation by Kaminsky and co-workers[41] that traces of water actually increases the rate of polymerisation, (in the presence of the Al co-catalyst) despite the sensitivity of the metallocene system towards hydrolysis, gave birth to the co-catalyst methylaluminoxane (MAO). MAO is a poorly characterized polymeric glassy substance, usually of molar mass 900 – 1200g/mol and approximated composition of $[\{MeAlO\}_n]$, which consists of linear, cyclic and cross-linked compounds, containing predominantly four coordinate Al centres and some $OAlMe_2$ end groups. In addition, MAO is much more effective in activating metallocenedihalides than aluminium alkyl halides.[41] Metallocene catalytic systems are very sensitive to any impurities and water, but the addition of a large excess of MAO neutralises those impurities and the catalytic system is not compromised. The draw-backs of MAO is the inconsistency of concentration as well as the large mole ratio of catalyst to co-catalyst (usually $1:10^3$–10^4 mole ratio) to be added, but the ratio should not be too large either. High concentrations of MAO relative to low ethylene pressure results in a competition between the rate of chain transfer to the aluminium and the rate of β-hydride transfer, leading to the formation of a fully saturated low molar mass fraction in addition to the high molar mass vinyl terminated polymer. Despite these drawbacks, MAO has become the most widely used activator for metallocene-based catalytic systems. Attempts have been made to replace MAO with better catalytic activators such as triisobutylaluminium (TiBAl) in

combination with $B(C_6F_5)_3$, but these were less efficient co-catalysts. Modified methylaluminoxane (MMAO) has been used with some success.[42] It consists of a unit formula $-[(R)AlO]_n-[(Me)AlO]_p-$ where p and n are integers between 1 and 60. The R-group represents a straight-chained or branched hydrocarbon alkyl, alkenyl or aryl moiety or a mixture of the three. The structure of MMAO is either in a linear or ring-like sequence with the two structural units either as random or block homopolymers.[43]

Cationic alkyl complexes of Group 4 metallocenes of the general formula $[MCp_2R]^+$ with M = Ti, Zr or Hf and Cp = C_5H_5 and half-sandwich titanium-amide complexes have been recognised as catalytically active species in metallocene-based olefin polymerisation catalysts. These complexes are 14 electron species (with the Cp ligand formally a 6 electron donor), highly electrophilic and highly active polymerisation catalysts with great stereoselectivities and narrow polydispersity indexes. Specific steric interactions controlling the C-C bond formation step in chain propagation must be the success behind the remarkable stereo specificities displayed by various modified Group 4 metallocene/methyl aluminoxane catalysts. Bochmann and co-workers[44] have found the activity order: $[Cp_2MR]^+ > [CpMR^2]^+ > [MR_3]^+$. Metallocene catalysts are soluble in hydrocarbon solvents; have only one type of active site and their chemical structure can easily be changed to suit ones requirements of polymer product. Zirconocene-based metallocene catalysts are regarded as the most successful metallocenes to date. When activated by MAO, up to 100 tons of ethylene can be polymerised by one gram of catalyst.[45]

In olefin polymerisation (Scheme 1.3)[46] by metallocene catalysts, MAO undergoes a fast ligand exchange reaction with the metallocene dichloride and, in typical Lewis acid fashion, another MAO molecule also binds a chloride ligand forming a metallocene alkyl cation and $(MAO)Cl^-$ anion (Step I). The monomer (olefin) is introduced to the active catalyst and coordinates at the vacant coordination site (Step II). Chain growth (Step III) follows by the insertion of the alkene, the association of more monomer units and further insertions. When the rate of chain transfer becomes equal to the rate of propagation, β-elimination occurs; the active centre carrying the hydride accepts a "new" alkene and the

process are repeated. The active site can also be quenched by addition of terminating agents such as water, methanol or dihydrogen and the catalyst is destroyed by mineral acids such as HCl.

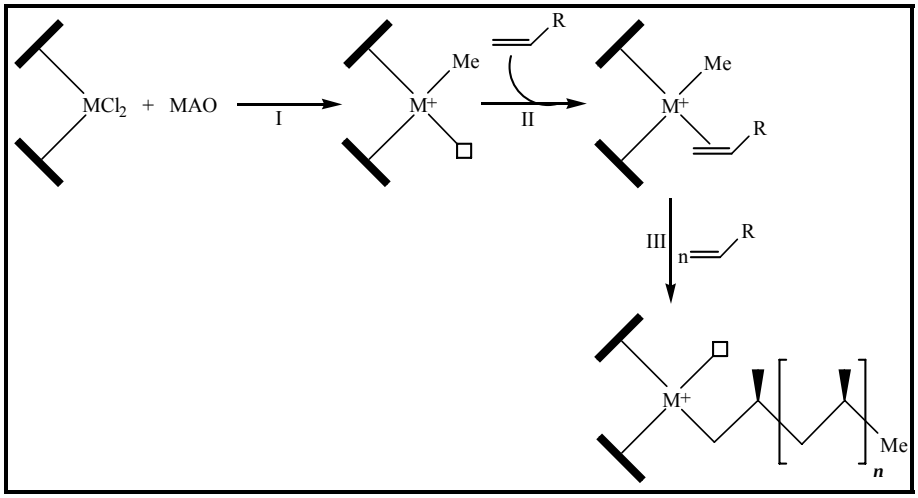

Scheme 1.3

Recently Erker and co-workers[47] have introduced an alternative to the classical activation methods by treating [Cp_2Zr(butadiene)] with $B(C_6H_5)_3$ (Equation 1.4). This forms a zwitterionic metallocene-borate-betaine system which is highly active in polymerisation reactions.[48,49]

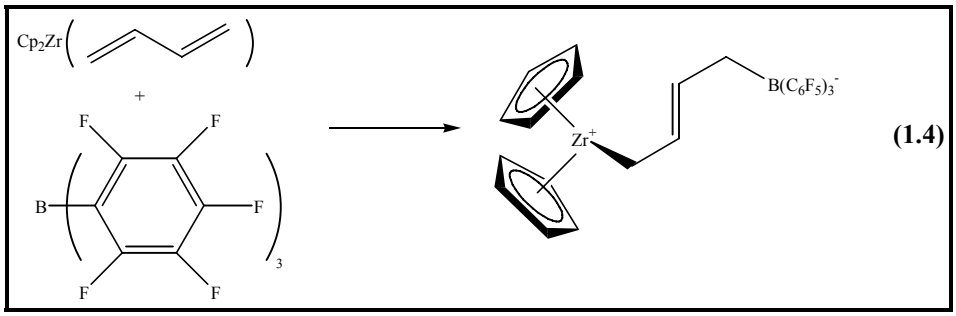

(1.4)

The same principles for constrained-geometry Ti complexes (Fig. 1.5) have been demonstrated by Devore and co-workers,[50] and also work done in the laboratory of Piers (Fig. 1.6)[51] to form zwitterionic metallocenes capable of initiating olefin polymerisation.

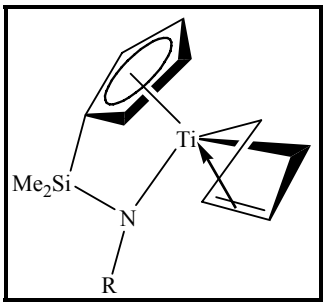

Fig. 1.5: Constrained-geometry Ti complex

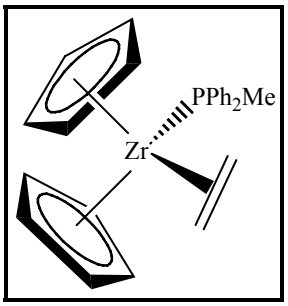

Fig. 1.6: Zwitterionic metallocenes.

When anionic Fischer-type carbene complexes are coordinated to zirconocene dichloride, active catalysts for the polymerisation of olefins are formed. The first Fischer-type metal carbene complex, the tungsten carbonyl carbene complex, was reported in 1964[52] and, since then, a significant amount of work has been done to elucidate the chemistry of many metal carbene complexes. Carbenes are defined as neutral organic species in which a carbon atom has a valency of only 2 and in which the two non-bonded electrons may ether be paired (singlet carbene) or unpaired (triplet carbene). Carbenes are electron deficient, thus behave more as transient electrophilic intermediates. In the 1960's Wanzlick proposed that electron-donating substituents such as amino-groups, can increase the stability of the singlet carbene species.[53] The first ferrocenyl carbene complex of chromium has been reported by Fischer[54] in 1970 using lithioferrocene as lithiation source. These types of metal carbene complexes, including the tungsten and molybdenum derivatives, have been researched further by Connor.[55] Carbene compounds containing the ferrocenyl-moiety show remarkable stability and are also of interest in the biomedical field.[56] Recently, carbene complex precursors or anionic carbene complexes were used as bidentate ligands to prepare a series of "complex of complexes" (Fig 1.7).[57]

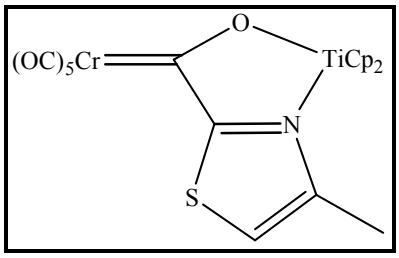

Fig. 1.7: Complex of complexes involving anionic carbene complexes (bidentate carbene ligand)

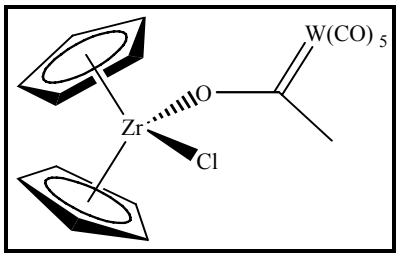

Fig. 1.8: Complex of complexes involving anionic carbene complexes (monodentate carbene ligand)

As mentioned above, when coordinating in monodentate fashion, such anionic carbenes afford useful and stable complexes with zirconium and a new type of polymerisation pre-catalyst is created in this manner [Fig. 1.8].[58] These complexes are probably transferred onto MAO to form a suitable initial counter ion in the real low-pair catalyst. This idea is substantiated by the relatively long Zr-O bond length (1.95 Å). The chloride atom present on the zirconocene fragment is also easily substituted by MAO to form the cationic alkyl species and polymerisation proceeds *via* the normal metallocene-based route. High molar mass polymers with narrow polydispersities of ethylene were synthesised.[58]

Three classes of metallocene pre-catalysts exist, namely the covalently bridged (Fig. 1.9), the half-sandwich amide or constrained-geometry catalysts[45] (Fig. 1.10) and the unbridged (fig. 1.11) sandwich compounds.[59]

In the covalently bridged sandwich compound catalysts, covalent bridging of the Cp rings forces and defines a smaller centroid-metal-centroid angle with the practical result that sterically demanding monomers can also be readily linked. Such catalysts are particularly suitable for homopolymerisation of propene as well as higher α-olefins. Structure-optimized *ansa* compounds of specific symmetry (C_2, C_s) allow near perfect stereocontrol for isotactic and syndiotactic polypropylene. π-Donor ligand (D) substituents donate a lone pair of electrons to acceptor (A) substituents with an electron vacancy. This results in a strong polarised coordinative $D^+ \rightarrow A^-$ bonding interaction between the two π ligands (Fig. 1.9). These bonds inhibit the spinning of the two Cp-rings with respect to each other and at the same time the dihedral angle of the metallocene is influenced which offers additional control. Thus, different π-donor atoms (O, N, P) and different acceptor atoms (B, Al), including their substituents, can influence catalytic behavior.

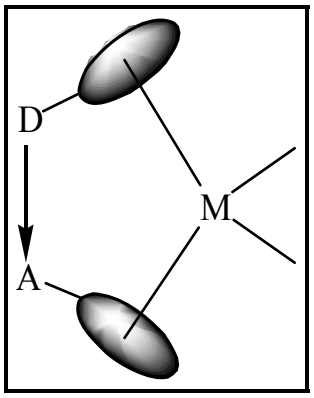

Figure 1.9: Covalently bridged pre-catalyst

The second class of metallocene-based pre-catalysts, the half-sandwich amide or constrained-geometry catalysts (Fig. 1.10), are multihapto ligands which engage in a variety of bonding modes. Devore and co-workers found that the constrained-geometry ancillary ligands stabilises the Ti-diene coordination predominantly in both π-diene and metallacyclopentene bonding geometries.[50] Upon activation by the co-catalyst such as MAO, $B(C_6F_5)_3$ or $(HNMe_2Ph)[B(C_6F_5)_4]$, these constrained-geometry complexes prove to be highly active olefin polymerisation catalysts.

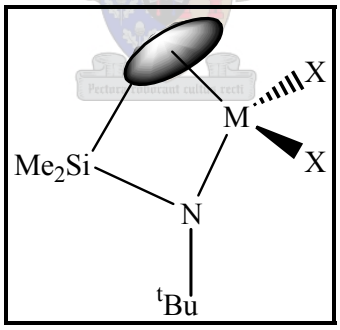

Figure 1.10: Half-sandwich amide/constrained-geometry catalysts

The latter class (unbridged sandwich compounds) [Fig. 1.11], are highly active in polymerising small molecules such as ethylene, but larger monomer molecules combine at such low rates coupled with a lack of stereo control, that oligomers are the most probable products.

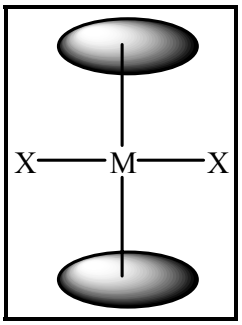

Figure 1.11: Unbridged sandwich compound

Very few α-olefin polymerisation pre-catalysts bearing the ferrocene moiety as ligand or active center have been described in the literature [Fig. 1.12]. These catalysts are restricted to α-diimine ligand-metal complexes of Ni and Pd.[60]

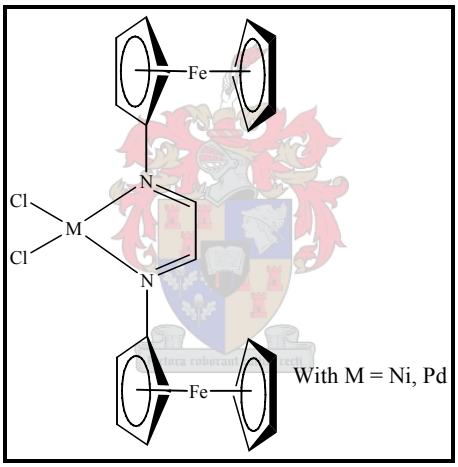

Fig. 1.12: α-Olefin polymerisation pre-catalysts bearing the ferrocene

Polymerisation of ethylene with MAO as co-catalyst was carried out with these complexes. Results obtained when using these metals, indicated that Metal-DFDAB (DFDAB = diferrocenyldiazabutadiene) complexes are highly active catalysts for ethylene polymerisation.[60]

1.6 Aims of the present study

The research on α-diimine-metal complexes by Brookhart and Gibson and its application to the polymerisation of monomers such as olefins and methacralates (2-methylpropenoic acid) are known extensively only for certain metals such as Ni and Pd to afford highly active catalysts. Other middle- to late-transition metals were not investigated by these groups.

The aims of this study were:

1. The synthesis of two known ligands with varying steric bulk and then to characterise them completely. The two ligands chosen were N,N'-diferrocenyl diazabutadiene and the N,N'-dimesityl diazabutadiene.
2. To coordinate these ligands (and others to be developed as the study progressed) to metals in the middle to late transition area of the periodic table and characterise these products fully where possible. The metal centres chosen were chromium(0), iron(II), silver(I) and zinc(II). All of these metals are commercially available, they are relatively inexpensive and comparatively easy to handle. Furthermore, they differ in oxidation state as well.
3. To study the polymerisation of olefinic monomers with all the products obtained and to evaluate the catalytic activity thereof. Ethylene should serve as olefin monomer due to its high activity and availability. The characterisation of the polymeric products should develop in its own right and should allow the calculation of molar mass distribution and its polydispersity indexes. Thermal distribution determinations were also envisioned to establish the density of the polymer products.
4. To compare results obtained from the polymerisation study to results found in literature for similar pre-catalysts as well as to the metallocene-based polymerisation catalysts used industrially. The comparison was done to evaluate the effect of metal centre chosen, steric bulk of the ligand and activity of the pre-catalyst complex.

References:

1. K. Ziegler, E. Holzkamp, H. Breil and H. Martin, *Angew. Chem.,* **1955**, *67,* 541.
2. G. Natta, *Angew. Chem.,* **1956**, *68*, 393 and **1964**, *76*, 553.
3. A. Behr, *Angew. Chem,. Int. Ed., Engl.,* **1988**, *27*, 661.
4. B.J. Burger, M.E. Thompson, W.D. Cotter and J.E. Bercaw, *J. Am. Chem. Soc.,* **1990**, *112,* 1566.
5. P.J. Shapiro, W.D. Cotter, W.P. Schaefer, J.A. Labinger and J.E. Bercaw, *J. Am. Chem. Soc.,* **1994**, *116*, 4623.
6. T.C. Chung, *Macromolecules*, **1988**, *21*, 865.
7. M.R. Kesti, G.W. Coates and R.M. Waymouth, *J. Am. Chem. Soc.,* **1992**, *112*, 9679.
8. M.M. Marques, S.G. Correira, J.R. Ascenso, A.F.G. Ribeiro, P.T. Gomes, A.R. Dias, P. Foster, M.D. Rausch and J.C.W. Chien, *J. Polym. Sci. Part A: Polym. Chem.,* **1999**, *37*, 2457.
9. S.J. McLain, E.F. McCord, S.D. Arthur, E. Hauptman, J. Feldman, W.A. Nugget, L.K. Johnson, S. Mecking and M. Brookhart, *Polym. Mat. Sci. Eng.* **1997***, 76*, 246.
10. B. Mohr, D.M. Lynn and R.H. Grubbs, *Organometallics*, **1996**, *15*, 4317.
11. D.M. Lynn, S. Shokyoku and R.H. Grubbs, *J. Am. Chem. Soc.,* **1996***, 118*, 784.
12. H.D. Maynard, S.Y. Okada and R.H. Grubbs, *Macromolecules*, **2000***, 33*, 6239.
13. J.F. Hagman and J.W. Crary, *Encyclopedia of Polymer Science and Engineering*, H.F. Mark, N.M. Bikales, C.G. Overberger and J.I Kroschwitz, Eds., *Wiley-Interscience*: New York, **1985**, Vol. 1, p. 325.
14. For the Review on Late Transition metal catalysts, see: S.D. Ittel, L.K. Johnson and M. Brookhart, *Chem. Rev.* **2000**, *100*, 1169.
15. L.K. Johnson, C.M. Killian and M. Brookhart, *J. Am. Chem. Soc.,* **1995***, 117,* 6414.
16. C.M. Killian, D.J. Temple, L.K. Johnson and M. Brookhart, *J. Am. Chem. Soc.,* **1996***, 118,* 11664.
17. G.J.P. Britovsek, V.C. Gibson, S.K. Spitzmesser, K.P. Tellmann, A.J.P. White and D.J. Williams, *J. Chem. Soc., Dalton Trans.,* **2002**, 1159.
18. V.C. Gibson, R.K. O'Reilly, D.F. Wass, A.J.P. White and D.J. Williams, *Macromolecules,* **2003**, *36*, 2591.

19. B.L. Small and M. Brookhart, *J. Am. Chem. Soc.,* **1998**, *120*, 7143.
20. B.L. Small and M. Brookhart, *Macromolecules,* **1999**, *32*, 2120.
21. S.C. Bart, E.J. Hawrelak, A.K. Schmisseur, E. Lobkovsky and P.J. Chirik, *Organometallics*, **2004**, *23*, 237.
22. D. Walther, T. Döhler, N. Theyssen and H. Görls, *Eur. J. Inorg. Chem.,* **2001**, 2049.
23. K. Yang, R.J. Lachicotte and R. Eisenburg, *Organometallics*, **1998**, *17*, 5102.
24. C.R. Baar, H.A. Jenkins, G.P.A. Yap and R.J. Puddephatt, *Organometallics,* **1998**, *17*, 4329.
25. M.S. Brookhart, L.K. Johnson, C.M. Killian, S.D. Arthur, J. Feldman, E.F. McCord, S.J. MacLain, K.A. Kreutzer, A.M.A. Bennet, E.B. Coughlin, E.B. Ittel, A. Parthasasrathy and D.J. Temple, WO Patent Application 9623010 to DuPont, **1995**.
26. L. Wang and T.C Flood, *J. Am. Chem. Soc.,* **1992**, *114*, 3169.
27. V.C. Gibson, A. Tomov, D.F. Wass, A.J.P. White and D.J. Williams, *J. Chem. Soc., Dalton Trans.,* **2002**, 2261.
28. (a.) M. Svoboda, H. tom-Dieck, *J. Organomet. Chem.,* **1980***, 191*, 321. (b.) T. Schleis, J. Heineman, T.P. Spaniol and J. Okuda, *J. Inorg. Chem. Commun.* **1998**, *1 (11)*, 431.
29. L.K. Johnson, S. Mecking and M. Brookhart, *J. Am. Chem. Soc.,* **1996***, 118,* 267.
30. S. Mecking, L.K. Johnson, L. Wang and M. Brookhart, *J. Am. Chem. Soc.,* **1998**, *120*, 888.
31. T. Schleis, T.P. Spaniol, J. Okuda, J. Heinemann and R. Mulhaupt, *J. Organomet. Chem.,* **1998**, *569,* 159.
32. D.G. Musaev, R.D.J. Froese and K. Morukuma, *Organometallics*, **1998**, *17(9)*, 1850.
33. P.J. Flory, *J. Am. Chem. Soc.,* **1940**, *62*, 1561.
34. Y.V.J. Kissin, *J. Polym. Sci., Part A: Polym. Chem.,* **1989**, *27,* 623.
35. W. Keim, F.H. Kowaldt, R. Goddard and C. Kruger, *Angew. Chem., Int. Ed. Engl.,* **1978**, *17*, 466.
36. Y. Kubo, L.S. Pu, A. Yamamoto and S. Ikeda, *J. Organomet. Chem.,* **1975**, *84*, 369.
37. G.J.P. Britovsek, V.C. Gibson, B.S. Kimberley, P.J. Maddox, S.J. McTavish, G.A. Solan, A.J.P. White and D.J. Williams, *Chem. Comm.,* **1998**, 849.
38. B.L. Small, M. Brookhart and A.M.A. Bennett, *J. Am. Chem. Soc.,* **1998**, *120*, 4049.
39. K.A.O. Starzewski, W.M. Kelly, A. Stumpf and D. Freitag, *Angew. Chem., Int. Ed.,*

Pectora roborant cultus recti

Eng., **1999**, *38*, 2439.

40. G. Wilkinson, P.L. Pauson, J.M. Birmingham and F.A. Cotton, *J. Am. Chem. Soc.,* **1953**, 1011.
41. H. Sinn, W. Kaminsky, H.J. Vollmer and R. Woldt, *Angew. Chem.,* **1980**, *92*, 396.
42. E. Kaji, Y. Tokuyama-shi, K. Toyota, Y. Hikari-shi, T. Tokuyama-shi, H. Kanazawa and Y. Shinnanyou-shi, *European Patent Application*, EP1352913 A1, **2003**.
43. A.A. Andersen, H.G. Cords, J. Herwig, W. Kaminsky, A. Merck, R. Mottweiler, J. Pein, H. Sinn and H.J. Vollmer, *Angew. Chem., Int. Ed., Engl.,* **1976**, *15*, 630.
44. M. Bochmann and S.J. Lancaster, *Organometallics*, **1993**, *12*, 633.
45. G.J.P. Britovsek, V.C. Gibson and D.F Wass, *Angew. Chem., Int. Ed., Engl.,* **1999**, *38*, 428.
46. W. Kaminsky, *J. Chem. Soc., Dalton Trans.,* **1998**, 1413.
47. B. Temme, G. Erker, J. Karl, H. Luftmann, R. Fröhlich and S. Kotila, *Angew. Chem., Int. Ed., Engl.,* **1995**, *34*, 1755.
48. B. Temme, G. Erker and J. Karl, *Chem. Eur. J.,* **1996**, *2*, 919.
49. G. Erker and J. Karl, *Chem. Ber.,* **1997**, *130,* 1261.
50. D.D Dovore, F.J. Timmers, D.L. Hasha, R.K. Rosen, T.J. Marks, P.A. Deck and C.L. Stern, *Organometallics.,* **1995**, *14*, 3132.
51. Y. Sun, W.E. Piers and S.J. Rettig, *Chem. Comm.,* **1998**, 127.
52. G.A. Moser, E.O. Fischer and M.D. Rausch, *J. Organomet Chem.,* **1971**, *27,* 379.
53. J.A. Connor and J.P. Lloyd, *J.C.S Dalton,* **1972**, 1470.
54. M. Zora, B. Yucel and N. Peynircioglu, *J. Organomet. Chem.,* **2002**, *11*, 656.
55. E.O. Fischer and A. Maasböl, *Angew. Chem.,* **1964**, *76*, 645.
56. H.-W. Wanzlick, *Angew. Chem, Int. Ed. Eng.,* **1962**, *1*, 75.
57. H.G. Raubenheimer, A. du Toit, M. du Toit, J. An, L. van Niekerk, S. Cronje, C. Esterhuysen and A.M. Crouch, *Dalton Trans.*, **2004**, 1173.
58. N. Luruli, V. Grumel, R. Brüll, A. du Toit, H. Pasch, A.J. van Reenen and H.G. Raubenheimer, *J. Polymer Science: Part A: Polymer Chemistry*, **2004**, *42*, 5121.
59. M. Bochmann, *J. Chem. Soc., Dalton Trans.,* **1996**, 255.
60. A. Gonioukh, W. Micklitz, B. Bildstein, M. Malaun and A. Hradsky, DE Patent 19920486 A1, 9 November 2000.

Chapter 2: Preparation of α-diimine ligands

Introduction

In this chapter, the synthesis and characterisation of the two α-diimine ligands are described (Scheme 2A) separately. These ligands differ in terms of the substituents on the imine nitrogen donor atoms. Although both ferrocenyl and phenyl moieties are aromatic and bulky, they nevertheless, differ in terms of their steric influences.

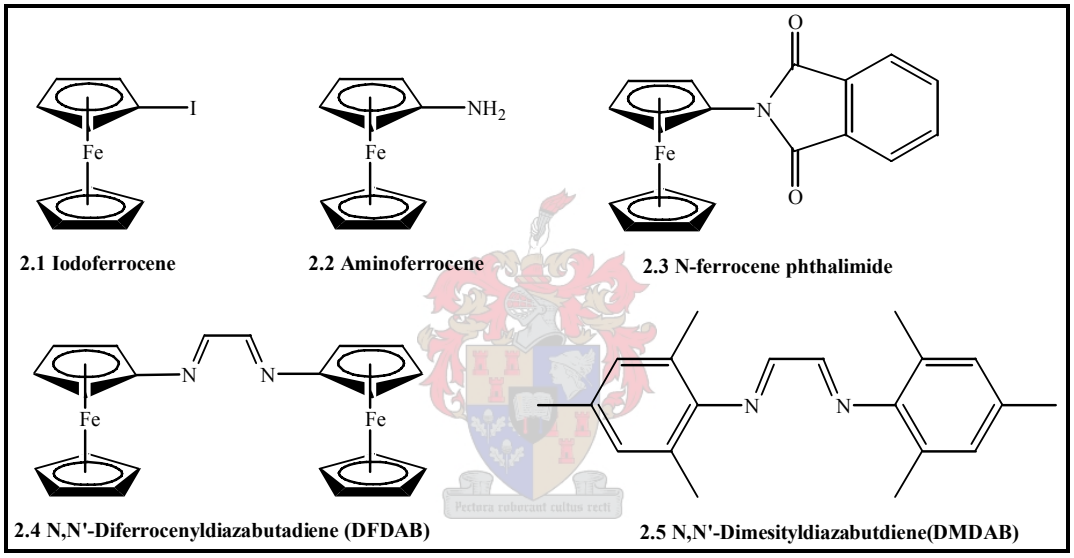

Scheme 2A

Here some background information regarding the ferrocene complex, from which ferrocenyl compounds derives, is given.

The independent discovery of dicyclopentadienyl iron(II) (ferrocene) [Fig. 2A] in 1951 by Wilkinson has transformed the field of organometallic chemistry. These sandwich-like compounds still holds the imagination of many scientists over fifty years after its discovery. The entire class of transition metal dicyclopentadienyl compounds is known as metallocenes, ferrocene having the chemical notation $[(\eta^5\text{-}C_5H_5)_2Fe]$.

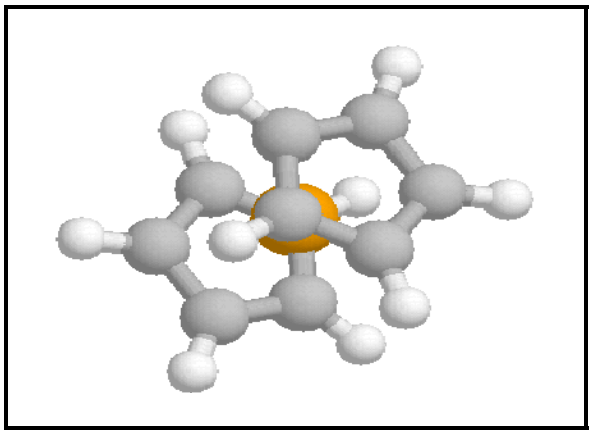

Fig. 2A: Molecular illustration of dicyclopentadienyl iron(II)

Ferrocene is isolated as an orange, crystalline solid with a melting point of 173 ^{o}C and a boiling point of 249 ^{o}C. It is stable to air, water and acids, soluble in most organic solvents and insoluble in water. Ferrocene is deprotonated in super-bases such as *tert*-butyllithium and the mixture of potassium *tert*-butoxide in butyllithium.

Wilkinson has found that the iron atom is located between two parallel cyclopentadienyl (Cp) rings with a staggered conformation. The sandwich structure is due to good orbital overlap of the sextet of the π-electrons in the *p*-orbitals of the Cp rings and the *d*-orbitals of the metal gives it a delocalised covalent bond between the metal atom and the cyclopentadienyl ring as a whole, resulting in high stability due to the π-complexation.

Woodward has discovered that the Cp rings were of aromatic nature paving the way for aromatic substitution reactions such as the Friedel-Crafts reaction. Due to its great stability and the ability to maintain the metal-ligand bonding under harsh conditions, there is a vast range of organic chemistry associated with this molecule and it is possible to carry out a variety of transformations on the Cp-ligands. For their independent contribution to the elucidation of the ferrocene structure and the chemistry of other metallocenes, Fischer and Wilkinson shared the Nobel Prize for Chemistry in 1973.

Ferrocene has a zero dipole moment and therefore the molecule is symmetrical. Furthermore, its infrared spectrum shows that all the C-H bonds are equivalent. The

molecule possesses interesting structural variations depending on the phase, i.e. it can crystallize in monoclinic, triclinic and orthorhombic modifications. Gas-phase electron diffraction observations project a D_{5h} geometry.

Removing hydrogen from the sp^3-carbon in cyclopentadiene results in an sp^2-carbon and full conjugation within the ring is established. This results in aromaticity of the Cp ring. The cyclopentadienyl anion has an MO-diagram as illustrated in Fig. 2B. Note the filled-shell configuration affording to aromaticity.

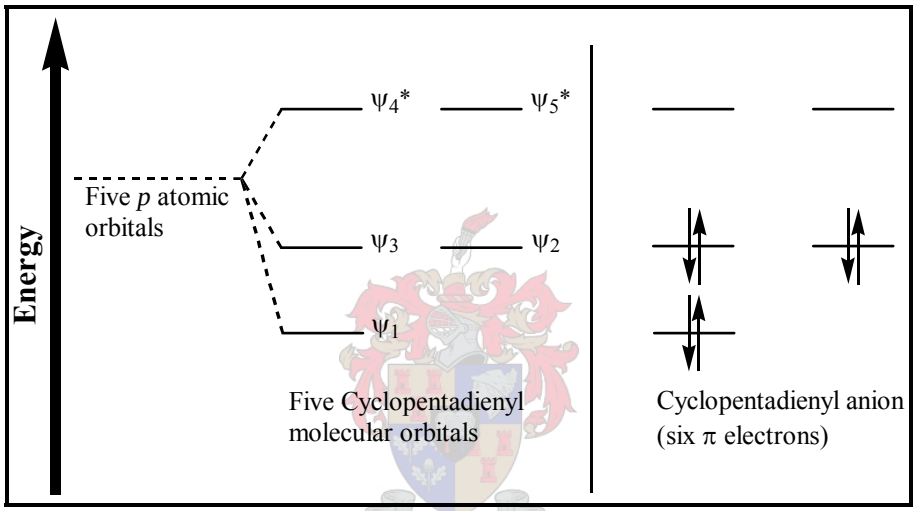

Fig. 2B: The MO-diagram of the cyclopentadienyl anion

More recent results for the crystal indicates that the superfluidity or lambda point is below Λ=164 K, the triclinic form persists and the configuration is ordered with a D_5 structure and only 9° rotation from the D_{5h} eclipsed configuration. The room temperature monoclinic crystalline form is a disordered species, indicating a staggered conformation, whilst in the orthorhombic form (T< 110 K) the rings are fully eclipsed (D_{5h}). Theoretical studies have shown that the eclipsed form is slightly more stable than the staggered form by 2.78 kJ/mol. Experimental evidence concurred with the theoretical studies.[2]

X-ray structures of ferrocenium salts formed upon oxidation (conc. H_2SO_4); indicate that the loss of an electron (from the frontal orbital located on the metal) has a minimal effect on the conformation of the Cp-rings. They remain in the staggered configuration at room

temperature as in ferrocene. There is also a slight increase in the C-Fe bond lengths as well as within the rings, but this is to be expected with removal of a bonding electron.

The reaction of cyclopentadienyl magnesium bromide with anhydrous ferrous(III) chloride in ether was an attempt to synthesise fulvalene *via* the oxidation of the cyclopentadienyl Grignard reagent.[3] However, the reduction of the iron(III) to iron(II) species yielded orange crystals that was analysed to be $FeC_{10}H_{10}$ (Scheme 2B).

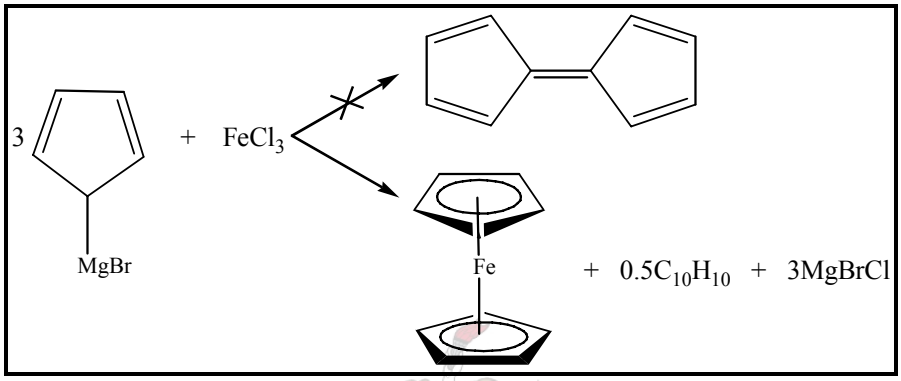

Scheme 2B

Although the prefered synthetic pathways towards ferrocene involve transmetallation or alkali ferrocenyls, Miller prepared ferrocene by the direct reaction (reaction 2.1) of cyclopentadiene with iron in the presence of aluminium, potassium or molybdenum oxides at 300 ^{0}C.[4]

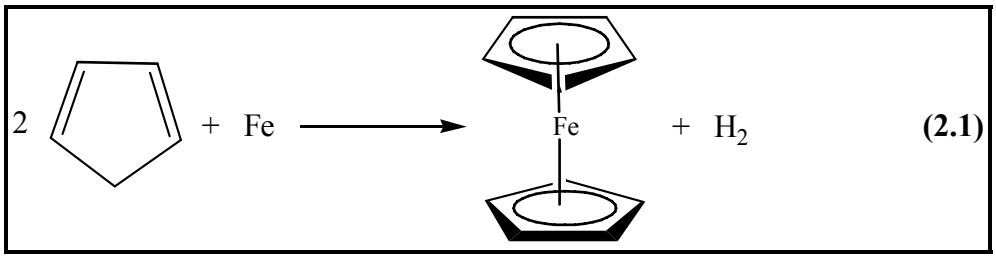

Ferrocene and ferrocene-derivatives cover a wide variety of reactions, including polymerization reactions, such as ring opening polymerization (ROP), where silicon, germanium, phosphorous and hydrocarbon-bridged ferrocenophanes form the back-bone of the polymer.

The banning of chlorofluorocarbons (CFC's) due to their negative impact on the ozone layer has prompted the search for alternative sources of coolants for refrigeration and many other applications, including fire suppressants. Fire suppressants such as CF_3Br are no longer useful. Pentacarbonyliron $Fe(CO)_5$ is more effective than CF_3Br, but much more toxic and flammable. In contrast to $Fe(CO)_5$, ferrocene is less toxic and flammable, but equally effective.[5]

The ferrocenyl-containing diimine ligand, N,N′-diferrocenyldiazabutadiene (DFDAB), has been chosen specifically to investigate the effect the presence a second metal centre has on the catalysis of olefin polymerisation. The metal centres of iron, zinc and chromium were chosen for their reputation of being low-activity catalysts. The question was whether the old dogs were prepared to learn new tricks? It is known from literature that comparable imine-type ligands readily coordinate to metal centres, especially those in the 2+ oxidation state.[6,7]

The synthesis of the DFDAB ligand is quite tedious and involves five steps starting with the very unstable and very sensitive pyrophoric lithioferrocene, which was not isolated. Despite the fact that the synthesis of N,N′-diferrocenyldiazabutadiene has been published[8], the synthetic steps were carefully repeated in this study and each intermediate product analysed by NMR spectroscopy. The description of compound 2.2 (N-ferrocenylphthalimide), however, includes a molecular structure determination and crystal data as well. Where applicable, the numbering of the hydrogen atoms corresponds to that of the carbon atoms.

2.1 <u>Iodoferrocene</u>:

Iodoferrocene was synthesised according to the modified method of Bildstein and co-workers.[8] Former synthetic methods of halogenated ferrocene involved the synthesis of (tri-*n*-butylstannyl)ferrocene[9] or ferrocene boronic acid[10] as precursors. In the method used here, mono-lithiated ferrocene obtained by deprotonation of ferrocene with Schlosser's base (a mixture of ^{t}BuOK and BuLi in THF), was converted directly to the

halogenated ferrocene using the appropriate halogen. The dark oil was extracted with diethyl ether and the solvent removed under vacuum. Equation 2.1 illustrates the reaction sequence.

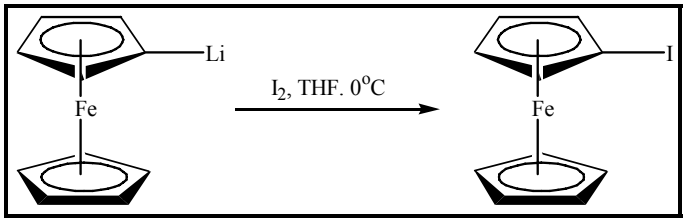

Equation 2.1

2.1.1 NMR Spectroscopy

The spectrum is consistent with that published by Guillaneux and co-workers.[9] Table 2.1.1 summarises the ^{1}H and ^{13}C NMR data for iodoferrocene that were now obtained.

Table 2.1.1: ^{1}H and ^{13}C NMR data for iodoferrocene.

Complex:	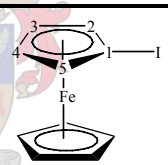
Solvent	$CDCl_3$
Temperature (K)	273
^{1}H NMR (600 MHz)	**δ**
$H^{2,5}$	4.40 (s, 2H)
$H^{3,4}$	4.15 (s, 2H)
Cp	4.18 (s, 5H)
^{13}C NMR (150 MHz)	**δ**
C^{1}	77.6
$C^{2,5}$	68.8
$C^{3,4}$	74.5
Cp	71.0

The proton NMR spectrum displays 3 signals in the region δ 4.15 to 4.40. Protons H^3 and H^4 encounter an equivalent, but different, chemical environment and correspond to the singlet signal at δ 4.15. Protons H^2 and H^5 experience an equivalent chemical environment and correspond to the singlet signal at δ 4.40. The large singlet signal at 4.18 ppm was assigned to the unsubstituted cyclopentadienyl ring proton atoms.

The substituted carbon atom (C^1) displays a signal at δ 77.56 in the ^{13}C NMR spectrum. Carbon atoms C^3 and C^4 endure an equivalent chemical environment and correspond to the signal at δ 74.46. C^2 and C^5 are also identical and resonate at δ 68.80. The strong signal at δ 71.0 belongs to the carbon atoms in the unsubstituted cyclopentadienyl ring.

2.2 N-ferrocene phthalimide:

N-ferrocene phthalimide is the precursor for aminoferrocene. Previous methods to prepare aminoferrocene have included the synthesis of ferrocenoyl azide, N-ferrocenyl acetamide or ferrocene phthalimide as intermediates.[21,22] The method that has been employed by Bildstein and co-workers[8] converts halogenated ferrocene directly into N-ferrocene phthalimide and then to aminoferrocene. N-ferrocene phthalimide was thus synthesised in this investigation by refluxing the halogenated ferrocene with phthalimide and Cu_2O followed by column chromatography. Equation 2.2 illustrates the reaction process.

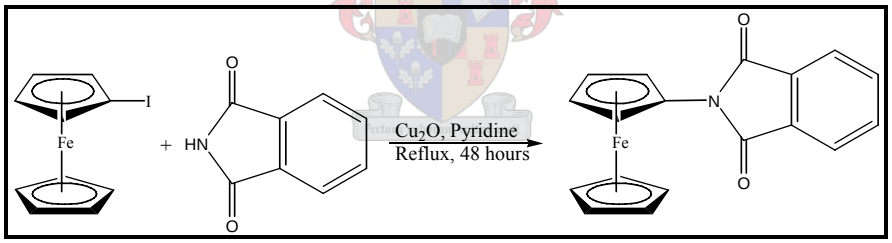

Equation 2.2

2.2.1 NMR Spectroscopy:

The NMR spectroscopic data were consistent with that found in literature.[8] The proton NMR spectrum display 5 signals in the region δ 4.17 to 7.86. Protons H^3 and H^4 are chemically equivalent and the singlet signal at δ 4.17 are assigned to these proton atoms, which experience a very small chemical shift downfield compared to the corresponding atoms of the halogenated ferrocene. This chemical shift is mainly due to the almost insignificant influence from the imine nitrogen atom and two carbonyl oxygen atoms. The unsubstituted cyclopentadienyl ring proton atoms resonate at δ 4.19. These proton

atoms do not undergo any change in chemical shift whatsoever. Proton atoms H^2 and H^5 are found at δ 4.98 as a singlet signal. These proton atoms do experience a large chemical shift downfield due to the electron withdrawing effect of the two carbonyl oxygen atoms. The phenyl proton atoms account for the two multiplet signals at δ 7.75 and δ 7.86 which are consistent with the absorption position of aryl proton atoms.

Table 2.2.1: ^{1}H and ^{13}C NMR data for N-ferrocene phthalimide.

Complex:	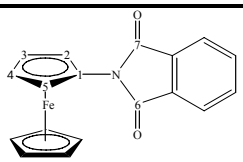
Solvent	$CDCl_3$
Temperature (K)	273
^{1}H NMR (300 MHz)	**δ**
$H^{2,5}$	4.98 (s, 2H)
$H^{3,4}$	4.17 (s, 2H)
Cp	4.19 (s, 5H)
Ph	7.75 (m, 2H)
Ph	7.86 (m, 2H)
^{13}C NMR (75 MHz)	**δ**
C^1	88.7
$C^{2,5}$	62.8
$C^{3,4}$	65.5
C^6	167.3
C^7	165.1
Ph	123.3
Ph	132.1
$Cp_{unsubst}$	69.5

In the ^{13}C NMR spectrum, the substituted carbon atom (C^1) of the cyclopentadienyl ring gives a signal at δ 88.68. This carbon atom is coordinated directly to the imine nitrogen atom and fairly close to two electron withdrawing carbonyl oxygen atoms accounting for the downfield shift compared to the substituted carbon atom on the halogenated ferrocene; all the other carbon atom NMR signals display a chemical shift upfield. The signal at δ 65.5 is assigned to the C^3 and C^4 atoms and similarly to the proton NMR spectrum, experiencing a small chemical shift upfield. The signal at δ 62.8 is allocated to carbon atoms C^2 and C^5. The signal with high intensity at δ 69.5 represents the unsubstituted cyclopentadienyl ring carbon atoms with almost no change in chemical

shift in comparison to iodoferrocene. The two signals at δ 123.3 and δ 132.1 correspond to the phenyl ring carbon atoms respectively. The two resonances at δ 165.1 and δ 167.3 are assigned to the carbonyl carbon atoms (C^6 and C^7) respectively. Table 2.2.1 summarises the ^1H and ^{13}C NMR data for N-ferrocene phthalimide.

2.2.2 X-Ray Diffraction:

N-ferrocene phthalimide was recrystallised from ethanol and single crystal obtained subjected to an X-ray diffraction study at room temperature. A red, needle-like crystal was mounted on a glass fibre and transferred to a Bruker Smart Apex[11] X-Ray diffractometer. The molecular structure and numbering of relevant atoms of N-ferrocenylphthalimide are illustrated in Figure 2.2.1.

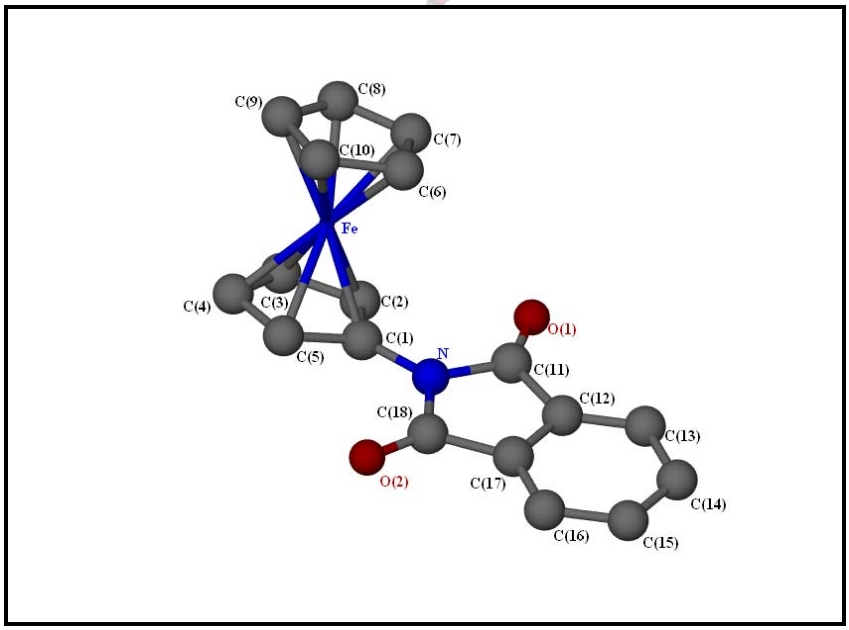

Fig 2.2.1: Molecular structure of N-ferrocenyl phthalimide

The crystals were radiated with a monochromatic Mo-Kα X-ray source at a wavelength of 0.71073Å and were corrected for Lorentz- and polarisation effects. The position of the heaviest atom (iron) was determined using direct methods and anisotropic displacement parameters for all the atoms, excluding hydrogen atoms, which were placed in calculated

positions. Structure determination and refinement of the atom coordinates were accomplished using the SHELX-97[12] and X-Seed[13] software.

The experimental and crystallographic data is reported are Table 2.2.2.

Table 2.2.2: Experimental and crystallographic data for N-ferrocene phthalimide

Empirical formula	$C_{18}H_{13}NO_2Fe$
Formula weight	331.14
Colour	Red needles
Crystal system	Monoclinic
Space group	$P2_1/n$
Unit cell dimensions	a = 5.830(3) α = 90.00
	b = 18.555(8) β = 96.689(7)
	c = 13.111(6) γ = 90.00
Z	4
V (Å^3)	1408.6(10)
Density (g/cm^3)	1.561
Radiation (Mo-Kα) [Å]	0.71073
$2\theta_{max}$	56.4°
Monochromator	Graphite
Absorption coefficient (μ) [mm^{-1}]	1.076
Temperature (K)	273(2)
F (000)	680
Diffractometer	Bruker Smart Apex®
Scan range (θ)	$-6 \leq h \leq 7$
hkl ranges	$-24 \leq k \leq 23$
	$-13 \leq l \leq 17$
Reflections measured	8477
Unique reflections used	3271
Number of parameters refined	200
Deepest hole	1.91
Highest peak	28.22
R_{int} (%)	2.95
R1 (%)	4.27
Goodness of fit (GooF)	1.055

The R value obtained in this study (4.27%) is significantly smaller than that found by Heinze and co-workers[14] (6.0%) and the molecular structure is therefore briefly discussed again in this thesis. The bond lengths for N-ferrocenyl phthalimide are reported in Table 2.2.3. The bond lengths for the phenyl ring, ferrocene fragments as well as the five membered imine ring are consistent with published values.[15,16] Within the ferrocene unit, however, some important differences are observed. In the substituted cyclopentadienyl ring, the bond lengths are all of the same length. However, in the unsubstituted Cp ring, the bond between C(6) and C(10) is considerably longer than the other bonds (1.452(6) Å compared to 1.380 Å for the other bonds). When comparing the bond distances of the two

Cp rings, one finds that, on average, the substituted Cp ring have longer bond distances than the unsubstituted Cp ring. The carbon-carbon bonds in the substituted Cp ring have less double bond character due to less delocalisation of these bonds. This is possibly brought about by the presence of not only the imine nitrogen atom, but also the two carbonyl oxygen atoms.

Table 2.2.3: Bond lengths for N-ferrocenyl phthalimide

Selected Bond Lengths (Å)							
C(1)-C(2)	1.419(3)	C(4)-Fe	2.032(3)	C(8)-Fe	2.042(3)	C(12)-C(17)	1.377(4)
C(1)-C(5)	1.419(3)	C(5)-Fe	2.038(3)	C(9)-C(10)	1.385(5)	C(13)-C(14)	1.382(5)
C(1)-N	1.420(3)	C(6)-C(7)	1.393(6)	C(9)-Fe	2.040(3)	C(14)-C(15)	1.378(5)
C(1)-Fe	2.037(2)	C(6)-C(10)	1.452(6)	C(10)-Fe	2.022(3)	C(15)-C(16)	1.385(4)
C(2)-C(3)	1.407(4)	C(6)-Fe	2.016(3)	C(11)-N	1.410(3)	C(16)-C(17)	1.376(4)
C(2)-Fe	2.047(2)	C(7)-C(8)	1.362(5)	C(11)-C(12)	1.478(4)	C(17)-C(18)	1.485(4)
C(3)-C(4)	1.416(4)	C(7)-Fe	2.030(3)	C(11)-O(1)	1.201(3)	C(18)-N	1.412(3)
C(3)-Fe	2.041(3)	C(8)-C(9)	1.375(4)	C(12)-C(13)	1.378(4)	C(18)-O(2)	1.201(3)
C(4)-C(5)	1.418(4)						

The bond angles for N-ferrocenylphthalimide are reported in Table 2.2.4. All the carbon atoms of the phthalimide ring are sp^2 hybridised thus, as expected, the ring is planar. The plane formed by the substituted Cp ring makes an angle of 17.62° with the bent plane through the atoms of the phthalimide ring. This angle was calculated using the Mean Plane (MPLA) function of SHELX.

Pectora roborant cultus recti

Table 2.2.4: Bond lengths for N-ferrocenyl phthalimide

Bond Angles (in degrees)					
C(1)-Fe-C(6)	107.9(1)	C(4)-Fe-C(8)	127.1(1)	C(12)-C(17)-C(16)	121.7(2)
C(1)-Fe-C(7)	120.5(1)	C(4)-Fe-C(9)	108.7(1)	C(12)-C(17)-C(18)	108.4(2)
C(1)-Fe-C(8)	154.4(1)	C(4)-Fe-C(10)	119.4(2)	C(12)-C(11)-N	106.1(2)
C(1)-Fe-C(9)	164.4(1)	C(5)-Fe-C(6)	120.5(2)	C(13)-C(14)-C(15)	121.4(3)
C(1)-Fe-C(10)	127.0(1)	C(5)-Fe-C(7)	155.2(2)	C(13)-C(12)-C(17)	121.0(3)
C(3)-Fe-C(6)	162.4(2)	C(5)-Fe-C(8)	164.0(1)	C(14)-C(15)-C(16)	120.9(3)
C(3)-Fe-C(7)	125.8(2)	C(5)-Fe-C(9)	127.1(1)	C(15)-C(16)-C(17)	117.4(3)
C(3)-Fe-C(8)	109.2(1)	C(5)-Fe-C(10)	107.8(1)	C(16)-C(17)-C(18)	129.9(2)
C(3)-Fe-C(9)	120.6(1)	C(11)-C(12)-C(13)	130.2(3)	C(16)-C(17)-C(12)	121.7(2)
C(3)-Fe-C(10)	153.9(2)	C(11)-C(12)-C(17)	108.8(2)	C(17)-C(18)-N	106.0(2)
C(4)-Fe-C(6)	155.5(2)	C(11)-N-C(18)	110.7(2)	C(17)-C(18)-O(2)	128.7(2)
C(4)-Fe-C(7)	162.8(2)	C(12)-C(13)-C(14)	117.5(3)	Fe-C(1)-N	126.5(2)

The bond angles at C(12) and C(17) [121° and 121.7°, respectively] within the phenyl ring are marginally larger than the norm of 120°. The five membered imine ring is

sterically demanding, which causes some disorder within the phenyl rings. The rigidity of the phenyl ring compensates for this disorder by decreasing the bond angles at C(13) and C(16) to 117.5° and 117.4° respectively. The angles formed by the carbon atoms of the substituted cyclopentadienyl ring to their corresponding atoms in the unsubstituted cyclopentadienyl ring through Fe are approximately 108°. The crystal data proved that the two cyclopentadienyl rings of the ferrocene are in an eclipsed configuration with D_{5h} symmetry.

The packing of the crystal structure is depicted in Figure 2.2.2. It is clear from this figure that molecular packing proceeded very economically in a sterical sense. The molecules are packed inversely along the *b*-axis. Between two molecules, the phenyl ring overlaps with an imine ring of adjacent molecules, but the distances between each centroid of overlapping rings (5.83 Å) are too large for π-stacking to occur.

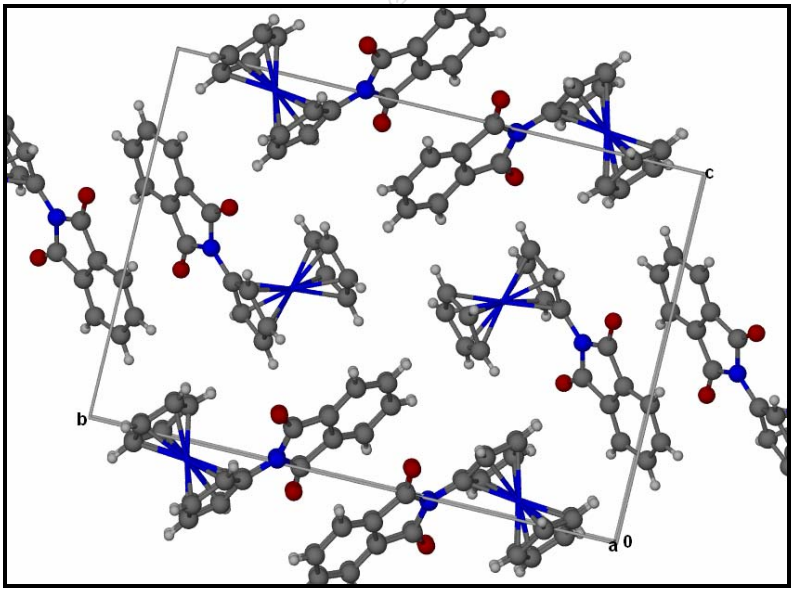

Fig. 2.2.2: Packing of N-ferrocenyl phthalimide along the *b*-axis

The hydrogen atoms are placed theoretically, thus their exact vector position can not be determined. The Van der Waals forces between the molecules O(2)···H(161)···C(16) with a distance of 2.547 Å and a second set between atoms O(1)···H(41)···C(4) with a distance of 2.539 Å, contribute to the stable packing of the crystal structure. Figure 2.2.3 illustrates these hydrogen bonds and the manner in which the molecule is held together.

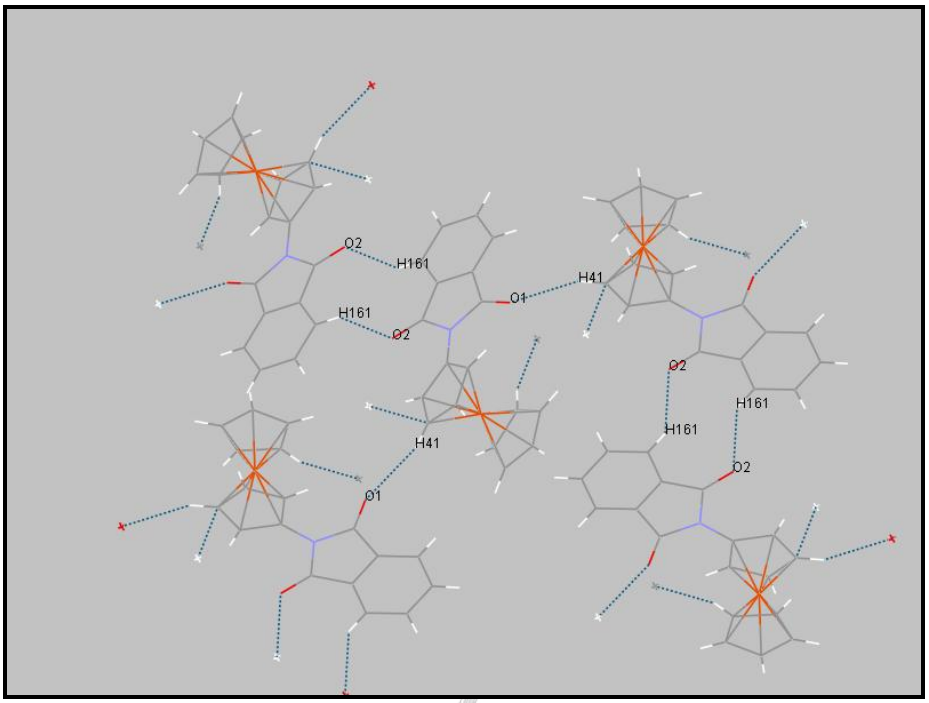

Fig. 2.2.3: Van der Waals forces in N-ferrocenyl phthalimide

2.3 Aminoferrocene:

Aminoferrocene was synthesised using the modified and optimised method described by Bildstein and co-workers.[8] Ferrocene phthalimide was refluxed with hydrazine hydrate in pyridine. Aqueous work-up yielded a bright orange, microcrystalline material. Equation 2.3 demonstrates the reaction succession.

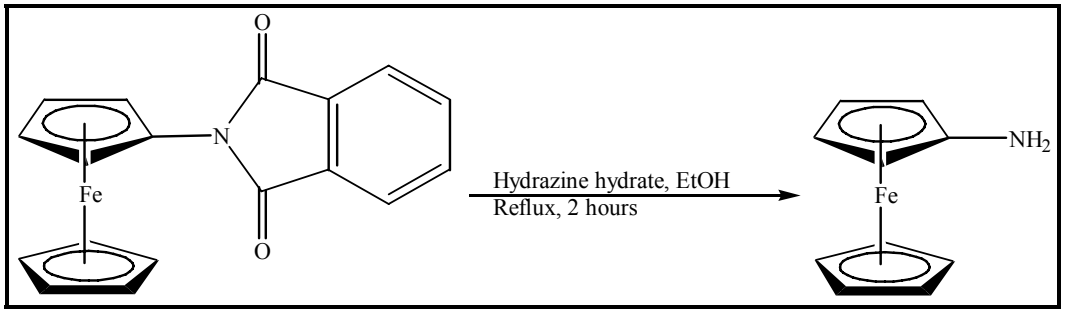

Equation 2.3

2.3.1 NMR Spectroscopy:

The NMR spectroscopic data are mainly consistent with published results of Herberhold and co-workers[17] in which they discuss alternative methods for the preparation of ferrocenylamines from acetomidoferrocene.

The signals assigned to the proton atoms in the ^{1}H NMR spectrum experience a chemical shift upfield compared to the corresponding proton atoms of N-ferrocene phthalimide. This is mainly due to the absence of the two electron withdrawing carbonyl oxygen atoms on N-ferrocene phthalimide. The broad signal at δ 2.50 is assigned to the amine proton atoms. Protons H^2 and H^5 are adjacent to the electron donating nitrogen atom of the amide group, thus experiencing the largest change in chemical shift (in excess of 1 ppm) and appear at δ 3.97. Protons H^3 and H^4 endure an equivalent chemical environment and the singlet signal at δ 3.83 are assigned to these atoms. The large singlet signal at δ 4.08 is assigned to the unsubstituted cyclopentadienyl ring proton atoms.

Table 2.3.1: ^{1}H and ^{13}C NMR data for aminoferrocene

Complex:	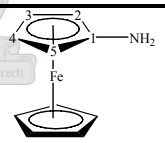
Solvent	$CDCl_3$
Temperature (K)	273
^{1}H NMR (300 MHz)	**δ**
$H^{2,5}$	3.97 (s, 2H)
$H^{3,4}$	3.83 (s, 2H)
Cp	4.08 (s, 5H)
NH_2	2.50 (bs, 2H)
^{13}C NMR (75 MHz)	**δ**
C^1	105.3
$C^{2,5}$	58.6
$C^{3,4}$	63.3
Cp	68.7

The signal at δ 105.3 is allocated to the substituted Cp carbon atom (C^1) in the ^{13}C NMR spectrum. C^1 is the only carbon atom to demonstrate a chemical shift downfield compared to the corresponding atom on the N-ferrocene phthalimide compound.

Although almost insignificant, all the other carbon atoms experience chemical shift up field in comparison to those in the aforementioned compound. The signal at δ 63.3 is assigned to C^3 and C^4, which endure equivalent chemical environments. Carbon atoms C^2 and C^5 experience equivalent chemical environments and the signal at δ 58.7 is allocated to these atoms. The large signal at δ 68.7 is assigned to the unsubstituted cyclopentadienyl ring carbon atoms. Table 2.3.1 summarises the ^1H and ^{13}C NMR data for aminoferrocene.

2.4 N, N'-Diferrocenyldiazabutadiene (DFDAB):

The final step in the synthesis of the N,N'-Diferrocenyldiazabutadiene ligand which will later be coordinated to several metals is discussed now. N,N'-Diferrocenyldiazabutadiene was prepared using a well tested method[8] according to Bildstein in which aminoferrocene is stirred with an aqueous solution of glyoxal at room temperature for several hours. The product was precipitated with water, filtered and dried under vacuum. Equation 2.4 depicts the sequence.

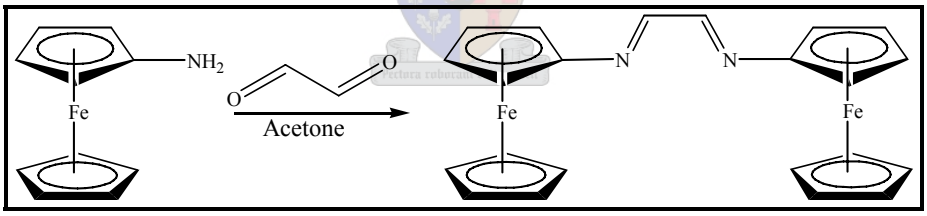

Equation 2.4

2.4.1 NMR Spectroscopy:

The spectroscopic data indicated that the desired compound was prepared. Fortunately no indication of impurities or side-reactions was found. Table 2.4.1 summarises the ^1H and ^{13}C NMR data for N,N'-Diferrocenyldiazabutadiene. The singlet signals at δ 4.63 and δ 4.38 are assigned to proton atoms H^2 and H^5 and proton atoms H^3 and H^4 respectively. The large singlet signal at δ 4.19 is assigned to unsubstituted cyclopentadienyl ring proton atoms. The singlet signal at δ 8.35 is allocated to the imine proton atoms. All the

proton atoms undergo a considerable change in chemical shift downfield compared to those in aminoferrocene. This is due electron donating effect of the nitrogen atoms.

In the ^{13}C NMR spectrum, the signal at δ 103.5 is assigned to carbon atom (C^1) and is the only carbon atom to exhibit a change in chemical shift upfield compared to the ^{13}C NMR spectrum of aminoferrocene, all the other carbon atoms display a large change in chemical shift downfield. The signal at δ 69.1 is allocated to carbon atoms C^3 and C^4. Carbon atoms C^2 and C^5 experience equivalent chemical environments and the signal at δ 64.1 is allocated to them. The large signal at δ 70.4 is assigned to the unsubstituted cyclopentadienyl ring carbon atoms, almost equivalent to that of N-ferrocene phthalimide. To the imide carbon atoms, the signal at δ 158.9 is allocated.

Table 2.4.1: ^1H and ^{13}C NMR data for N,N'-Diferrocenyldiazabutadiene

Complex:	
Solvent	Dichloromethane D-2
Temperature (K)	273
^1H NMR (300 MHz)	**δ**
$H^{2,5}$	4.63 (s, 2H)
$H^{3,4}$	4.38 (s, 2H)
Cp	4.19 (s, 5H)
-N=C-	8.35 (s, H)
^{13}C NMR (75 MHz)	**δ**
C^1	103.5
$C^{2,5}$	64.1
$C^{3,4}$	69.1
Cp	70.4
-N=C-	158.9

2.4.2 UV/Vis Spectroscopy:

The UV/Vis spectrum was recorded on a GBC-UV/Vis spectrophotometer with a solution of the compound in THF at a concentration of 94.31 μM using a 1 cm^2 quartz cuvette. Spectrophotometric data are represented in Table 2.4.2.

Table 2.4.2: Spectrophotometric data for N,N'-Diferrocenyldiazabutadiene

UV/Vis spectrum	Peak 1	Peak 2
Solvent:	THF	THF
λ (nm)	333.4	526.7
A	0.8995	0.2472
ε (M^{-1})	9537.7	2621.1

The DFDAB compound has an intense dark purple color (λ_{max} = 526.72 nm) indicating a metal-to-ligand charge transfer which is to be expected for molecules incorporating redox-active ferrocenyl groups and a DAB backbone with two low-lying antibonding π^* orbitals.[18] A single band in the region of 280 to 360nm usually indicates an $n \rightarrow \pi^*$ transition. This value is consistent for that of other -N=C- fragments. From Table 2.4.2, it is clear that the band at 333nm (ε = 9538 M^{-1}) is that of the imine fragment.

2.4.3 Mass Spectrometry:

The mass spectral data for N,N'-Diferrocenyldiazabutadiene are reported in Table 2.4.3. The most abundant ion formed in the ionization chamber was that of N_2 which formed the base peak *m/z* 28. The molecular ion, $[M]^+$, formed at *m/z* 424, obeying the nitrogen rule.[19] This rule states that if a compound contains an even number of nitrogen atoms, the molecular ion will appear at an even mass value. The N,N'-diferrocenyl-diazabutadiene compound fragments into Fe-Cyclopentadienyl (Fe-Cp) and ferrocene-diazabutadiene-cyclopentadienyl fragments corresponding to the two low intensity peaks at *m/z*303 and *m/z* 121. The next fragmentation step takes place at the weakest bond, namely the single bond between the ferrocene and diazabutadiene-Cp moieties resulting in the low intensity peak at *m/z* 186.

Table 2.4.3: Mass spectral data for N,N'-Diferrocenyldiazabutadiene

Fragment-ion	$[M]^+$	$[M - \text{Fe-Cp}]^+$	$[\text{Fc}]^+$	$[\text{Fc - Cp}]^+$	$[N_2]^+$
m/z (I%)	424 (33)	303 (8)	186 (6.5)	121 (12)	28 (100)

2.4.4 Infrared Spectroscopy:

The infrared spectrum (KBr) of this compound displayed a characteristic -C=N- stretching frequency at 1633 cm^{-1}.

2.5 N,N'-dimesityldiazabutadiene (DMDAB):

The second ligand prepared with an eye on eventual metal coordination is N,N'-dimesityldiazabutadiene. The two phenyl moieties on each ligand could indicate the influence of pure aromatic units on conjugated N-donors in catalysis. Furthermore, differences with aromaticity in the ferrocene Cp-rings could become clear. The Arduengo group[20] and the Grubbs group[23] amongst others synthesised N,N'-dimesityldiazabutadiene as a pre-cursor for the 1,3-bis-(2,4,6-trimethylphenyl)imidazolin-2-ylidene ligand (Figure 2.5.1). Substitution of one of the two tricyclohexyl phosphine ligands on the First Generation Grubbs catalyst by this ylidene affords the Second Generation Grubbs catalyst. This catalyst was employed for Ring Opening Metathesis Polymerisation (ROMP) of strained cyclic olefin monomers such as norbornene and cyclooctadiene.

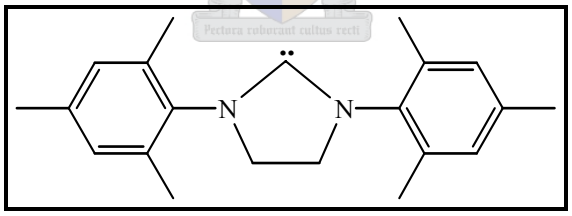

Fig. 2.5.1: The 1,3-bis-(2,4,6-trimethylphenyl)imidazolin-2-ylidene ligand

N,N'-dimesityldiazabutadiene (DMDAB) was constructed using the method described by Arduengo and co-workers.[20] An aqueous solution of glyoxal was stirred with 2,4,6-trimethylaniline in *n*-propanol at room temperature. The yellow powder was precipitated with water, filtered and dried under vacuum. Equation 2.5 illustrates the synthetic pathway.

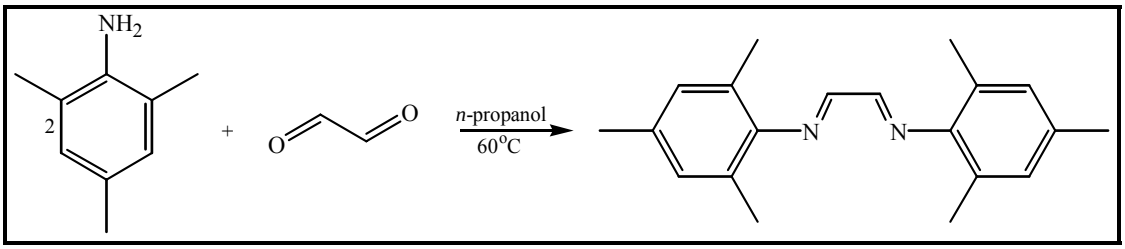

Equation 2.5

2.5.1 NMR Spectroscopy:

The NMR data reported in Table 2.5.1 showed all the expected chemical shifts revealing that the favoured product has been obtained after synthesis. All signals could be assigned more completely than in previous work .[20] The methyl proton atoms, due to the aromatic rings, experience some deshielding and hence resonate somewhat downfield (δ 2.14) from ordinary alkyl proton atoms (0.9-1.5 ppm).

Table 2.5.1: ^{1}H and ^{13}C NMR data for N,N'-dimesityldiazabutadiene

Complex:	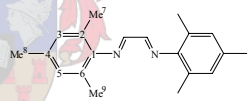
Solvent	Dichloromethane D-2
Temperature (K)	273
^{1}H NMR (300 MHz)	**δ**
$Me^{7,9}$	2.14 (s, 24H)
Me^{8}	2.28 (s, 12H)
$C^{3,5}$	6.94 (s, 8H)
-N=C-H	8.12 (s, 4H)
^{13}C NMR (75 MHz)	**δ**
$Me^{7,9}$	18.2
Me^{8}	20.8
$C^{2,6}$	127.0
$C^{3,5}$	129.5
C^{4}	134.8
Ipso C	148.3
-N=C-	164.3

The ring proton atoms (*meta* H) exhibit low-field resonance characteristic of aromatic proton atoms. The imine proton atoms experience a chemical shift somewhat upfield compared to that of the diferrocenyldiazabutadiene ligand due to the presence of the

phenyl ring that causes some shielding. On the other hand, the imine carbon atoms appear somewhat downfield compared to the corresponding carbon atoms of the diferrocenyldiazabutadiene ligand in the ^{13}C NMR spectrum.

2.5.2 UV/Vis Spectroscopy:

The UV/Vis spectrum was recorded on a GBC-UV/Vis spectrophotometer with a solution of the compound in THF (0.1368 mM) using a 1 cm^2 quartz cuvette. The ultraviolet spectrum of benzene contains three absorption bands and electronic transitions are probably of the $\pi \rightarrow \pi^*$ type. The primary bands occur at 184 and 202 nm. Being in the vacuum ultraviolet region, they are difficult to detect with most commercial instruments. The secondary band appears at 255 nm. Substitution of the benzene ring shifts the bands to higher wavelengths. Aniline has a primary absorption band at 230 nm (ε = 8600 M^{-1}) and a secondary band at 280 nm (molar absortivity, ε = 1430 M^{-1}). A single band in the region of 280 to 360 nm usually indicates an $n \rightarrow \pi^*$ transition. This value is consistent for that of –N=C- fragments.

Table 2.5.2: Spectrophotometric data for N,N'-dimesityldiazabutadiene

UV/Vis spectrum	Peak 1	Peak 2
Solvent:	THF	THF
λ (nm)	272.32	367.04
Absorbance	1.82	1.16
ε (M^{-1})	13 307	8 499

From Table 2.5.2, it is clear that Peak 1, the 272.3 nm (ε = 13 307 M^{-1}) band, belongs therefore, to the aromatic ring and Peak 2, the 367 nm (ε = 8499 M^{-1}) band, is that of the imine fragment. These results are also in line with reported values for similar compounds.[20]

2.5.3 Molecular Structure:

The molecular structure and numbering of relevant atoms of the N,N'-dimesityl diazabutadiene ligand is illustrated in Figure 2.5.2.

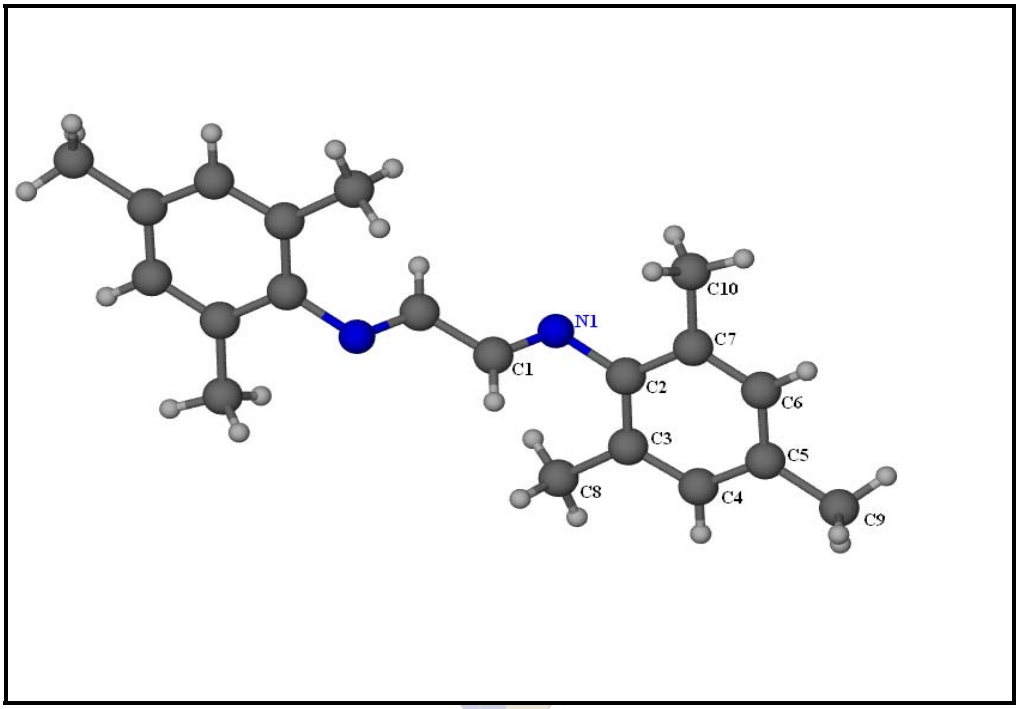

Fig 2.5.2: The molecular structure of N,N'-dimesityl diazabutadiene

N,N'-dimesityldiazabutadiene was dissolved in methylene chloride and single crystals suitable for crystallographic investigation collection formed after a week. A yellow, needle-like crystal was mounted on a glass fibre and transferred to a Bruker Smart Apex[11] X-Ray diffractometer. The crystals were radiated with a monochromatic Mo-Kα X-ray source at a wavelength of 0.71073Å and the data were corrected for Lorentz- and polarisation effects. The position of the heaviest atom (nitrogen) was found using direct methods and anisotropic displacement parameters for al the atoms, excluding hydrogen atoms, were calculated. The hydrogen atoms were placed in calculated positions. Structure determination and refinement of the atom coordinates were accomplished using the SHELX-97[12] and X-Seed[13] software. The collection was done at 173K and Table

2.5.3 summarises the collection as well as the structural data. Bond distances and angles are reported in Table 2.5.4 and 2.5.5 respectively.

Table 2.5.3: Experimental and crystallographic data for N,N'-dimesityldiazabutadiene

Empirical formula	$C_{20}H_{24}N_2$
Formula weight	292.41
Colour	Yellow needles
Crystal system	Monoclinic
Space group	$P2_1/c$
Unit cell dimensions	a = 13.261(5) α = 90.00
	b = 4.4151(18) β = 107.982(6)
	c = 15.347(6) γ = 90.00
Z	2
V (Å^3)	854.6(6)
Density (g/cm^3)	1.136
Radiation (Mo-Kα) [Å]	0.71073
$2\theta_{max}$	56.4°
Monochromator	Graphite
Absorption coefficient (μ) [mm^{-1}]	0.067
Temperature (K)	173(2)
F (000)	316
Diffractometer	Bruker Smart Apex®
Scan range (θ)	
hkl ranges	$-14 \leq h \leq 17$
	$-5 \leq k \leq 5$
	$-20 \leq l \leq 19$
Reflections measured	4503
Unique reflections used	1913
Number of parameters refined	88
Deepest hole	2.76
Highest peak	28.20
R_{int} (%)	6.19
R1 (%)	11.74
Goodness of fit (GooF)	1.120

The C-C bond lengths originating from the methyl carbon atoms [C(8) to C(10)] are consistent with those for C(sp^3)-C$_{(aryl)}$ bonds (~1.506Å).[15] The bond length of 1.43 Å between atoms C(2) and N(1) is consistent with published values.[16] The bond distance of 1.47 Å between C(1) and C(1)' indicates C(sp^2)-C(sp^2) overlap.

Table 2.5.4: Bond lengths for N,N'-dimesityldiazabutadiene

Bond Lengths (Å)					
C(1)-N(1)	1.269(5)	C(2)-C(7)	1.405(5)	C(5)-C(6)	1.389(6)
C(1)-C(1)'	1.470(8)	C(3)-C(4)	1.392(6)	C(5)-C(9)	1.516(5)
C(2)-N(1)	1.431(5)	C(3)-C(8)	1.508(5)	C(6)-C(7)	1.387(5)
C(2)-C(3)	1.410(6)	C(4)-C(5)	1.388(5)	C(7)-C(10)	1.506(6)

The bond angles for the mesitylene ring deviates from the theoretical value of 120°, but still retains its planar geometry. The angle at C(2) remains in the order of 120°, but the two adjacent angles [C(7) and C(3)] are smaller than 120° (118.6 and 117.9° respectively) and the two angles at C(4) and C(6) are somewhat larger (122.8 and 122.4° respectively). The steric crowding caused by the two methyl groups [C(8) and C(10)] results in a pushing effect away from N(1), which in turn results in the deviation in the aromatic bond angles. The planes formed by the two mesitylene rings are parallel to each other, but at different elevated levels.

Table 2.5.4: Bond angles for N,N'-dimesityldiazabutadiene

Bond Angles (in degrees)					
C(1)-N(1)-C(2)	117.8(4)	C(4)-C(5)-C(9)	120.7(4)	C(5)-C(6)-C(7)	122.4(4)
C(1)-C(1)'-N(1)'	119.9(5)	C(3)-C(2)-C(7)	120.7(3)	C(6)-C(5)-C(9)	121.6(4)
C(2)-C(3)-C(4)	117.9(3)	C(3)-C(4)-C(5)	122.8(4)	C(6)-C(7)-C(10)	121.0(3)
C(2)-C(3)-C(8)	122.3(4)	C(4)-C(3)-C(8)	119.8(4)	N(1)-C(2)-C(3)	121.5(3)
C(2)-C(7)-C(6)	118.6(4)	C(4)-C(5)-C(6)	117.6(4)	N(1)-C(2)-C(7)	117.8(4)
C(2)-C(7)-C(10)	120.4(3)				

The crystal packing of the dimesityldiazabutadiene complex is illustrated in Figure 2.5.3. The step-like orientation of the mesitylene rings to each other results in an efficient layered stacking along the *b*-axis.

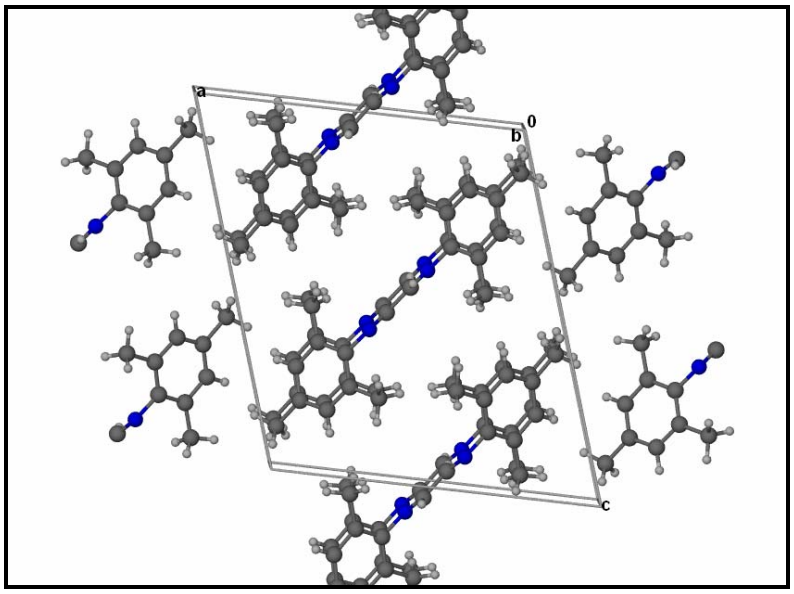

Fig. 2.5.3: Crystal packing of N,N'-dimesityldiazabutadiene along the *b*-axis

The hydrogen positions are calculated and exact vector positions are not be known. Extremely weak hydrogen contacts between N(1) and C(11), N(1)···H(11)···C(11) at 3.687 Å, could contribute to the stable packing of the crystal structure. The centroid distance between overlapping mesitylene fragments is too large (4.42 Å) for π-stacking to occur. Figure 2.5.4 illustrates these hydrogen contacts and the manner in which the molecules are held together.

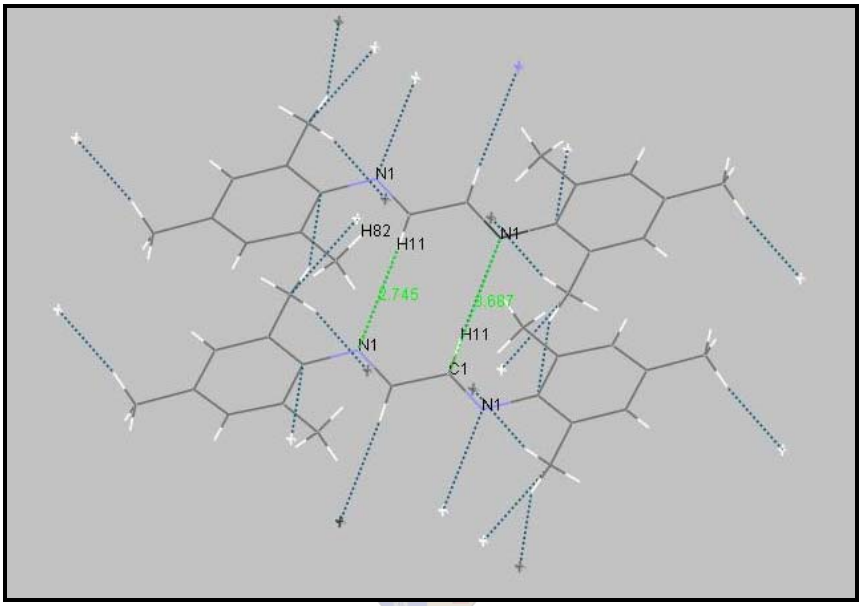

Fig. 2.5.4: Hydrogen bonds present in N,N'-dimesityldiazabutadiene

2.5.4 Mass Spectrometry:

The mass spectral data of the dimesityldiazabutadiene ligand is given in Table 2.5.6. The molecular ion peak is formed at *m/z* 292. Expulsion of the first methyl group yielded the base peak at *m/z* 277 with an intensity of 97%. Subsequent fragmentation of another methyl group leads to the two low intensity peaks at *m/z* 262 and *m/z* 247. The fragmentation to form a phenyl moiety and a methyl group occurs simultaneously yielding a peak at *m/z* 158 with a low intensity. The cleavage of the β-amine bond is characteristic of secondary and tertiary amines.

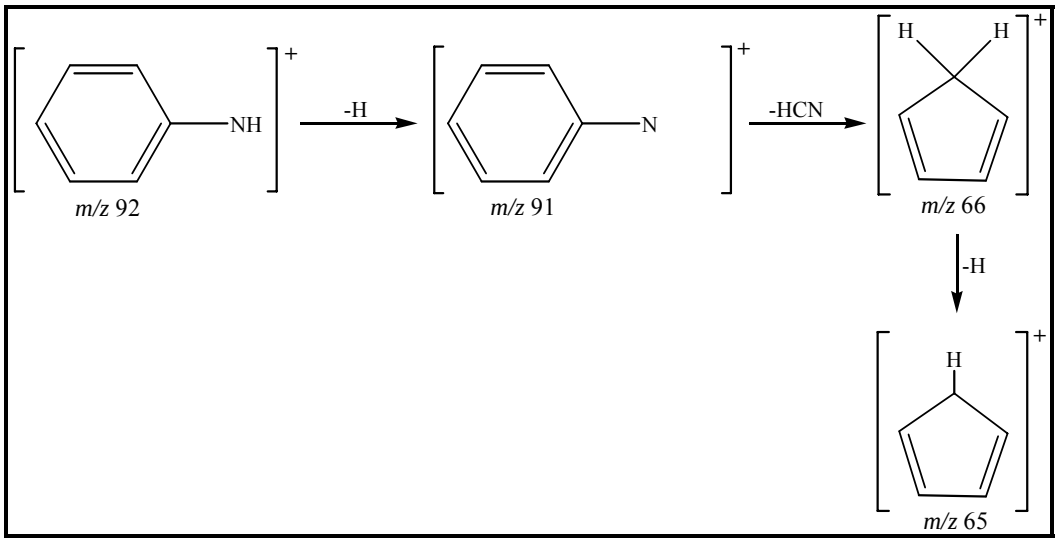

Scheme 2.5.1:

The medium intensity peak at *m/z* 91 and the low intensity peak at *m/z* 65 represent the classic fragmentation of aniline which is illustrated in Scheme 2.5.1.

Table 2.5.6: Mass spectral data for N,N'-dimesityldiazabutadiene

Fragment-ion	***m/z (I%)***	**Fragment-ion**	***m/z (I%)***
$[M]^+$	292 (3)	$[C_9H_{10}N_2 - CH_3]^+$	131 (42)
$[M - CH_3]^+$	277(97)	$[C_7H_7N_2]^+$	119 (31)
$[M - 2CH_3]^+$	262 (5)	$[C_6H_5N]^+$	91 (32)
$[M - 3CH_3]^+$	247 (4)	$[C_5H_5]$	65 (5)
$[M - 4CH_3 - Ph]^+$	158 (8)	$[N_2]^+$	28 (63)
$[C_9H_{10}N_2]^+$	146 (85)		

2.5.5 Infrared spectroscopy:

The infrared stretching frequencies for the dimesityldiazabutadiene complex are reported in Table 2.5.7 and are consistent with those of a previous study.[18]

Table 2.5.7: The infrared stretching frequencies for N,N'-dimesityldiazabutadiene

Moiety	Aryl-H	Aliphatic C-H	-N=C-	C=C
$\nu(cm^{-1})$	3014 (w)	2914 (*s*)	1617 (*s*)	1476 (*m*)
$\nu(cm^{-1})_{theoretical}$	3100-3000	2960-2850	1660-1480	≈ 1500

Conclusions:

N,N'-diferrocenyldiazabutadiene and N,N'-dimesityldiazabutadiene were synthesized and all products that formed were characterised by comparison of the NMR data to published results. The crystal and molecular structures of N-ferrocene phthalimide and N,N'-dimesityldiazabutadiene were determined. Different bond types are clearly indicated and the molecular packing of the compounds described.

References:

1. G. Wilkinson, *J. Organomet. Chem.,* **1975**, *100*, 273.
2. F.A. Cotton, G. Wilkinson and P.L. Gaus, *Basic Inorganic Chemistry,* John Wiley and sons, New York, **1995**, *3rd Edition*, 689.
3. T.J. Kealy and P.L. Pauson, *Nature*, **1951**, *168*, 1039.
4. I. Manners, *Advances in Organometallic Chemistry*, **1995**, *37*, 131.
5. G.T. Linteris, *et al, 28th Symposium on Combustion*, **2000**.
6. C.M. Killian, D.J. Temple, L.K. Johnson and M. Brookhart, *J. Am. Chem. Soc.,* **1996**, *118*, 11665.
7. G.J.P. Britovsek, M. Bruce, V.C. Gibson, B.S. Kimberley, P.J. Maddox, S. Mastroianni, S.J. MacTavish, J. Redshaw, G.A. Solan, S. Strömberg, A.J.P. White and D.J. Williams, *J. Am. Chem. Soc.,* **1999**, *121*, 8728.
8. B. Bildstein, M. Malaum, H. Kopacka, K. Wurst, M. Mitterböck, K. Ongania, G. Opromolla and P. Zanello, *Organometallics*, **1999**, *18*, 4325.
9. D. Guillaneux and H.B. Kagan, *J. Org. Chem*, **1995**, *60*, 2502.
10. F.S. Kamounah and J.B. Christensen, *J. Chem. Res., Synop,* **1997**, 150.
11. SMART Data collection software (version 5.629), Bruker AXS Inc., Madison, WI, **2003**.
12. G. Sheldrick, *SHELX Program for Crystal Structure Determination,* University of Göttengen, **1997**.
13. L.J. Barbour, *J. Supramol. Chem.,* **2001**, *1*, 189.
14. K. Heinze and M. Schlenker, *Eur. J. Inorg. Chem.,* **2004**, *14*, 2974.

15. C.L. Foster, C.A. Kilner, M. Thornton-Pett and M.A. Halcrow, *Acta Crystallographica,* **2000**, *C56*, 319.
16. F.H. Allen, O. Kennard, D.G. Watson, L. Brammer, A.G. Orpen and R. Taylor, *J. Chem. Soc., Perkin Trans. II*, **1987**, S1.
17. M. Herberhold, M. Ellinger and W. Kremnitz, *J. Organomet. Chem.*, **1983**, *241*, 227.
18. M. Hesse, H. Meier and B. Zeeh, *Spectroscopic Methods in Organic Chemistry*, Foundations of Organic Chemistry Series, **1997**, Georg Thieme Verlag, Stuttgart-New York, 365.
19. D.L. Pavia, G.M. Lampman and G.S. Kriz, *Introduction to Spectroscopy,* **2001**, *3rd Edition*, Harcourt College Publishers, 398.
20. A.J. Arduengo (III), R. Krafczyk, R. Schmutzler, J.R. Goerlich, W.J. Marshall and M. Unverzagt, *Tetrahedron*, **1999**, *55*, 14523.
21. M. Sato and S. Ebine, *Synthesis*, **1981**, 472.
22. N. Montserrat, A.W. Parkins and A.R. Tomkins, *J. Res., Synop.,* **1995**, 336.
23. H.D. Maynard, S.Y. Okada and R.H. Grubbs, *Macromolecules*, **2000***,* *33*, 6239.

Pectora roborant cultus recti

Chapter 3: Metal-α-diimine and two carbonyl complexes

Introduction

Until the mid 1990's, as mentioned in Chapter 1, it was assumed that middle to late transition metal α-diimine ligand complexes were not suitable as effective pre-catalysis for lower olefin polymerisation. Catalysts of this kind yielded polyolefins of low molar mass and with broad polydispersities. This assumption was proved incorrect in the late 1990's by Brookhart and co-workers[1-3] and Gibson and co-workers[4] when sterically hindered substituents were incorporated on the α-diimine ligand backbone. These new catalysts yielded polyethylene, polypropylene and polymethylmethacralates of high molar mass and low polydispersities.

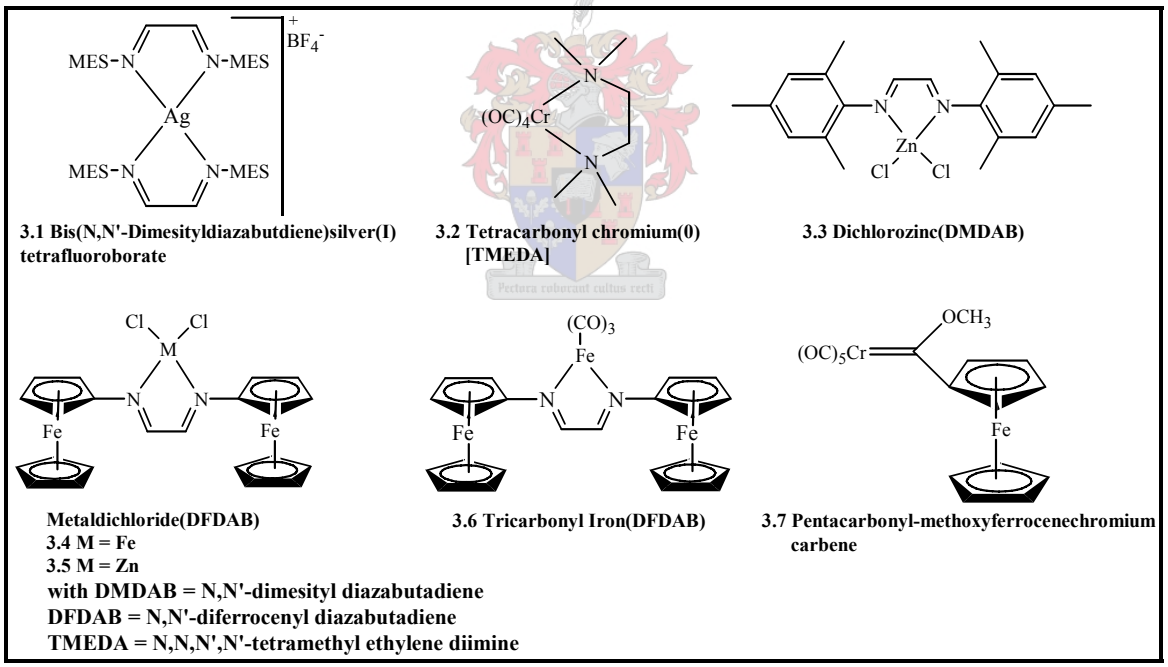

Fig. 3.1: Compounds discussed in Chapter 3

The aim of the present study was to coordinate α-diimine ligands (such as N,N'-diferrocenyl diazabutadiene, N,N'-dimesityl diazabutadiene and N,N,N',N'-tetramethyl ethylene diimine) to middle and late transition metals (Ag, Cr, Fe and Zn) and where possible, study them as potential pre-catalysts. While having prepared the appropriate

ligands, it was also planned to include complexes of iron and chromium in low oxidation (carbonyl containing complexes) states. In this chapter a series of complexes are described (Fig. 3.1) and then, in Chapter 4, certain applications, especially catalytic activity towards the polymerisation of ethylene and in some cases 1-pentene is reported. The Fischer-type carbene complex [pentacarbonyl(methoxy)ferrocenylchromium(0) carbene) was prepared previously by Zora and co-workers[5], but this study did not include a crystal structure, thus the complex is discussed fully in this chapter in (Section 3.8).

3.1 Bis(dimesityldiazabutadiene)silver(I) tetrafluoroborate $[Ag(DMDAB)_2]^+(BF_4)^-$:

Bis(dimesityldiazabutadiene)silver(I) tetrafluoroborate was synthesised by stirring $AgBF_4$ and N,N'-dimesityldiazabutadiene for two hours in THF at room temperature. The red, microcrystalline material was collected after filtration. Equation 3.1.1 illustrates the reaction sequence.

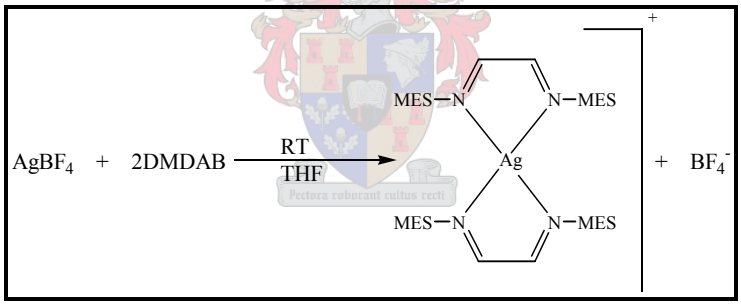

Equation 3.1.1

3.1.1 NMR Spectroscopy:

Comparing the ^1H and ^{13}C NMR spectrum of the free dimesityldiazabutadiene ligand to that of the coordinated dimesityldiazabutadiene ligand, one finds almost no change in chemical shifts. The Me[7,9] proton and carbon resonances are exactly the same (Table 2.1, Chapter 2) as that of the non-coordinated ligand. A very small chemical shift upfield is shown by the Me[8] proton and carbon atom group compared to the uncoordinated ligand. The imine proton and carbon atoms demonstrate a chemical shift downfield (to δ 6.79 and δ 20.8 for the proton and carbon atoms respectively) experienced upon coordination.

The C^2, C^3 and C^4 carbon atoms resonate downfield compared to the corresponding atoms of the uncoordinated ligand. The *ipso* carbon atoms display a chemical shift upfield.

Table 3.1.1: ^{1}H and ^{13}C NMR data of bis(DMDAB)Ag(I) tetrafluoroborate

Complex:	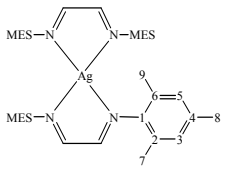
Solvent	Dichloromethane D-2
Temperature (K)	273
^{1}H NMR (300 MHz)	**δ**
$Me^{7,9}$	2.10 (s, 24H)
Me^8	2.28 (s, 12H)
$C^{3,5}$	6.79 (s, 8H)
-N=C-H	8.16 (s, 4H)
^{13}C NMR (75 MHz)	**δ**
$Me^{7,9}$	18.0
Me^8	20.8
$C^{2,6}$	127.7
$C^{3,5}$	129.8
C^4	137.1
Ipso C	146.3
-N=C-	159.8

3.1.2 Molecular Structure:

The red, microcrystalline material was dissolved in toluene and layered with *n*-pentane and slowly cooled to 0°C. After a week small single crystals suitable for single X-ray analysis were obtained. A red, prism-shaped crystal was mounted on a glass fibre and transferred to a Bruker Smart Apex[6] X-Ray diffractometer. The crystals were radiated with a monochromatic Mo-Kα X-ray source at a wavelength of 0.71073Å and the data were corrected for Lorentz- and polarisation effects. The position of the heaviest atom (silver) was determined using direct methods and anisotropic displacement parameters for al the atoms were achieved. The hydrogen atoms are placed in calculated positions. Structure determination and refinement of the atom coordinates were accomplished using the SHELX-97[7] and X-Seed[8] software. The Experimental data and crystallographic data are reported in Table 3.1.2.

Table 3.1.2: Experimental and crystallographic data of bis(DMDAB)Ag(I)BF_4

Empirical formula	$C_{40}H_{48}N_4AgBF_4$
Formula weight	779.50
Colour	Deep Red
Crystal system	Orthorhombic
Space group	P*bcn*
Unit cell dimensions	a = 15.5436(16) α = 90.00
	b = 16.7347(18) β = 90.00
	c = 14.0779(16) γ = 90.00
Z	4
V (Å^3)	3661.9(7)
Density (g/cm^3)	1.414
Radiation (Mo-Kα) [Å]	0.71073
$2\theta_{max}$	56.6°
Monochromator	Graphite
Absorption coefficient (μ) [mm^{-1}]	0.605
Temperature (K)	100(2)
F (000)	1616
Diffractometer	Bruker Smart Apex®
Scan range (θ)	
hkl ranges	$-20 \leq h \leq 17$
	$-21 \leq k \leq 22$
	$-15 \leq l \leq 18$
Reflections measured	21585
Unique reflections used	4366
Number of parameters refined	233
Deepest hole	2.30
Highest peak	28.30
R_{int} (%)	14.74
R1 (%)	8.10
Goodness of fit (GooF)	1.029

Pectora roborant cultus recti

The molecular structure of the bis(dimesityldiazabutadiene)silver(I) tetrafluoroborate complex, as well as the numbering of relevant atoms are shown in Figure 3.1.1. Selected bond lengths and angles are given in Table 3.1.3 and 3.1.4 respectively. The silver(I) source, $AgBF_4$, lacks a robust coordination shell and readily interacts with the N-donor ligands. In this complex, the silver(I) metal exhibits a square planar arrangement, somewhat disordered towards a *pseudo*-tetrahedral configuration. The only comparable complex to the Ag(I) dimesityldiazabutadiene complex in the literature is a Cu(I) analogue.[9] The Cu complex displays a planar twist around the Cu-atom. The authors ascribe this to the formation of π-π interactions between the mesityl groups on adjacent ligands, probably during packing in the crystal. Planar twist in the Ag-complex does occur, but to a much lesser degree than in the Cu-compound.

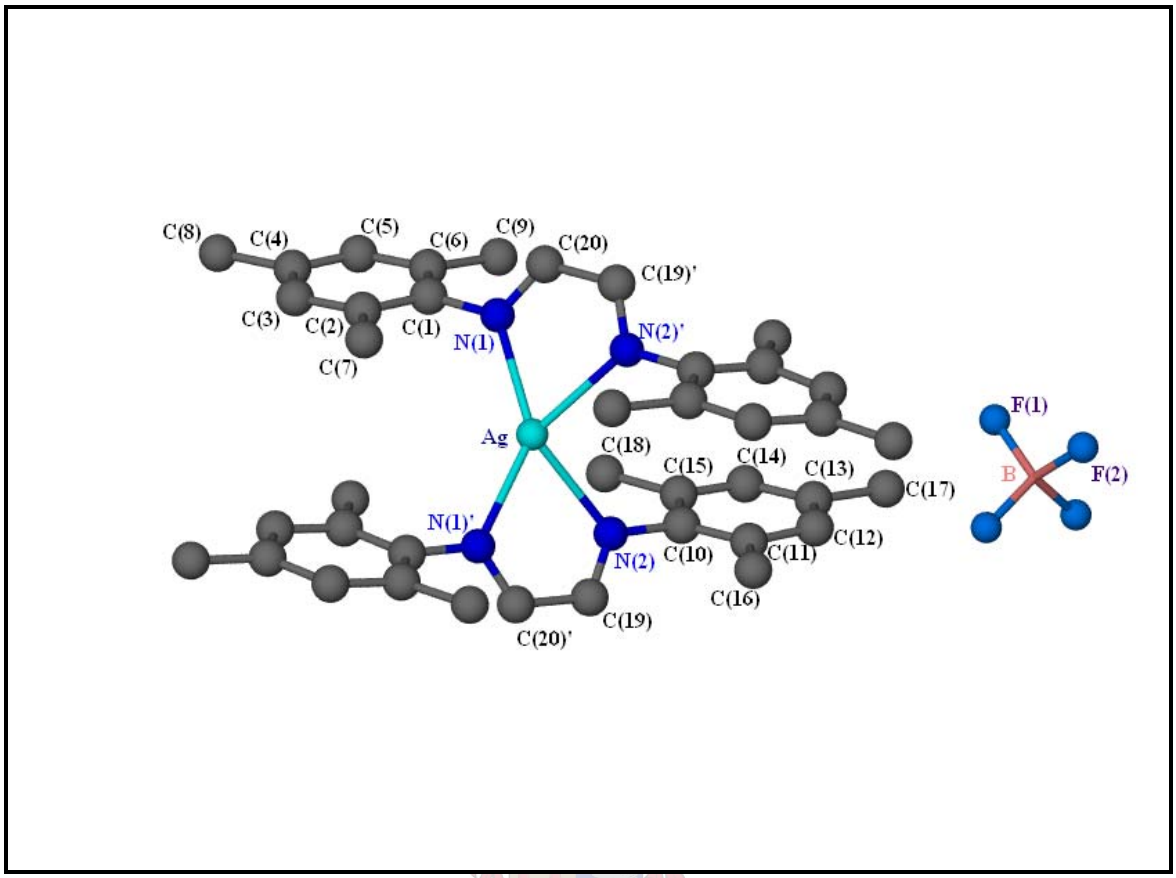

Fig. 3.1.1: Molecular structure of bis(DMDAB)silver(I) tetrafluoroborate

The slightly longer bond distance between the Ag-atom and the four N-atoms compared to that of Cu (2.384 Å vs. 2.020 Å) could explain the smaller degree of twist in the Ag structure. The complex adopts an orthorhombic crystal system with a dihedral angle of 56.6° between the planes formed by the two ligand molecules.

The Ag-N bond lengths, especially Ag-N(1) and Ag-N(2), differ remarkably in the solid state, a fact not reflected in the NMR data of the dissolved complex. This is due to the steric interaction of the two adjacent mesityl ligands. The bond lengths in the coordinated dimesityldiazabutadiene ligand and the free dimesityldiazabutadiene ligand (Chapter 2, Fig. 2.2, and Table 2.3) do not differ significantly. The bond lengths between the boron and fluorine atoms are consistent with published values.[10]

Table 3.1.3: Bond lengths of bis(DMDAB)Ag(I)BF_4

Bond Lengths (Å)					
Ag-N(1)	2.301(4)	C(3)-C(4)	1.385(8)	C(12)-C(13)	1.393(7)
Ag-N(2)	2.384(4)	C(4)-C(5)	1.378(8)	C(13)-C(14)	1.385(7)
N(2)-C(19)	1.265(6)	C(4)-C(8)	1.512(8)	C(13)-C(17)	1.510(7)
N(1)-C(1)	1.433(6)	C(5)-C(6)	1.395(7)	C(14)-C(15)	1.392(7)
N(1)-C(20)	1.270(7)	C(6)-C(9)	1.513(7)	C(15)-C(18)	1.514(7)
C(1)-C(2)	1.403(7)	C(10)-C(15)	1.390(7)	C(19)-C(20)	1.489(7)
C(1)-C(6)	1.405(7)	C(10)-C(11)	1.398(7)	B-F(1)	1.383(6)
C(2)-C(3)	1.395(7)	C(11)-C(12)	1.396(8)	B-F(2)	1.389(6)
C(2)-C(7)	1.506(7)	C(11)-C(16)	1.509(8)		

The bond angles of the coordinated dimesityldiazabutadiene ligand compared to the free dimesityldiazabutadiene ligand (Fig. 2.1 and Table 2.3 in Chapter 2) are almost identical, with one exception. The mesityl group bonded to N(1)' in Fig. 2.2 (Chapter 2) twists by 180° to allow coordination to the Ag atom (Fig. 3.1.1) with a retention of bond angle between C(20)-C(19)'-N(2)'. The coordinated ligand of the Ag-complex has similar bond angles and bond lengths to those of the Cu-complex ligand with the exception of the N-M-N angles. The Ag-complex has much smaller N-M-N angles compared to the same angles in the Cu-complex [the inner N-M-N angles (71.65° *vs*. 82.30°), outer N-M-N angles (98.50° and 139.94° *vs*. 108.29° and 145.46°) and the cross angles (139.94° *vs*. 145.46°)]. These differences are due to the larger atomic radius of the Ag-atom compared to that of Cu.

Table 3.1.4: Bond angles of bis(DMDAB)Ag(I)BF_4

Bond Angles (in degrees)					
C(1)-N(1)-C(20)	119.7(5)	C(19)-N(2)-Ag	113.3(4)	N(2)-C(19)-C(20)'	119.0(5)
C(1)-N(1)-Ag	124.9(3)	C(19)-C(20)'-N(1)'	120.2(5)	N(2)-Ag-N(2)'	98.5(2)
C(2)-C(1)-N(1)	117.5(5)	C(20)-N(1)- Ag	115.4(4)	C(20)'-N(1)'-Ag	115.4(4)
C(6)-C(1)-N(1)	120.7(5)	N(1)-C(20)-C(19)'	120.2(5)	F(1)-B-F(1)'	110.2(7)
C(10)-N(2)-C(19)	120.3(5)	N(1)-Ag-N(1)'	139.6(2)	F(1)-B-F(2)	109.8(2)
C(10)-N(2)-Ag	126.0(3)	N(1)-Ag-N(2)	139.9(2)	F(1)-B-F(2)'	108.8(2)
C(11)-C(10)-N(2)	121.6(5)	N(1)-Ag-N(2)'	71.7(2)	F(2)-B-F(1)'	108.8(2)
C(14)-C(15)-C(18)	120.8(5)	N(1)'-Ag-N(2)'	139.9(2)	F(2)-B-F(2)'	109.4(6)
C(15)-C(10)-N(2)	116.4(5)	N(1)'-Ag-N(2)	71.7(2)	F(1)'-B-F(2)'	109.8(2)

In comparison with the silver(I) complex described by Patra and co-workers[11], the angle between the two nitrogen atoms of the bidentate ligand at the silver atom is of similar magnitude. The dihedral angle between the two planes formed by the N(1)-C(19)-C(20)'-

N(1)'-Ag and N(2)-C(19)-C(20)'-N(1)'-Ag atoms using the Mean Plane (MPLA) function of the SHELX program is 54.2° (0.1). This is much smaller than the 89° of the comparable Cu-complex with the result that the two ligand molecules coordinated to the Ag are more in a parallel arrangement to each other than those of the Cu-analogue.

The crystal packing for the bis(dimesityldiazabutadiene)silver(I) tetrafluoroborate complex is illustrated in Figure 3.1.2. The mesitylene rings do overlap in the packing, but distances between overlapping centroids (7.04 Å) are too great for π-stacking to be of any significance. Hydrogen bonds are absent from the packing structure, thus the system is held together by Van Der Waals interactions. There are Van Der Waals interactions between C(20) and F(2) and C(19) and F(1) with Van Der Waals distances of 2.543 and 2.581 Å respectively. Packing proceeds in a zigzag pattern along the *a*-axis and a roof tile-like packing along the c-axis. The main interactions occur between the cationic H(20) and the anionic F(2) atoms with a Van Der Waals length of 2.54 Å and the cationic H(19) and anionic F(1) atoms with a Van Der Waals length of 2.58 Å.

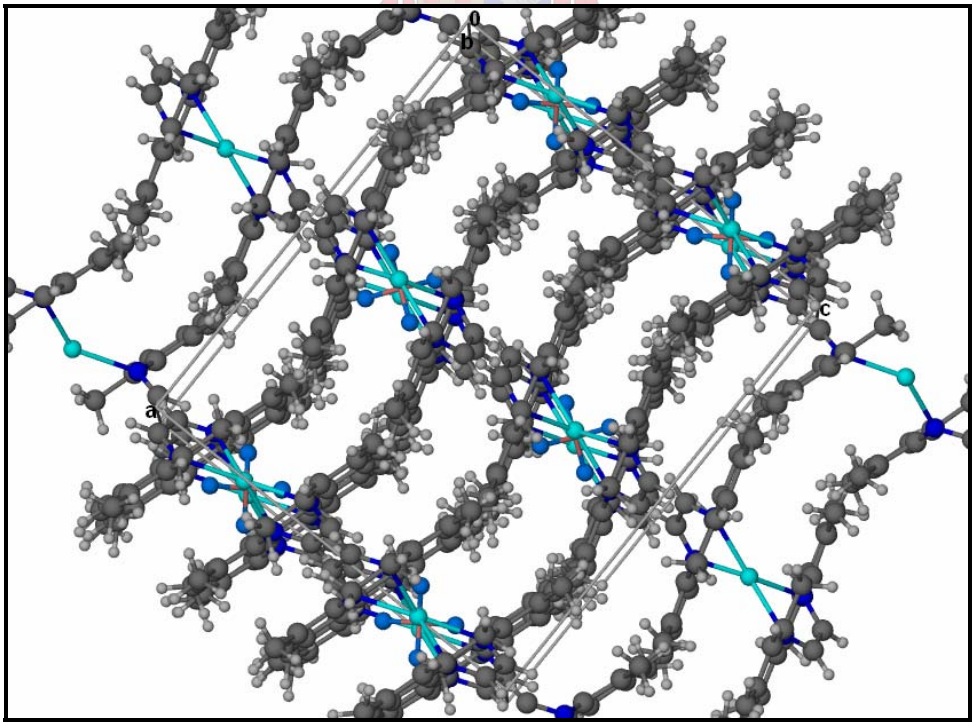

Fig. 3.1.2: Crystal packing of bis(DMDAB)silver(I) tetrafluoroborate along the *a*-axis

3.1.3 Infrared spectroscopy:

The infrared stretching frequencies for the Bis(dimesityldiazabutadiene)silver(I) tetrafluoroborate complex are reported in Table 3.1.5 and are consistent with published data[12] for similar fragments occurring elsewhere.

Table 3.1.5: The infrared stretching frequencies for bis(DMDAB)Ag(I)BF_4

Moiety	Aryl-H	Aliphatic C-H	-N=C-	C=C
$\nu(cm^{-1})$	3000 (*w*)	2916 (*s*)	1618 (*s*)	1477 (*m*)
$\nu(cm^{-1})_{theoretical}$[12]	3100-3000	2960-2850	1660-1480	≈ 1500

3.1.4 Mass Spectrometry:

The MALDI-TOF Mass Spectrum data are collected in Table 3.1.6. The most abundant ion that forms in the ionization chamber corresponds with the ligand (dimesityl-diazabutadiene) peak and thus formed the base peak. The molecular mass of the cation corresponds with the peak at *m/z* 693. One of the ligand molecules is lost from the cationic molecule to yield a ligand-metal peak at *m/z* 401 and a ligand peak at *m/z* 292. The ligand-metal fragment then subsequently fragments into the ligand and silver fragments. The fragmentation pattern of the coordinated dimesityldiazabutadiene ligand is similar to that of the free ligand (compare Scheme 2.2 for the fragmentation of aniline).

Table 3.1.6: MALDI-TOF Mass Spectra data for bis(DMDAB)Ag(I)BF_4

Fragment-ion	***m/z (I%)***	**Fragment-ion**	***m/z (I%)***
$[M]^+$	693 (49)	$[L - 2CH_3]^+$	262 (53)
$[M - L_1]^+$	401 (58)	$[L - 3CH_3]^+$	247 (20)
$[L]^+$	292 (100)	$[Ag]^+$	108 (76)
$[L - CH_3]^+$	277 (54)		

3.2 Tetracarbonylchromium(0)(N,N,N',N'-tetramethylethylenediamine):

The $(CO)_4Cr(TMEDA)$ complex has previously been synthesised by Kruger and co-workers.[13] Its use as a catalyst for the polymerisation of olefins has not been investigated. Thus, when it unexpectedly formed in the attempted synthesis of bis[pentacarbonyl(methoxy)methylchromium(0)carbene]bis(benzene)chromium it was included in the study. Since the crystals were satisfactory, an X-ray diffraction study was also undertaken. Except for the zirconocene-chromium carbene complexes[14], chromium metal complexes are not well known for catalytic ability in the polymerisation of lower olefin monomers. Possible reasons for this could be the difficult synthesis of most chromium complexes due to their sensitivity towards air and moisture. Low temperature column chromatography under inert conditions makes purification a relatively complicated process. The dreaded green colour of the oxidized chromium(III) always looms in the background in every low oxidation state chromium complex synthesis.

Traditionally the metal centre in olefin polymerisation catalysts is of a cationic oxidation state caused by the presence of an anionic leaving group (e.g. halogen atoms). This poses a conundrum for the cationic polymerisation process. The zero oxidation state of the metal combined with the loss of neutral carbonyl groups upon the activation with MAO implies that a pseudo-cationic mechanism has to prevail during the polymerisation process.

The complex was initially obtained as a by-product during the attempted synthesis of a bis-carbene complex connected to bis(benzene)chromium. We discovered that the same product forms readily when $Cr(CO)_6$ is treated simultaneously with BuLi and TMEDA. Initially BuLi and TMEDA was employed for the double deprotonation of the bis(benzene)chromium, similar to the double deprotonation of ferrocene. This means that the anion carbene ligand in $[Cr(CO)_5{=}C(O)Bu]Li$ and one carbonyl group are substituted by the bidentate anion- a process certainly driven by the chelate effect. Equation 3.2.1 illustrates the process.

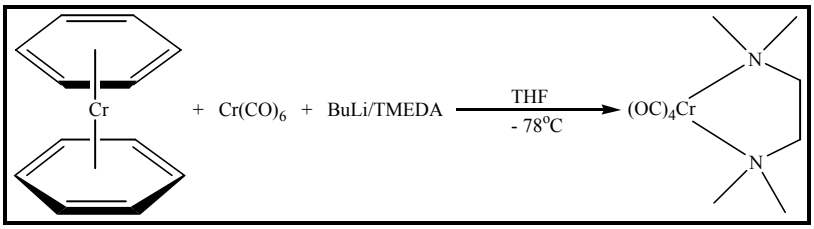

Equation 3.2.1

Although Cr(0) complexes are diamagnetic, the $Cr(CO)_4$[TMEDA] complex decomposed slowly to products that exhibited paramagnetic behaviour, thus the collection of a sharp ^{1}H NMR spectrum was not possible. This complex is also very sensitive towards the atmosphere and the MS spectrum gave inaccurate signals for $Cr(CO)_6$ and the free ligand.

3.2.1 Molecular Structure:

The purified $(CO)_4$Cr(TMEDA) was dissolved in a minimum of methylene chloride and layered with *n*-pentane. Single crystals suitable for single X-ray diffraction were collected after a few weeks. The data collection proceeded at low temperature (100K). A yellow, prism-shaped crystal was mounted on a glass fibre and transferred to a Bruker Smart Apex[6] X-Ray diffractometer. The crystals were radiated with a monochromatic Mo-Kα X-ray source at a wavelength of 0.71073Å and were corrected for Lorentz- and polarisation effects. The position of the heaviest atom (chromium) is determined using direct methods and anisotropic displacement parameters for al the atoms, excluding proton atoms.

The proton atoms were placed in calculated positions. Structure determination and refinement of the atom coordinates were accomplished using the SHELX-97[7] and X-Seed[8] software. Table 3.2.1 lists the experimental and crystal data for this complex. The molecular structure and numbering of relevant atoms of the tetracarbonyl Chromium(0)(N,N,N',N'-tetramethylethylenediamine) complex is illustrated in Figure 3.2.1.

Table 3.2.1: Experimental and crystal data for $(CO)_4$Cr(TMEDA)

Empirical formula	$C_{10}H_{16}N_2O_4Cr$
Formula weight	280.28
Colour	Yellow
Crystal system	Monoclinic
Space group	$P2_1/n$
Unit cell dimensions	a = 8.258(1) α = 90.00 b = 11.81(2) β = 91.866(3) c = 13.123(2) γ = 90.00
Z	2
V (Å^3)	1279.0(3)
Density (g/cm^3)	1.455
Radiation (Mo-Kα) [Å]	0.71073
$2\theta_{max}$	56.5°
Monochromator	Graphite
Absorption coefficient (μ) [mm^{-1}]	0.899
Temperature (K)	100(2)
F (000)	584
Diffractometer	Bruker Smart Apex®
Scan range (θ)	$-10 \leq h \leq 8$
hkl ranges	$-15 \leq k \leq 13$ $-17 \leq l \leq 17$
Reflections measured	7909
Unique reflections used	2933
Number of parameters refined	158
Deepest hole	2.32
Highest peak	28.24
R_{int} (%)	6.43
R1 (%)	6.20
Goodness of fit (GooF)	0.932

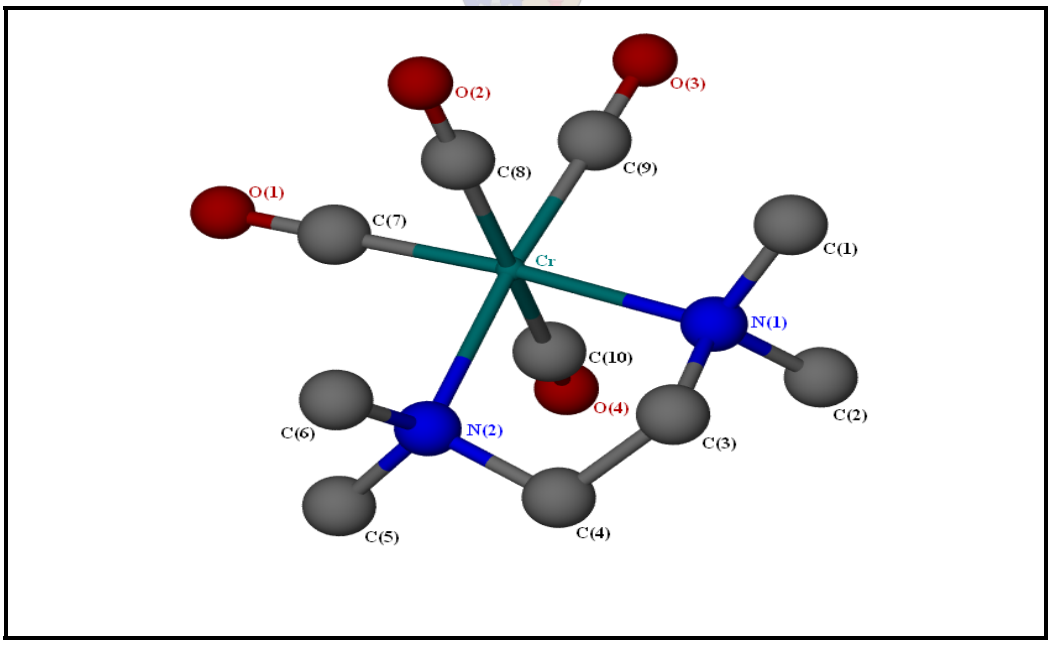

Fig. 3.2.1: The molecular structure of tetracarbonyl chromium(0)(TMEDA)

The chelate ligand coordinates to the metal in a bidentate fashion to form a five membered heterocyclic chelate. The chromium metal adopts a disordered octahedral coordination with the bidentate five membered chelate ring (tetramethylenediammine). The average single bond length between the carbon and nitrogen atoms of the chelate ring (1.483 and 1.493 Å) are slightly longer than that reported for sp^2 hybridised carbon and coordinated nitrogen atoms (1.452 Å).[13] The logical explanation for this is that the C-atoms are, therefore, sp^3 hybridised. The average bond lengths between the chromium metal and the carbonyl groups (1.829 to 1.904 Å), as well as the distances between the coordinated nitrogen atoms and the chromium metal (2.207 and 2.215 Å) are comparable with that of published values (1.820 and 2.199 Å respectively).[15] The distance between C(3) and C(4) are consistent with that for C_{sp3}-C_{sp3}. The retention of this value causes the chelated ring to undergo distortion. The dihedral angle at C(3) [the dihedral angle between the two planes N(2)-C(4)-C(3) and C(3)-N(2)-Cr] of approximately 40° is evidence for this effect. The respective bond lengths of this complex are reported in Table 3.2.2.

Table 3.2.2: Bond lengths for $(CO)_4Cr(TMEDA)$

Bond Lengths (Å)					
C(1)-N(1)	1.484(4)	C(6)-N(2)	1.478(4)	C(9)-O(3)	1.157(4)
C(2)-N(1)	1.492(4)	C(7)-Cr	1.829(3)	C(10)-Cr	1.904(4)
C(3)-N(1)	1.483(4)	C(7)-O(1)	1.164(4)	C(10)-O(4)	1.147(4)
C(3)-C(4)	1.510(5)	C(8)-Cr	1.891(4)	N(1)-Cr	2.215(3)
C(4)-N(2)	1.493(4)	C(8)-O(2)	1.157(4)	N(2)-Cr	2.207(3)
C(5)-N(2)	1.478(4)	C(9)-Cr	1.842(4)		

The carbonyl groups situated in an axial orientation to the TMEDA and two equatorial carbonyls [C(8) and C(10)], are bent away from the bidentate ligand. This creates a C(8)-Cr-C(10) angle of 167.63°. The coordination within the five membered chelate ring is the explanation for this phenomenon. The angle of 81.1° between the two nitrogen atoms at the chromium metal is consistent with that of other -N-M-N- chelated complexes in literature.[9] The same chelating effect results in an enlarged angle between the equatorial carbonyl groups and the nitrogen atoms at the chromium metal (93.4 and 94.3° respectively). The angle between the two equatorial carbonyl groups are virtually unaffected by the chelating effect. The respective bond angles are reported in Table 3.2.3.

Table 3.2.3: Bond angles for $(CO)_4Cr(TMEDA)$

Bond Angles (in degrees)					
C(1)-N(1)-C(2)	106.6(3)	C(5)-N(2)-C(6)	106.6(3)	C(8)-Cr-C(10)	167.6(1)
C(1)-N(1)-C(3)	108.5(3)	C(5)-N(2)-Cr	113.3(2)	C(9)-Cr-N(1)	94.3(1)
C(1)-N(1)-Cr	113.6(2)	C(6)-N(2)-Cr	112.8(2)	C(9)-Cr-N(2)	175.3(1)
C(2)-N(1)-C(3)	109.2(3)	C(7)-Cr-N(1)	174.5(1)	C(9)-Cr-C(10)	85.5(2)
C(2)-N(1)-Cr	112.1(2)	C(7)-Cr-N(2)	93.4(1)	C(10)-Cr-N(1)	95.5(1)
C(3)-N(1)-Cr	106.9(2)	C(7)-Cr-C(8)	86.2(1)	C(10)-Cr-N(2)	93.7(1)
C(3)-C(4)-N(2)	110.2(3)	C(7)-Cr-C(9)	91.2(2)	O(1)-C(7)-Cr	179.4(3)
C(4)-C(3)-N(1)	110.3(3)	C(7)-Cr-C(10)	85.4(1)	O(2)-C(8)-Cr	171.1(3)
C(4)-N(2)-C(5)	108.0(3)	C(8)-Cr-N(1)	93.8(1)	O(3)-C(9)-Cr	178.6(3)
C(4)-N(2)-C(6)	109.6(3)	C(8)-Cr-N(2)	95.9(1)	O(4)-C(10)-Cr	171.3(3)
C(4)-N(2)-Cr	106.4(2)	C(8)-Cr-C(9)	85.7(2)	N(1)-Cr-N(2)	81.1(1)

The crystal packing of the $Cr(CO)_4$[TMEDA] complex is illustrated in Figure 3.2.2. The molecules are packed in columns along the *b*-axis with a plane of inversion running in the *ab*-plane. Hydrogen bonds between the atoms O(1)···H(51)···C(5) (with a distance of 3.303 Å), O(1)···H(42)···C(4) (with a distance of 3.343 Å) and O(2)···H(32)···C(3) (with a distance of 3.686 Å) contribute to the stable packing of the crystal structure.

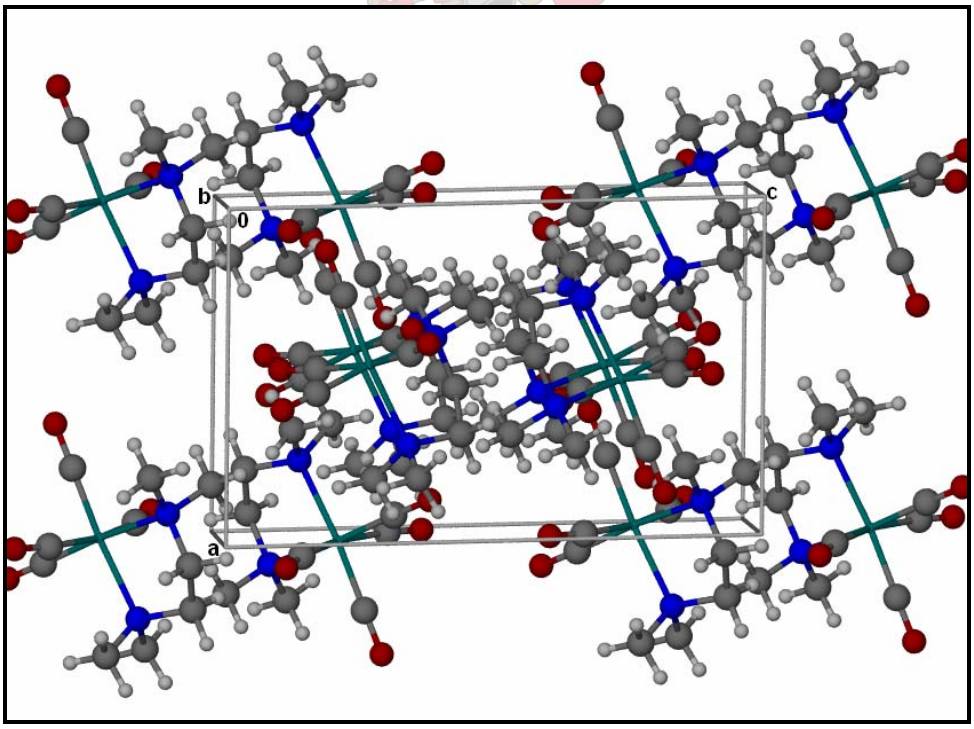

Fig. 3.2.2: Crystal packing of $Cr(CO)_4$[TMEDA] along the *b*-axis

3.2.2 Infrared Spectroscopy:

The stretching frequencies for the carbonyl groups for this complex are reported in Table 3.2.4. These stretching frequencies are characteristic of complexes with C_{4v} symmetry operators.

Table 3.2.4: Stretching frequencies for the carbonyl groups for $(CO)_4Cr(TMEDA)$

CO	$A_1^{(1)}$	$A_1^{(2)}$	B_1	B_2
ν [cm^{-1}]	2030.5 (*s*)	1954.4 (*w*)	1885.8 (*w*)	1841.1 (*w*)

3.3 Dichloro[N,N'-diferrocenyldiazabutadiene]iron(II):

Metal-α-diimine complexes can be treated with compounds such as methyl aluminoxane (MAO) or similar compounds to yield highly active catalysts for the polymerisation of ethylene into polyethylene (HDPE, LLDPE or LDPE) or α-olefins with a Schulz-Flory distribution.[16] As mentioned in Chapter 1, the substituents as well as their position on the diazabutadiene backbone plays a crucial role on the activity of the catalyst. By varying the number, position and type of substituents on this backbone, one can manipulate the density, molar mass and polydispersity of the polymer product. Ultimately, the chain-transfer rate can be manipulated by varying the steric hindrance of the substituents. Brookhart and co-workers[1-3] as well as Gibson and co-workers[4] have shown that chain-transfer rate is disfavored by steric hindrance in the axial positions of the propagating iron-alkyl species, in particular the *Ortho*-substituents on the arylimino rings. Bianchini and co-workers[17] have indicated that the simultaneous formation of both polyethylene and α-olefins with a Schulz-Flory distribution using a single catalyst pre-cursor in the same reaction is possible by the use of C_1-symmetric [2,6-bis(arylimino)-pyridyl]iron dichloride complexes. In their efforts, they proved that C_s-symmetric complexes of low steric hindrance (no substituents on the aryl rings) oligomerise ethylene.

In the past, most iron-based catalysts for polymerisation of ethylene proved to yield polymers of high polydispersity and low molar mass. As will be mentioned in Chapter 4, the iron catalyst discussed in this section yielded high density polyethylene (HDPE) in contrast to related results in literature.

Iron(II)[diferrocenyldiazabutadiene]dichloride was synthesised by stirring anhydrous $FeCl_2$ in THF with N,N'-diferrocenyldiazabutadiene for two hours during which time the product precipitated from solution as it was formed. Diethyl ether was added to precipitate the remainder of product left in solution. A dark green microcrystalline material was collected after filtration and washed with ether to remove all unreacted ligand. The reaction sequence is illustrated in Equation 3.3.1.

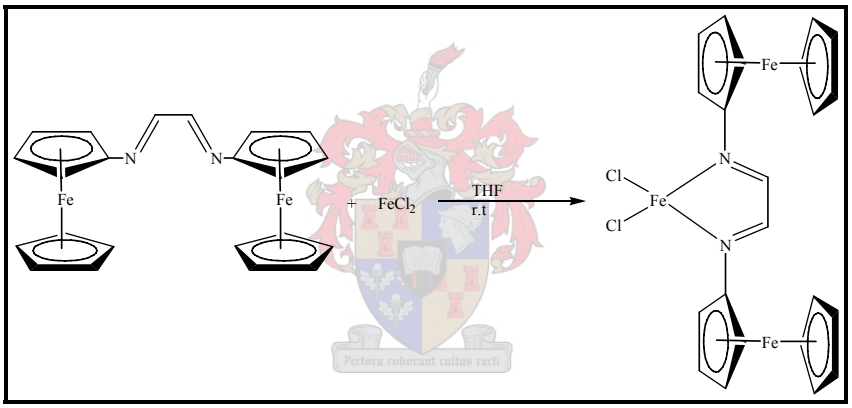

Equation 3.3.1

3.3.1 NMR Spectroscopy:

^{1}H and ^{13}C NMR data was collected on a 600 MHz NMR spectrophotometer due to the low solubility of this complex; for this reason also, single crystals suitable for a crystal structure determination could not be grown.

The resonance signals of the proton and carbon atoms of the coordinated ligand remain largely unchanged compared to the uncoordinated ligand. Carbon atom C^1 did undergo a chemical shift downfield compared to the same carbon atom on the uncoordinated ligand,

and the sharp signal at δ 109.8 was assigned to it. The ^{1}H and ^{13}C NMR data are reported in Table 3.3.1.

Table 3.3.1: ^{1}H and ^{13}C NMR data for iron(II)[diferrocenyldiazabutadiene]dichloride

Complex:	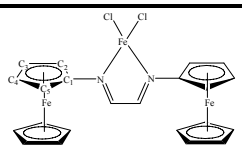
Solvent	Dichloromethane-D2
Temperature (K)	273
^{1}H NMR (600 MHz)	**δ**
$H^{2,5}$	4.70(s, 4H)
$H^{3,4}$	4.38 (s, 4H)
Cp	4.18 (s, 10H)
-N=C-	8.33 (s, 2H)
^{13}C NMR (150 MHz)	**δ**
C^{1}	109.8
$C^{2,5}$	65.8
$C^{3,4}$	69.6
Cp	71.5
-N=C-	155.6

3.3.2 Mass Spectrometry:

The two isotopes for chlorine at *m/z* 35 and *m/z* 37 were observed, but at very low intensities. The complex fragments into the metaldichloride and ligand fragments. The fragmentation of the ligand proceeds in its usual manner. The Electron Impact MS data for this complex are represented in Table 3.3.2.

Table 3.3.2: Electron Impact MS data for $Fe[(C_{10}H_9Fe)_2]Cl_2$

Fragment-ion	***m/z (I%)***	**Fragment-ion**	***m/z (I%)***
$[M]^+$	550 (1.0)	$[Fc - Cp]^+$	121 (14)
$[L]^+$	424 (24)	$[Fe]^+$	56 (8)
$[L – FeCp]^+$	304 (7)	$[Cl]^+$	35 and 37
$[Fc]^+$	186 (12)	$[N_2]^+$	28 (100)

3.3.3 Infrared spectroscopy:

A sharp peak characteristic of -N=C- compounds was observed at 1623.5 cm^{-1}. This peak shifted from the 1633 cm^{-1} frequency encountered for the uncoordinated ligand.

3.4 Dichloro[N,N'-diferrocenyldiazabutadiene]zinc(II):

Nickel(II)- α-diimine complexes have been synthesised by Evans and co-workers[18] and their activity towards the polymerisation of α-olefins investigated. Their aim was to synthesise a compound which would be able to polymerise olefinic monomers upon activation by a natural Lewis acid such as MAO or MMAO. During this activation process a substituent such as a halogen, alkyl or hydride is abstracted from the metal complex to form a cation. Evans and co-workers coordinated a vast number of different α-diimine ligands to mainly nickel(II) and palladium(II). In their communication, the activity of the dimesityl-diazabutadiene-metal complexes is not mentioned.

Dichlorozinc(II)[diferrocenyldiazabutadiene] was synthesised by stirring a suspension of $ZnCl_2$(anhydrous) and ligand (N,N'-diferrocenyldiazabutadiene) in THF for two hours during which time the product slowly precipitated from solution (Equation 3.4.1). Diethyl ether was added to precipitate the rest of the product. An olive green, microcrystalline material was collected after filtration and washed with ether to remove all unreacted ligand.

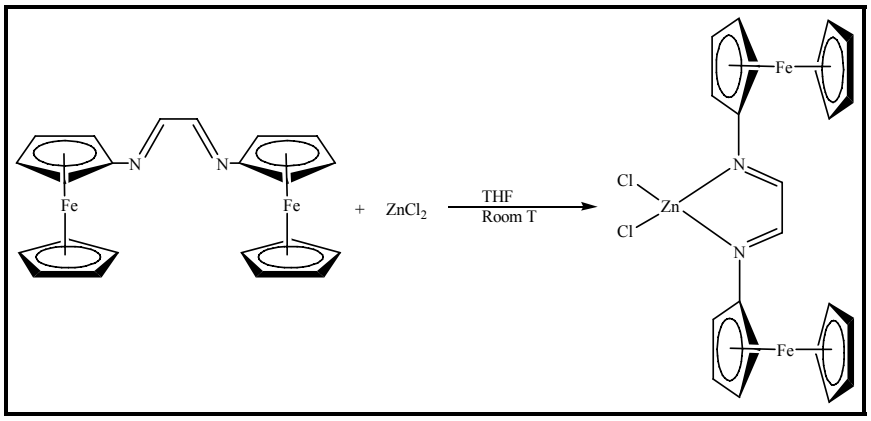

Equation 3.4.1

3.4.1 ^{1}H NMR spectroscopy:

Due to the extremely low solubility of this complex, only ^{1}H NMR data could be collected.

Table 3.4.1: ^{1}H NMR data for $Zn[(C_{10}H_9Fe)_2]Cl_2$

Complex:	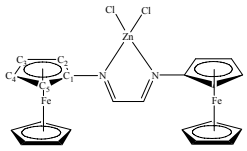
Solvent **Temperature (K)** **^{1}H NMR (300 MHz)** $H^{2,5}$ $H^{3,4}$ Cp -N=C-	Acetonitrile-D3 273 δ 5.02 (s, 4H) 4.81 (s, 4H) 4.44 (s, 10H) 8.41 (s, 2H)

A loss of electron density on the diferrocenyldiazabutadiene moiety occurs upon coordination. Deshielding of the proton atoms results in a downfield shift compared to the resonance of the free ligand. Even the unsubstituted cyclopentadienyl fragment indicates a larger electron loss. The ^{1}H and ^{13}C NMR data is represented in Table 3.4.1.

3.4.2 Mass Spectrometry:

The Electron Impact MS data for this complex are reported in Table 3.4.2. The molecular ion appears at *m/z* 560. The ferrocene fragment forms the base peaks at *m/z* 186. The complex fragments into the metaldichloride and ligand fragments. Part of the fragmentation pattern observed for this compound corresponds to the pattern observed for the free ligand (Chapter 2, Section 2.4).

Table 3.4.2: Electron Impact MS data $Zn[(C_{10}H_9Fe)_2]Cl_2$

Fragment-ion	***m/z (I%)***	**Fragment-ion**	***m/z (I%)***
$[M]^+$	560 (1.0)	$[Fc - Cp]^+$	121 (100)
$[L]^+$	424 (44)	$[Zn]^+$	65 (7)
$[L – FeCp]^+$	304 (19)	$[Fe]^+$	56 (95)
$[Fc]^+$	186 (100)	$[N_2]^+$	28 (100)

3.4.3 Infrared spectroscopy:

A sharp peak, characteristic of -N=C- compounds was observed at 1655 cm^{-1}. This value have shifted compared to than that of the uncoordinated ligand (1633 cm^{-1}) as well as the iron analogue (1623.5 cm^{-1}).

3.5 Dichloro[N,N'-dimesityldiazabutadiene]zinc(II) [$ZnCl_2$(DMDAB)]:

Applications of diazabiaryl compounds have prompted major research in fields such as photochemistry[19], biochemistry[20], organic synthesis[21] and polymerisation[1-4,22] of monomers such as lower α-olefins, styrenes, methyl methacralates and many more. These compounds incorporate ligands such as bipyridines, diquinolines and compounds containing polypyridyl subunits.[23]

Zinc(II), although not normally a well known catalytically active metal, was, nevertheless, included in this study to find out whether it will exhibit any activity. Zinc(II)[dimesityldiazabutadiene]dichloride was synthesised by stirring a suspension of $ZnCl_2$(anhydrous) and the N,N'-dimesityl diazabutadiene ligand in diethyl ether for two hours. A bright orange, clear solution formed almost immediately and the product precipitated slowly from solution as it was formed. Adding additional diethyl ether precipitated the rest of the product and a bright orange, microcrystalline material was collected after filtration and dried under vacuum. The reaction is illustrated in Equation 3.5.1.

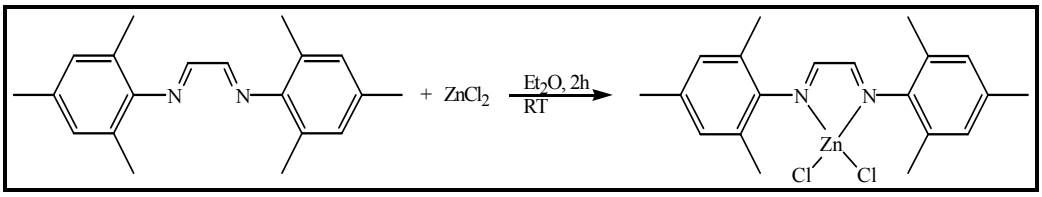

Equation 3.5.1

The zinc(II)[DMDAB] dichloride complex is virtually completely insoluble in most common solvents. The complex is somewhat soluble in chloroform; still, NMR data could not be collected.

3.5.1 Mass Spectrometry:

The MALDI-TOF MS data for this complex are reported in Table 3.5.1. The molecular ion peak formed at *m/z* 428. The complex is fragmented into the metaldichloride and ligand fragments that appeared at *m/z* 292 and *m/z* 136 respectively. The fragmentation pattern observed for the coordinated dimesityldiazabutadiene ligand is akin to that of the free ligand.

Table 3.5.1: MALDI-TOF MS data for $Zn(DMDAB)Cl_2$

Fragment-ion	***m/z (I%)***	**Fragment-ion**	***m/z (I%)***
$[M]^+$	428 (1)	$[ZnCl_2]^+$	136 (53)
$[M - ZnCl_2]^+$	292(97)	$[C_9H_{10}N_2 - CH_3]^+$	131 (42)
$[M - CH_3]^+$	277 (53)	$[C_7H_7N_2]^+$	119 (31)
$[M - 2CH_3]^+$	262 (20)	$[C_6H_5N]^+$	91 (32)
$[M - 3CH_3]^+$	247 (5)	$[C_5H_5]/[Zn]^+$	65 (5)
$[M - 4CH_3 - Ph]^+$	158 (61)	$[Cl]^+$	35 and 37
$[C_9H_{10}N_2]^+$	146 (57)	$[N_2]^+$	28 (100)

3.5.2 X-Ray diffraction:

Although, almost insoluble, the small amount of the $ZnCl_2$(DMDAB) product that did dissolve in chloroform, was transferred to a small Schlenk tube equipped with a bubbler to allow slow evaporation of the solvent. Single crystals suitable for crystallographic data collection formed after a couple of weeks. The refinement percentage for this complex is quite high (12.70%). The reason for this will be explained shortly.

An orange, needle-like crystal selected for the study and was mounted on a glass fibre and transferred to a Bruker Smart Apex[6] X-Ray diffractometer. The crystals were radiated with a monochromatic Mo-Kα X-ray source at a wavelength of 0.71073Å and were corrected for Lorentz-polarisation and absorption effects. The position of the heaviest atom (zinc) was determined using direct methods. Anisotropic displacement parameters for al the atoms were employed. Hydrogen atoms were placed in calculated positions. Structure determination and refinement of the atom coordinates were

accomplished using the SHELX-97[7] and X-Seed[8] software. The collection was done at 173K and Table 3.5.2 gives the conditions data and crystallographic data.

Table 3.5.2: Experimental conditions and crystallographic data for $Zn(DMDAB)Cl_2$

Empirical formula	$C_{40}H_{48}N_4Cl_4Zn_2$
Formula weight	587.36
Colour	Red
Crystal system	Monoclinic
Space group	$P2_1/c$
Unit cell dimensions	a = 16.653(2) α = 90.00 b = 13.975(1) β = 90.134(2) c = 17.271(2) γ = 90.00
Z	4
V (Å^3)	4019.4(7)
Density (g/cm^3)	1.417
Radiation (Mo-Kα) [Å]	0.71073
$2\theta_{max}$	56.5°
Monochromator	Graphite
Absorption coefficient (μ) [mm^{-1}]	1.493
Temperature (K)	100(2)
F (000)	1776
Diffractometer	Bruker Smart Apex®
Scan range (θ)	$-22 \leq h \leq 15$
hkl ranges	$-17 \leq k \leq 17$ $-21 \leq l \leq 19$
Reflections measured	24 559
Unique reflections used	9 080
Number of parameters refined	463
Deepest hole	2.32
Highest peak	28.24
R_{int} (%)	4.32
R1 (%)	12.70
Goodness of fit (GooF)	1.128

The crystal system is most likely monoclinic based on the $R_{int} = 0.043$ (*cf.* $R_{int} = 0.190$ for orthorhombic). The structure appears to have pseudo-symmetry namely a pseudo 2_1 screw axis parallel to [1 0 0] at (x, ¾, ½) relating the two molecules of the asymmetric unit to one another. However, the application of this symmetry produces an approximate overlap of molecules but not an exact overlap. This phenomenon resulted in the relatively high refinement value of 12.70%. The molecular structure of $ZnCl_2(DMDAB)$ is illustrated in Figure 3.5.1.

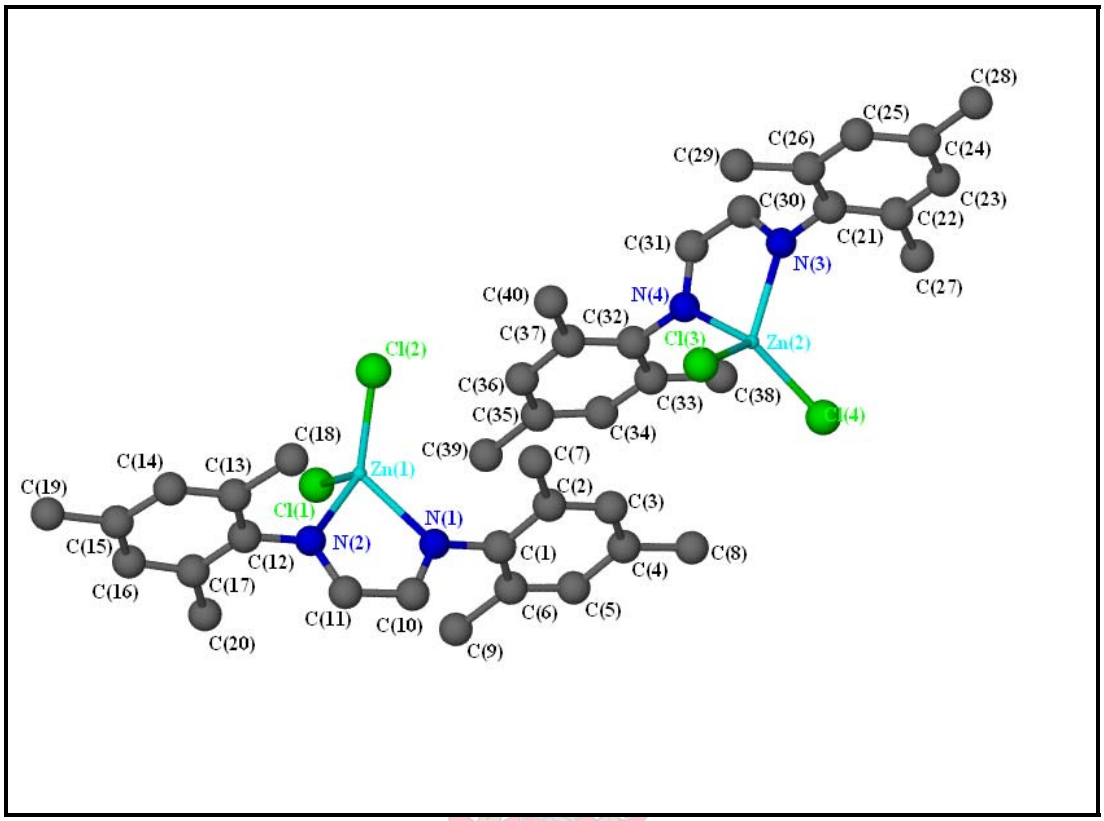

Fig. 3.5.1: Molecular structure of $ZnCl_2$(DMDAB)

The molecular structure of zinc(II)[dimesityldiazabutadiene]dichloride is reminiscent of the iron(II)[dimesityldiazabutadiene]dichloride compound published by Gibson and co-workers.[24] The bond distances from the zinc atom to the nitrogen and chloride atoms are consistent with published values (~ 2.09 Å for the Zn-N bond and ~2.2 Å for the Zn-Cl bond).[15] The bond distances within the mesityl moieties are also similar to these published values. The bond distances between the nitrogen atoms and that of the chelate carbon atoms are somewhat longer than the values reported by Gibson for the iron analogue [1.27(1) vs. 1.239(6)]. In turn, the distance between the chelate carbon atoms are somewhat shorter than that of the iron analogue [1.47(1) vs. 1.495(9)]. Table 3.5.3 contains selected bond lengths and Table 3.5.4 selected bond angles.

Table 3.5.3: Bond lengths for $Zn(DMDAB)Cl_2$

Bond Lengths (Å)					
C(1)-N(1)	1.45(1)	C(14)-C(15)	1.40(2)	C(26)-C(29)	1.49(1)
C(1)-C(2)	1.42(1)	C(15)-C(16)	1.38(2)	C(30)-N(3)	1.26(1)
C(1)-C(6)	1.40(1)	C(15)-C(19)	1.50(2)	C(30)-C(31)	1.47(1)
C(2)-C(3)	1.39(1)	C(16)-C(17)	1.41(1)	C(31)-N(4)	1.26(1)
C(2)-C(7)	1.51(1)	C(17)-C(20)	1.51(1)	C(32)-N(4)	1.44(1)
C(3)-C(4)	1.36(2)	N(1)-Zn(1)	2.091(7)	C(32)-C(33)	1.38(2)
C(4)-C(5)	1.41(1)	N(2)-Zn(1)	2.088(7)	C(32)-C(37)	1.42(1)
C(4)-C(8)	1.53(1)	Cl(1)-Zn(1)	2.219(3)	C(33)-C(34)	1.38(1)
C(5)-C(6)	1.39(1)	Cl(2)-Zn(1)	2.184(3)	C(33)-C(38)	1.52(2)
C(6)-C(9)	1.51(1)	C(21)-N(3)	1.44(1)	C(34)-C(35)	1.37(2)
C(10)-N(1)	1.27(1)	C(21)-C(22)	1.40(1)	C(35)-C(36)	1.39(2)
C(10)-C(11)	1.47(1)	C(21)-C(26)	1.40(1)	C(35)-C(39)	1.52(1)
C(11)-N(2)	1.27(1)	C(22)-C(23)	1.40(1)	C(36)-C(37)	1.40(1)
C(12)-N(2)	1.44(1)	C(22)-C(27)	1.51(2)	C(37)-C(40)	1.49(2)
C(12)-C(13)	1.39(2)	C(23)-C(24)	1.39(2)	N(3)-Zn(2)	2.087(7)
C(12)-C(17)	1.39(1)	C(24)-C(25)	1.40(1)	N(4)-Zn(2)	2.091(8)
C(13)-C(14)	1.40(1)	C(24)-C(28)	1.53(1)	Cl(3)-Zn(2)	2.201(3)
C(13)-C(18)	1.50(1)	C(25)-C(26)	1.40(1)	Cl(4)-Zn(3)	2.203(3)

The zinc atom is tetrahedrally surrounded by two nitrogen donor atoms and two chloride atoms and some distortion occurs. The bond angles at the zinc metals deviate from the theoretical value of 109.5°; this is true for both molecules within the unit cell. The angle between (N1)-Zn(1)-Cl(1) is the only bond angle to be close to 109° [108.9(2)°]. The acute angles at the bite of the chelate ligand [N(1)-Zn(1)-N(2) and N(3)-Zn(2)-N(4)] is somewhat larger than that reported by Gibson for the iron analogue[24] [79.9(3)° vs. 78.0(2)°] and contributes to the distortion of the tetrahedral angle. The larger metal centre could be responsible for the difference. The angles between the chloride atoms are smaller than in the iron analogue [114.2(1)° and 113.8(1)° vs. 120.1(1)°]. The angles formed within the mesityl phenyl rings are consistent with published values as well as with the bis(dimesityldiazabutadiene)silver(I) tetrafluoroborate complex. Figure 3.4.2 simplifies the description that follows. Molecule 1 contains Zn(1) and molecule 2 the Zn(2) metal centre.

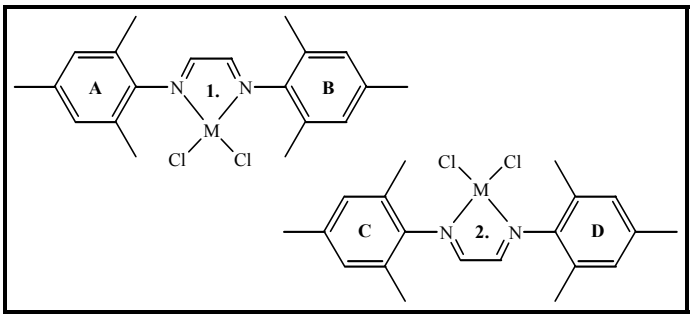

Fig. 3.4.2: Simplified diagram of $ZnCl_2$(DMDAB)

A certain degree of disorder within the chelate rings caused bending angles of 7.68(4)° for the molecule (1) ring and 3.42(5)° for molecule (2) ring.

Table 3.5.4: Bond angles for Zn(DMDAB)Cl_2

Bond Angles (in degrees)					
C(1)-N(1)-C(10)	118.9(8)	N(1)-Zn(1)-N(2)	79.9(3)	C(31)-C(30)-N(3)	120.0(8)
C(1)-N(1)-Zn(1)	129.4(4)	N(1)-Zn(1)-Cl(1)	108.9(2)	C(31)-N(4)-C(32)	118.9(4)
C(2)-C(1)-N(1)	117.5(8)	N(1)-Zn(1)-Cl(2)	121.5(2)	C(31)-N(4)-Zn(2)	112.1(6)
C(6)-C(1)-N(1)	120.1(7)	N(2)-Zn(1)-Cl(1)	106.7(2)	C(32)-N(4)-Zn(2)	129.0(6)
C(10)-N(1)-Zn(1)	110.8(6)	N(2)-Zn(1)-Cl(2)	121.1(2)	C(33)-C(32)-N(4)	117.6(8)
C(10)-C(11)-N(2)	117.5(8)	Cl(1)-Zn(1)-Cl(2)	113.8(1)	C(37)-C(32)-N(4)	118.1(9)
C(11)-C(10)-N(1)	119.4(8)	C(21)-N(3)-C(30)	119.0(8)	N(3)-Zn(2)-N(4)	79.9(3)
C(11)-N(2)-C(12)	119.9(8)	C(21)-N(3)-Zn(2)	130.1(6)	N(3)-Zn(2)-Cl(3)	112.5(2)
C(11)-N(2)-Zn(1)	111.8(6)	C(22)-C(21)-N(3)	118.1(9)	N(3)-Zn(2)-Cl(4)	117.7(2)
C(12)-N(2)-Zn(1)	128.1(6)	C(26)-C(21)-N(3)	118.7(8)	N(4)-Zn(2)-Cl(3)	110.8(2)
C(13)-C(12)-N(2)	117.8(8)	C(30)-N(3)-Zn(2)	110.5(6)	N(4)-Zn(2)-Cl(4)	117.3(2)
C(17)-C(12)-N(2)	119.6(9)	C(30)-C(31)-N(4)	117.4(8)	Cl(3)-Zn(2)-Cl(4)	114.2(1)

The mesityl rings of each molecule are not completely parallel to each other. A torsion angle of 7.97(1)° exists between Ring A and Ring B. This angle is somewhat larger between Ring C and Ring D with a value of 8.35(1)°. In molecule (1), the two chloride atoms are perfectly perpendicular to the chelate plane, but in molecule (2), this angle, although almost identical, is reduced somewhat to 89.16(5)°. The angle between the two planes is much smaller than the *ca.* 3° reported for the iron analogue. The conclusion that can be made from these statements is that the two molecules of the zinc compound are equivalent, but not identical.

Figure 3.5.3 illustrates the crystal packing of the [dimesityldiazabutadiene]zinc dichloride complex. The molecules are packed in inverse orientated columns along the *a*-axis. The centroid distance between the overlapping mesityl rings are too long [3.840(2) Å] for π-stacking to occur.

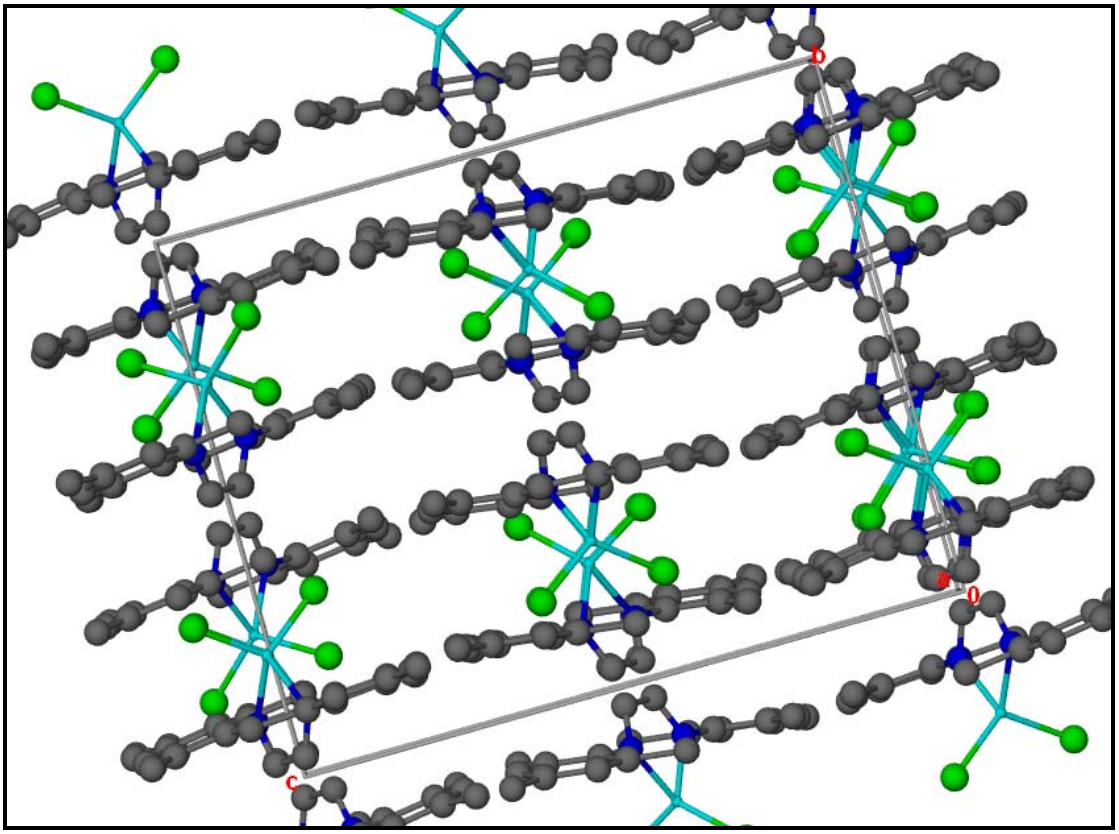

Fig. 3.5.3: Crystal packing of $ZnCl_2$(DMDAB) along the *c*-axis

The exact position of the hydrogen atoms could not be determined, so the atoms are placed theoretically. Hydrogen bonds between Cl(1)···H(101)···C(11) [3.510(2) Å], Cl(2)···H(101)···C(10) [3.679(2) Å], Cl(3)···H(311)···C(31) [3.679(2) Å] and Cl(4)···H(301)···C(30) [3.510(2) Å] contribute to the stable packing of the crystal structure. Figure 3.5.4 illustrates these hydrogen bonds and the manner in which the molecule is held together.

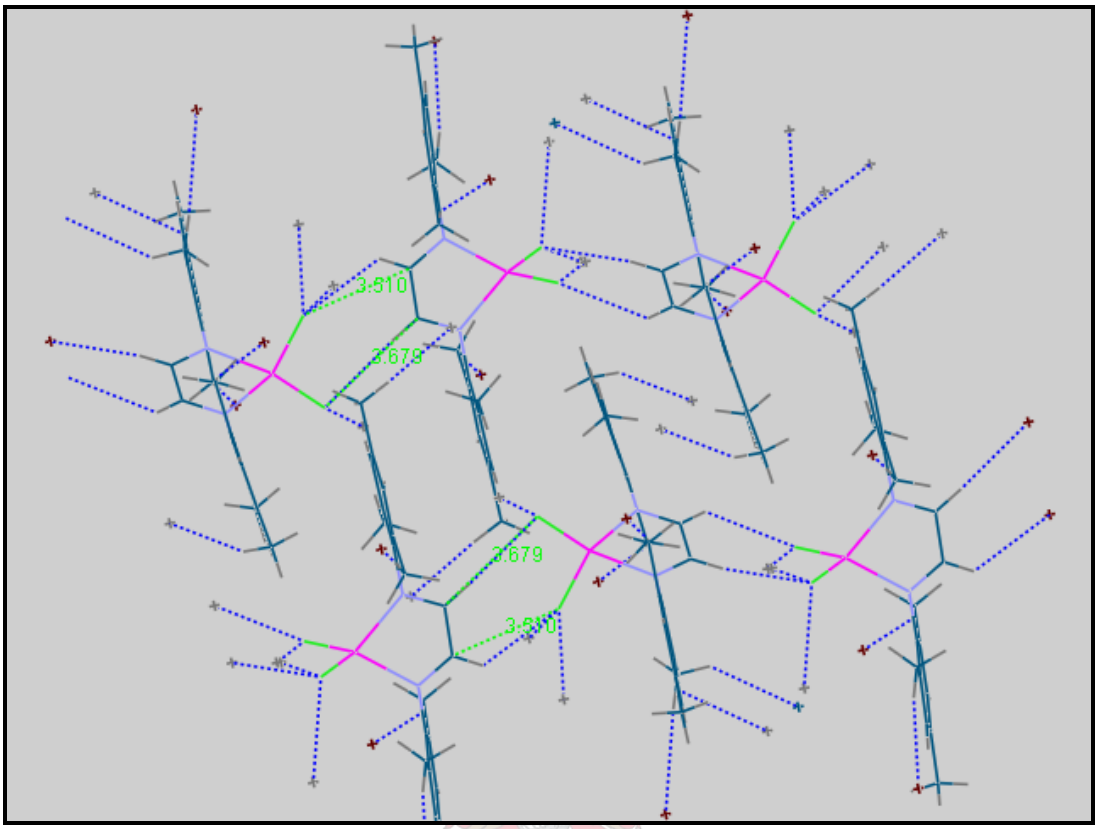

Fig. 3.5.4: Hydrogen bonds in $ZnCl_2$(DMDAB)

3.5.3 Infrared spectroscopy:

The infrared stretching frequencies for the zinc(II)[dimesityldiazabutadiene]dichloride complex are reported in Table 3.5.5 and are consistent with published data[12] for aryl-hydrogen bonds (broad) and aliphatic carbon-hydrogen bonds (sharp). A sharp peak, characteristic of -N=C- compounds was observed at 1646 cm^{-1} and a medium peak, characteristic of carbon-carbon double bonds at 1479 cm^{-1}.

Table 3.5.5: Infrared stretching frequencies for $Zn(DMDAB)Cl_2$

Moiety	Aryl-H	Aliphatic C-H	-N=C-	C=C
$\nu(cm^{-1})$	3028 (*w*)	2922 (*s*)	1646 (*s*)	1479 (*m*)
$\nu(cm^{-1})_{theoretical}$[12]	3100-3000	2960-2850	1660-1480	≈ 1500

Conclusions:

As mentioned before, most of the complexes discussed in this chapter displayed very low solubility in most common solvents. It is for this reason alone that they are not completely characterised.

The bis(dimesityldiazabutadiene)silver(I) tetrafluoroborate complex was characterised completely by means of ^{1}H and ^{13}C NMR spectra, molecular structure determination as well as FT-IR and MS refinements. This was the only complex to be so extensively analysed. The $Cr(CO)_4$(TMEDA) complex could only be characterised by means of FT-IR and molecular structure determination. The low solubility of the M(DFDAB)Cl_2 [M = Fe, Zn] complexes permitted NMR spectra measurements besides MS and FT-IR, but did not include molecular structure determinations. The Zn(DMDAB)Cl_2 complex was characterised by means of FT-IR, MS and a molecular structure determination. Since pure crystals could not be obtained of some of the complexes, the catalysis results of these complexes should be seen as "in sito" processes.

These five complexes were employed as pre-catalysts for the polymerisation of ethylene as described in Chapter 4. The Fe(DFDAB)Cl_2 complex was also used for the polymerisation of 1-pentene since it exhibited the highest activity as pre-catalyst for ethylene polymerisation.

Low oxidation-state complexes

3.6 Tricarbonyliron(N,N'-diferrocenyldiazabutadiene):

Tricarbonyliron(diferrocenyldiazabutadiene) was synthesised by first stirring $Fe_2(CO)_9$ in THF to form $Fe(CO)_4(THF)$; this complex was then added to a solution of N,N'-diferrocenyldiazabutadiene in THF. After purification by column chromatography, analytical data confirmed that the target complex had formed. Unfortunately, single crystals fit for X-ray diffraction data collection could not be collected. The reaction scheme is illustrated in Equation 3.6.1.

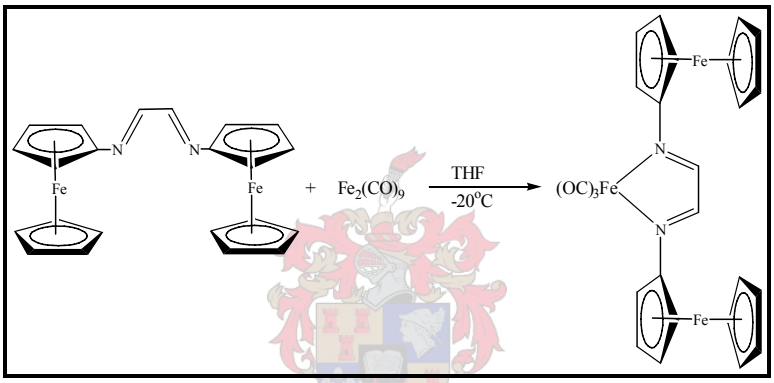

Equation 3.6.1

3.6.1 NMR Spectroscopy:

Proton atoms H^2 and H^5 endure a slight deshielding from the tricarbonyl fragment and resonate downfield compared to the free ligand. The diimine proton atoms as well as H^3 and H^4 resonate upfield from the free ligand due to the shielding from the applied field by the tricarbonyl fragment. The chemical shift of the unsubstituted cyclopentadienyl proton and carbon atoms remains unchanged. Most of the signals for the carbon atoms do not differ significantly from the free ligand except the C^1 atom which lies in the trigonal plane. This causes C^1 to experience minor deshielding and resonate downfield. The imine carbon atoms also resided in this plane, but far removed from the carbonyl fragment. The sharp peak at δ 214.4 is assigned to CO group, consistent with a tricarbonyl species. Only one signal is visible for the three carbonyls, indicating that the CO groups are chemically equivalent, or undergo exchange. Feiken and co-workers[25] have shown that Fe(α-

diimine)$(CO)_3$ complexes, where α-diimine is not a C_2-symmetrical ligand, form two diastereoisomeric configurations *via* Berry-pseudo rotation[22,26] in solution. The Berry-pseudo rotation occurs so rapidly that it is impossible to distinguish between the two diastereomers within the NMR timeframe even at low temperature.

Table 3.6.1: ^{1}H and ^{13}C NMR data for $Cr(CO)_3$(DFDAB)

Complex:	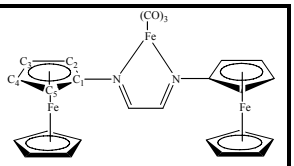
Solvent	Dichloromethane-D2
Temperature (K)	273
^{1}H NMR (300 MHz)	**δ**
$H^{2,5}$	4.79 (s, 4H)
$H^{3,4}$	4.28 (s, 4H)
Cp	4.19 (s, 10H)
-N=C-	8.11 (s, 2H)
^{13}C NMR (75 MHz)	**δ**
C^1	113.8
$C^{2,5}$	66.7
$C^{3,4}$	65.6
Cp	70.6
-N=C-	144.9
CO	214.4

3.6.2 Mass Spectrometry:

The ferrocene peak (*m/z* 186) forms the base peak. The stepwise fragmentation of the carbonyl groups proceeds first followed then by the fragmentation of the non-ferrocene iron metal. The fragmentation pattern for the coordinated ligand is similar to that of the uncoordinated ligand. Table 3.6.2 lists the Electron Spray Ionisation MS data for this complex.

Table 3.6.2: Electron Spray Ionisation MS data for $Cr(CO)_3$(DFDAB)

Fragment-ion	***m/z (I%)***	**Fragment-ion**	***m/z (I%)***
$[M]^+$	564 (1)	$[L - Cp]^+$	201 (37)
$[M - CO]^+$	536 (1)	$[Fc]^+$	186 (1)
$[M - 2CO]^+$	508 (2)	$[Fc - Cp]^+$	121 (68)
$[M - 3CO]^+$	480 (3)	$[Fe]^+$	56 (31)
$[L]^+$	424 (100)	$[N_2/CO]^+$	28 (62)

3.6.3 Infrared Spectroscopy:

Tricarbonyl *fac*-$(CO)_3M(L^\wedge L)$ complexes of C_{3v} symmetry have two infrared active stretching vibration frequencies. Table 3.6.3 reports the stretching frequencies for the tricarbonyliron(diferrocenyldiazabutadiene) complex. The infrared data are consistent with compounds with the C_{3v} symmetry.[27]

Table 3.6.3: FT-IR stretching frequencies for $Cr(CO)_3$(DFDAB)

Moiety	**A'**	**A''**	**-N=C-**
ν [cm^{-1}]	2048.0 (*s*)	1955.1 (*w*)	1659.77 (*w*)

To conclude, the objective behind the synthesis of this compound was the same as that for the tetracarbonylchromium(TMEDA) complex: to investigate the effect on polymerisation of olefinic monomers by the presence of carbonyl groups. Unfortunately, a low yield and extreme sensitivity of the complex was detrimental to this objective.

3.7 {Ferrocenyl(methoxy)-carbene}pentacarbonylchromium(0):

This complex was synthesised previously by Zora and co-workers[8], but their report did not include a crystal structure determination. The continuous interest of our group in carbene complexes as well as the availability of reagents and expertise gained in the present study in handling these compounds lead to the decision to synthesise and characterise them fully. This complex was, however, not included in the polymerisation study. The experimental procedure in given in Chapter 5.

Analogous to a carbonyl group, a carbene ligand could be regarded as a two-electron donor, as illustrated in Figure 3.7.1, since there is a lone pair of electrons present on what is formally a divalent carbon atom. This is chemically similar to a C=C double bond.

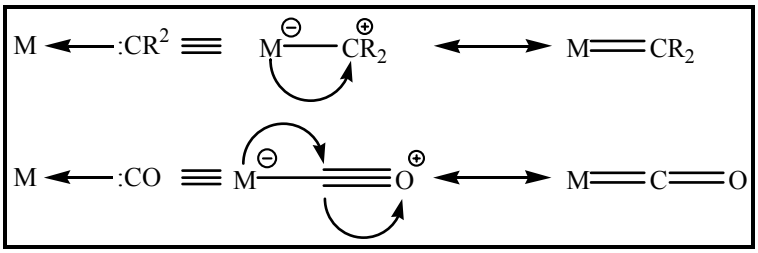

Fig. 3.7.1: Illustration of two-electron donor effect of the carbene ligand

Fischer-type carbene complexes are of the general kind illustrated in Figure 3.7.2, where L represent the acceptor ligands (e.g. carbonyl) and X and Y are substituents on the carbene carbon, that may also partake in π-interaction leading to another resonance structure.

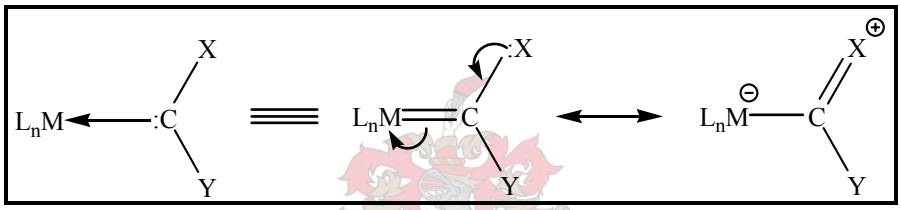

Fig. 3.7.2: General formula of Fischer-type carbene complexes

This π-contribution by a heteroatom requires α N-,O- or S- containing groups. The metal carbene bond is best described by the Dewar-Chatt-Duncanson model.[28] A synergistic σ-electron donation from the lone pair on the carbene carbon to an empty metal d_z^2 orbital takes place followed by back donation of π-electrons from the metal d_{xz} or d_{yz} orbitals to the empty $p(\pi)$ carbene carbon orbital. Figure 3.7.3 illustrates the overlap of atomic orbitals.

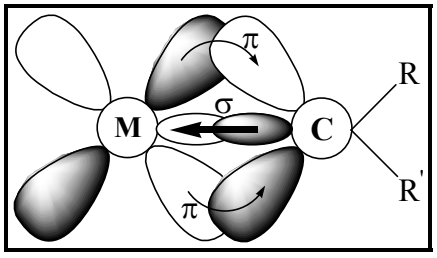

Fig. 3.7.3: Illustration of the overlap of molecular orbitals

The synthesis of {ferrocenyl(methoxy)-carbene}pentacarbonylchromium(0) was performed in three steps, which is illustrated in Equation 3.7.1. Ferrocene was lithiated with ^{t}BuLi in THF, or by the use of Schlosser's base. This "super base" is a mixture of butyllithium and potassium tertiary-butoxide.[29] The deprotonation of ferrocene with Schlosser's base is a new approach for lithiating metallocenes. The yield is significantly higher (~ 92% compared to the ~ 77% reported by Bildstein and co-workers). The suspension of lithiated ferrocene in THF was added dropwise to a suspension of the chromium hexacarbonyl for the nucleophilic addition of the ferrocenyl group to form the acylpentacarbonyl chromate salt. Trimethyloxonium tetrafluoroborate was used for the O-alkylation to generate the alkoxycarbene complex. Characterisation took place after purification *via* column chromatography and confirmed that a new carbene complex was present in the reaction mixture.

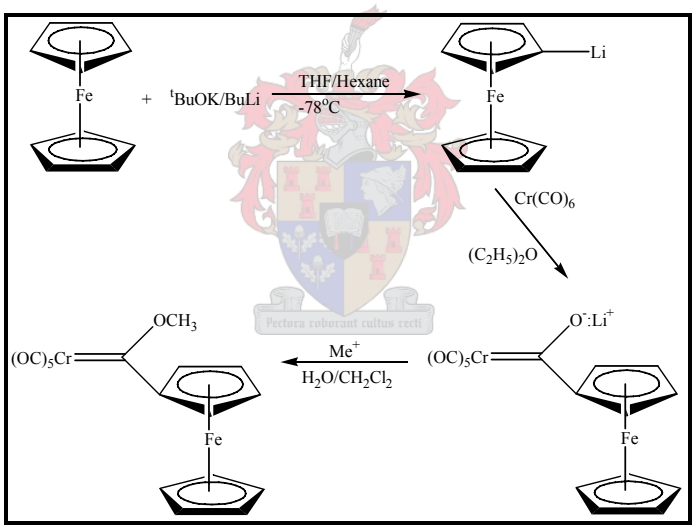

Equation 3.7.1:

3.7.1 <u>NMR Spectroscopy</u>:

A single resonance at δ 4.23 represents the proton atoms of the unsubstituted cyclopentadienyl ligands. The resonances of the proton atoms H^2 to H^5 appear somewhat downfield compared to the corresponding proton atoms of the ferrocenyl complexes reported earlier in this chapter. The deshielding effect of the pentacarbonyl fragment leads to chemical shifts at lower applied field strength. The ferrocenyl carbon atoms

experience the same effect of the deshielding effect and resonate thus downfield. The signals for the carbene carbon atom as well as the pentacarbonyl carbon atoms are consistent with signals observed in the ^{13}C NMR spectrum of Fischer-type carbene complexes. Note the extreme (carbocationic) deshielding of the carbene carbon. The ^{1}H and ^{13}C NMR data are summarised in Table 3.7.1.

Table 3.7.1: ^{1}H and ^{13}C NMR data for $(CO)_5Cr{=}C(OMe)(C_{10}H_9Fe)$

Complex:	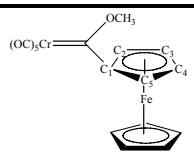
Solvent	Chloroform-D
Temperature (K)	273
^{1}H NMR (300 MHz)	**δ**
$H^{2,5}$	4.78 (s, 2H)
$H^{3,4}$	4.67 (s, 2H)
Cp	4.23 (s, 5H)
OMe	4.13 (m, 3H)
^{13}C NMR (75 MHz)	**δ**
C^{1}	93.6
$C^{2,5}$	72.2
$C^{3,4}$	74.6
$Cp_{(unsubstituted)}$	70.5
CO_{cis}	217.5
CO_{trans}	223.1
Carbene C	333.3

3.7.2 Mass Spectrometry:

Peaks showing the sequential loss of five carbonyl groups were visible in the MS spectrum of the carbene complex. Q (in Table 3.7.2) represents the carbene complex minus the five carbonyl and chromium fragments.

Table 3.7.2: MS data for the ferrocenyl methoxycarbene complex

Fragment-ion	***m/z (I%)***	**Fragment-ion**	***m/z (I%)***
$[M]^+$	420 (3)	$[Q - OC_{carb}]^+$	237 (42)
$[M - CO]^+$	392 (2)	$[Fc]^+$	186 (8)
$[M - 2CO]^+$	364 (5)	$[Fc - Cp]^+$	121 (18)
$[M - 3CO]^+$	336 (7)	$[Fe]^+$	56 (17)
$[M - 4CO]^+$	308 (7)	$[Cr]^+$	52 (23)
$[Q]^+$	280 (30)	$[CO]^+$	28 (100)
$[Q – CH_3]^+$	265 (4)		

The methoxy CH_3 is severed from Q to yield a peak at *m/z* 265. The carbene carbon atom and the oxygen atom are cleaved from Q to yield a peak at *m/z* 237. The remainder of the original complex fragments into ferrocene and a Cr cation to yield peaks at *m/z* 186 and *m/z* 52 respectively. The fragmentation of ferrocene proceeds in the usual manner. The carbonyl peak, strengthen by atmospheric N_2, at *m/z* 28 forms the base peak.

3.7.3 Molecular structure:

The elucidation of the molecular structure of pentacarbonylmethoxy ferrocenyl-chromiumcarbene was achieved at low temperature (100K) using single crystal X-ray diffraction techniques.

Table 3.7.3: Experimental and crystallographic data for $(CO)_5Cr{=}C(OMe)(C_{10}H_9Fe)$

Empirical formula	$C_{10}H_{16}N_2O_4Cr$
Formula weight	560.50
Colour	Yellow
Crystal system	Monoclinic
Space group	$P2_1/n$
Unit cell dimensions	a = 8.258(1) α = 90.00
	b = 11.81(2) β = 91.866(3)
	c = 13.123(2) γ = 90.00
Z	2
V (Å^3)	1279.0(3)
Density (g/cm^3)	1.455
Radiation (Mo-Kα) [Å]	0.71073
$2\theta_{max}$	56.5°
Monochromator	Graphite
Absorption coefficient (μ) [mm^{-1}]	0.899
Temperature (K)	100(2)
F (000)	584
Diffractometer	Bruker Smart Apex®
Scan range (θ)	
hkl ranges	$-10 \le h \le 8$
	$-15 \le k \le 13$
	$-17 \le l \le 17$
Reflections measured	7909
Unique reflections used	2933
Number of parameters refined	158
Deepest hole	2.32
Highest peak	28.24
R_{int} (%)	6.43
R1 (%)	6.20
Goodness of fit (GooF)	0.932

A red, prism-like crystal was mounted on a glass fibre and transferred to a Bruker Smart Apex[6] X-Ray diffractometer. The position of the iron atom was obtained using direct methods and anisotropic displacement parameters for all the atoms, excluding hydrogen atoms. The hydrogen atoms were placed in calculated theoretical positions. Structure determination and refinement of the atom coordinates are accomplished using the SHELX-97[7] and X-Seed[8] software. The resultant structure shows a ferrocene moiety coordinated to an octahedral $Cr(CO)_5$ fragment. From the crystal data it is clear that the two cyclopentadienyl rings are in a staggered configuration with D_{5d} symmetry. Table 3.7.3 contains the experimental and crystallographic data collected for this complex. The molecular structure and numbering of relevant atoms of the {ferrocenyl(methoxy)carbene}pentacarbonylchromium(0) complex can be seen in Figure 3.7.4.

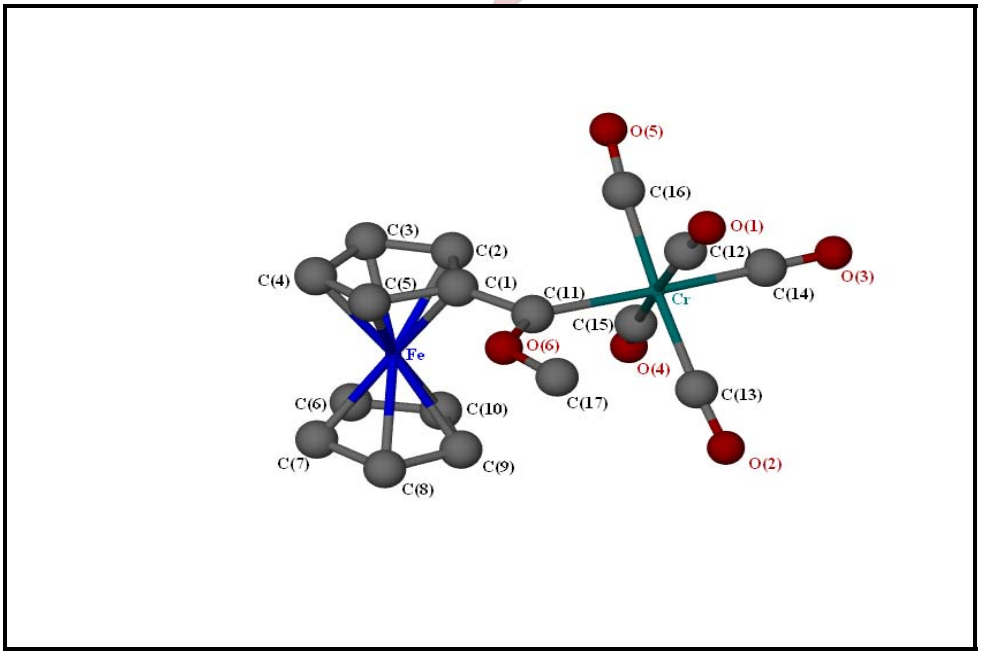

Fig. 3.7.4: Molecular structure of the $(CO)_5Cr{=}C(OMe)(C_{10}H_9Fe)$

The molecular structure of {ferrocenyl(methoxy)carbene}pentacarbonylchromium(0) can be compared with the {bromoferrocenyl(methoxy)carbene}pentacarbonyl chromium(0) complex of Hursthouse and co-workers[30] and the

$[(CO)_5Cr{=}C(OCH_3)(CH{=}CH)_2(C_5H_4)Fe(C_5H_5)]$ complex prepared by Jayaprakash and co-workers[10] (Figure 3.7.5).

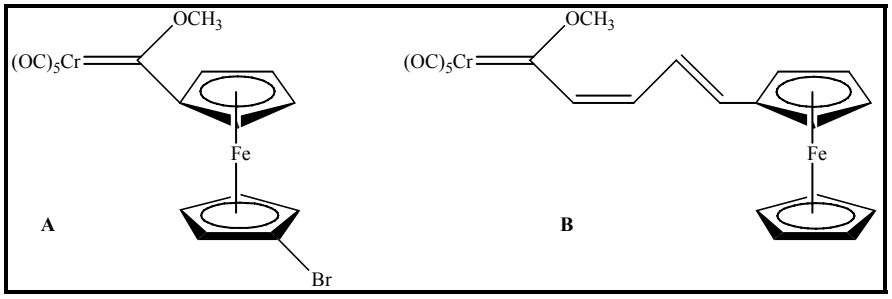

Fig. 3.7.5: Ferrocenyl Fischer carbene complexes by Hursthouse and Jayaprakash

Five carbonyl ligands and a carbene ligand surround the chromium metal which has a somewhat distorted octahedral configuration. The equatorial carbonyl groups [chosen as C(16), C(14) and C(13)] as well as the axial carbonyl groups' [C(12) and C(15)] bond lengths (Table 3.7.4) are slightly longer than the corresponding bond lengths in complex B, but equal to that of complex A. In comparison to complex B, the close proximity of the ferrocenyl group to these carbonyl groups could be the reason for this phenomenon. Other than these differences, the remaining bond lengths are consistent with data published for other carbene and ferrocene complexes.[10,15] Table 3.7.4 exhibits the bond lengths of the ferrocenyl carbene complex.

Table 3.7.4: Bond lengths of $(CO)_5Cr{=}C(OMe)(C_{10}H_9Fe)$

Bond Lengths (Å)					
C(1)-C(11)	1.46(1)	C(6)-C(10)	1.43(2)	C(12)-O(1)	1.15(1)
C(1)-C(2)	1.46(2)	C(6)-Fe	2.06(2)	C(13)-Cr	1.90(8)
C(1)-Fe	2.10(1)	C(7)-Fe	2.04(9)	C(13)-O(2)	1.16(1)
C(2)-Fe	2.04(9)	C(8)-Fe	2.05(9)	C(14)-Cr	1.86(9)
C(3)-C(4)	1.45(2)	C(9)-C(10)	1.42(1)	C(14)-O(3)	1.16(1)
C(3)-Fe	2.04(9)	C(9)-Fe	2.05(9)	C(15)-Cr	1.87(8)
C(4)-C(5)	1.35(2)	C(10)-Fe	2.07(9)	C(15)-O(4)	1.14(1)
C(4)-Fe	2.02(2)	C(11)-Cr	2.07(8)	C(16)-Cr	1.90(9)
C(5)-Fe	2.03(9)	C(11)-O(6)	1.33(1)	C(16)-O(5)	1.15(1)
C(6)-C(7)	1.42(2)	C(12)-Cr	1.92(1)	C(17)-O(6)	1.42(1)

The angles (Table 3.7.5) of the carbon atoms of the substituted cyclopentadienyl ring to their corresponding carbon atoms in the $Cp_{unsubst}$ ring through the iron atom have a

variation of approximately 7°. A variation in these angles suggests, as mentioned before, that the two Cp rings are in a staggered configuration relative to each other. The plane formed by the substituted cyclopentadienyl ring is not parallel to the square plane of the octahedral coordination sphere [formed by C(11), Cr and C(14)] and forms a dihedral angle of 15.8(3)°. The disorder in the octahedral sphere at the chromium metal results in some variation in angles between the carbonyl and carbene carbon substituents. The angle between the carbene carbon [C(11)] and the adjacent carbonyl carbon [C(13)] is larger than the proposed 90° right angle. The presence of the methoxy group, which lies parallel to the octahedral plane, causes this area to be sterically crowded and pushes the carbonyl group C(13) towards C(14) and this angle between C(11) and C(13) is subsequently increased to 94°. The angle formed between C(13) and C(14) is then decreased to 87.9°. This can be correlated with the almost 90° right angle between the carbene carbon and the other adjacent carbonyl group, C(16), where the methoxy group is not in close proximity. The rotation of the ferrocene group also pushes the axial carbonyl group away from the carbene carbon. The situation is valid for the other axial C(15) carbonyl group.

Table 3.7.5: Bond angles of $(CO)_5Cr{=}C(OMe)(C_{10}H_9Fe)$

Bond Angles (in degrees)					
C(1)-C(11)-Cr	125.4(7)	C(7)-C(8)-Fe	68.7(5)	C(12)-Cr-C(15)	175.0(4)
C(1)-C(11)-O(6)	105.2(8)	C(8)-C(9)-C(10)	108.6(8)	C(12)-Cr-C(16)	87.1(5)
C(1)-C(2)-Fe	71.7(6)	C(9)-C(10)-Fe	69.1(5)	C(13)-Cr-C(14)	87.9(4)
C(1)-C(5)-Fe	72.1(5)	C(10)-C(9)-Fe	70.7(5)	C(13)-Cr-C(15)	88.6(4)
C(2)-C(1)-C(11)	128.0(9)	C(10)-C(6)-Fe	70.3(7)	C(13)-Cr-C(16)	176.3(4)
C(3)-C(4)-Fe	69.9(6)	C(11)-O(6)-C(17)	124.0(7)	C(14)-Cr-C(15)	86.4(4)
C(4)-C(3)-Fe	68.2(7)	C(11)-C(1)-Fe	122.6(7)	C(14)-Cr-C(16)	88.5(4)
C(4)-C(5)-Fe	70.0(7)	C(11)-Cr-C(12)	93.4(4)	C(15)-Cr-C(16)	90.8(4)
C(5)-C(4)-Fe	71.0(7)	C(11)-Cr-C(13)	94.0(3)	Cr-C(11)-O(6)	129.0(5)
C(5)-C(1)-Fe	67.0(5)	C(11)-Cr-C(14)	176.8(4)	Cr-C(12)-O(1)	176.9(9)
C(5)-C(1)-C(11)	127.0(1)	C(11)-Cr-C(15)	91.0(3)	Cr-C(13)-O(2)	175.6(7)
C(6)-C(7)-Fe	70.5(7)	C(11)-Cr-C(16)	89.6(4)	Cr-C(14)-O(3)	179.3(8)
C(6)-C(10)-Fe	69.1(7)	C(12)-Cr-C(13)	93.2(4)	Cr-C(15)-O(4)	175.0(8)
C(7)-C(6)-Fe	69.0(7)	C(12)-Cr-C(14)	89.1(4)	Cr-C(16)-O(5)	176.1(9)

The crystal packing of the pentacarbonylmethoxyferrocenylchromiumcarbene complex is illustrated in Figure 3.7.6. The molecules are packed inversely in columns along the b-

axis. The hydrogen atoms are placed in calculated positions. Hydrogen bonds between N(1) and C(11) [3.687 Å] contribute to the stable packing of the crystal structure.

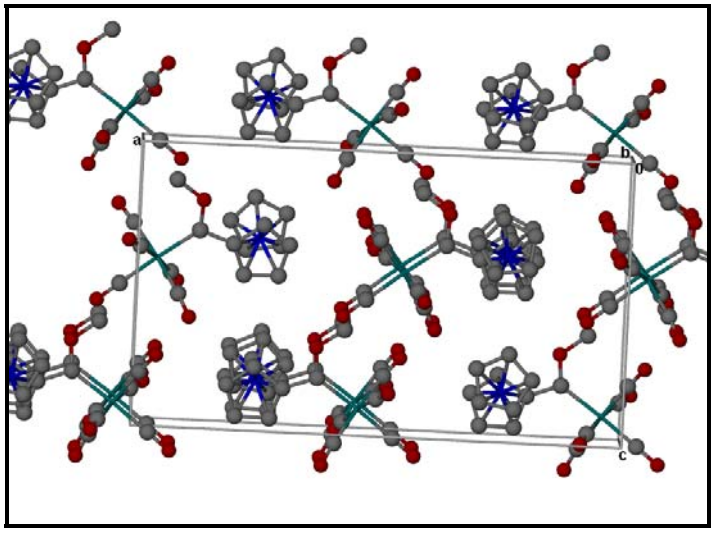

Fig. 3.7.6: Crystal packing of $(CO)_5Cr{=}C(OMe)(C_{10}H_9Fe)$ along the *b*-axis

3.7.4 Infrared Spectroscopy:

The ν(CO)-infrared vibration frequencies for the ferrocenyl(methoxy) carbene complex are represented in Table 3.7.6. Three active infrared frequencies are expected for pentacarbonyl compounds with C_{4v} carbonyl ligand symmetry. The B' band was not visible.

Table 3.7.6: ν(CO)-infrared vibration frequencies for $(CO)_5Cr{=}C(OMe)(C_{10}H_9Fe)$

Carbonyl	$A_1^{(1)}$	E	$A_1^{(2)}$
ν [cm^{-1}]	2055.3 (*s*)	1963.8 (*s*)	1892.8 (*w*)

References:

1. J.C. Jenkins and M. Brookhart, *Organometallics,* **2003**, *22*, 250.
2. F.A. Hicks and M. Brookhart, *Organometallics,* **2001**, *20*, 3217.
3. C.M. Killian, D.J. Temple, L.K. Johnson and M. Brookhart, *J. Am. Chem. Soc.,* **1996**, *118*, 11665.
4. G.J.P. Britovsek, M. Bruce, V.C. Gibson, B.S. Kimberley, P.J. Maddox, S. Mastroianni, S.J. MacTavish, J. Redshaw, G.A. Solan, S. Strömberg, A.J.P. White and D.J. Williams, *J. Am. Chem. Soc.,* **1999**, *121*, 8728.
5. M. Zora, B. Yucel and N.B. Peynircioglu, *J. Organomet. Chem.,* **2002**, *656,* 11.
6. SMART Data collection software (version 5.629), Bruker AXS Inc., Madison, WI, **2003**.
7. G. Sheldrick, *SHELX Program for Crystal Structure Determination,* University of Göttengen, **1997**.
8. L.J. Barbour, *J. Supramol. Chem.,* **2001**, *1*, 189.
9. C.L. Foster, C.A. Kilner, M. Thornton-Pett and M.A. Halcrow, *Acta Crystallographica,* **2000**, *C56*, 319.
10. K.N. Jayaprakash, P.C. Ray, I. Matsuoka, M.M. Bhadbhade, V.G. Puranik, P.K. Das, H. Nishihara and A. Sarkar, *Organometallics*, **1999**, *18*, 3851.
11. G.K. Patra and I. Goldberg, *J. Chem. Soc., Dalton Trans.,* **2002**, 1051.
12. M. Hesse, H. Meier and B. Zeeh, *Spectroscopic Methods in Organic Chemistry*, Foundations of Organic Chemistry Series, Georg Thieme Verlag, Stuttgart-New York, **1997**, p. 365.
13. G.J. Kruger, G. Gafner, J.P.R de Villiers, H.G. Raubenheimer and H. Swanepoel, *J. Organomet. Chem.,* **1980**, *187*, 333.
14. N. Luruli, V. Grumel, R. Brüll, A. du Toit, H. Pasch, A.J. van Reenen and H.G. Raubenheimer, *J. of Polymer Science: Part A: Polymer Chemistry*, **2004**, *42*, 5121.
15. F.H. Allen, O. Kennard, D.G. Watson, L. Brammer, A.G. Orpen and R. Taylor, *J. Chem. Soc., Perkin Trans. II*, **1987**, S1.
16. P.J. Flory, *J. Am. Chem. Soc.,* **1940**, *62*, 1561.
17. C. Bianchini, G. Giambastiani, I.R. Guerrero, A. Meli, E. Passaglia and T.

Gragnoli, *Organometallics,* **2004**, *23*, 6087.

18. C.H. Evans, S.J. MacLain and A.M.A. Bennet, WO Patent Application **WO 98/56832** to DuPont, December, 1998.
19. (a) S. Grammenudi and F. Vögtle, *Angew. Chem. Int., Ed., Engl.,* **1986**, *25*, 1122.
    (b) J.M. Lehn and R.J. Ziessel, *J. Chem. Soc., Chem. Comm.,* **1987**, 1292.
    (c) S.J. Riepert, C.B. Knobler and D.J. Cram, *Tetrahedron*, **1987**, *43*, 4861.
    (d) P.D. Beer and A.S.J. Rothin, *Chem. Comm.,* **1988**, 52.
20. (a) J.N. Demas, E.W. Harris, C.M. Flynn *jr.* and D.J. Diemente, *J. Am. Chem. Soc.,* **1975**, *97*, 3838.
    (b) D.M. Klassen, *Inorg. Chem.,* **1976**, *15*, 366.
    (c) B. Alpha, J.M. Lehn and G. Mathis, *Angew. Chem. Int., Ed., Engl.,* **1987**, *26*, 266.
    (d) E. Danielson, C.M. Elliott, J.W. Merkert and T.J. Meyer, *J. Am. Chem. Soc.,* **1987**, 109, 2519.
21. (a) H.Y. Mei and J.K. Barton, *J. Am. Chem. Soc.,* **1986**, *108*, 7414.
    (b) L.A. Basile and J.K. Barton, *J. Am. Chem. Soc.,* **1987**, *109*, 7548. (c) A.E. Friedman, J.C. Chambron, N.J. Turro and J.K. Barton, *J. Am. Chem. Soc.,* **1990**, *112*, 4960.
22. C.J. Marsden, *J. Chem. Soc.,* **1984**, 401.
23. X.C. Wang and H.N.C. Wong, *Tetrahedron*, **1995**, *51*, 6941.
24. V.C. Gibson, R.K. O'Kelly, W. Rees, D.F. Wass, A.J.P. White and D.J. Williams, *Chem. Comm.,* **2002**, 1850.
25. N. Feiken, P. Schreuder, R. Siebenlist, H.W. Frühauf and K. Vrieze, *Organometallics*, **1996**, *15*, 2148.
26. R.S. Berry, *J. Chem. Phys.,* **1960**, *32*, 933.
27. S. Lotz, *Ph.D Thesis*, Rand Afrikaans University, **1978**.
28. M. Cases, G. Frenking, M. Duran and M. Sola, *Organometallics*, **2002**, *21*, 4182.
29. L. Brandsma and H.H. Verkruijsse, *Preparative Polar Organometallic Chemistry*, **Vol. 1**,1987, p. 18, Springer-Verlag, Berlin.
30. M.B. Hursthouse, D.E. Hibbs and I.R. Butler, *CCDC Private Communications,* Code BAVBIK 217906, **2003**.

Chapter 4: Polymerisation of lower olefins by transition metal pre-catalysts

Introduction:

Polyolefins are the fastest growing sector in industrial production of polymers with a wide range in commercial application. Polyethylene represents 75% of these commercial polyolefins. As discussed in Chapter 1, there are three types of polyethylene namely high density PE (HDPE) [M_w > 200 000 g/mol], linear low density PE (LLDPE) [M_w < 100 000 g/mol] and low density PE (LDPE) [M_w < 100 000 g/mol].

Polydispersity ranges depend on the type of catalyst used. Metallocene catalysts are renowned to yield polymers of high molar mass coupled with narrow polydispersities. These catalysts are also used mainly for the industrial production of commercial polymer products.

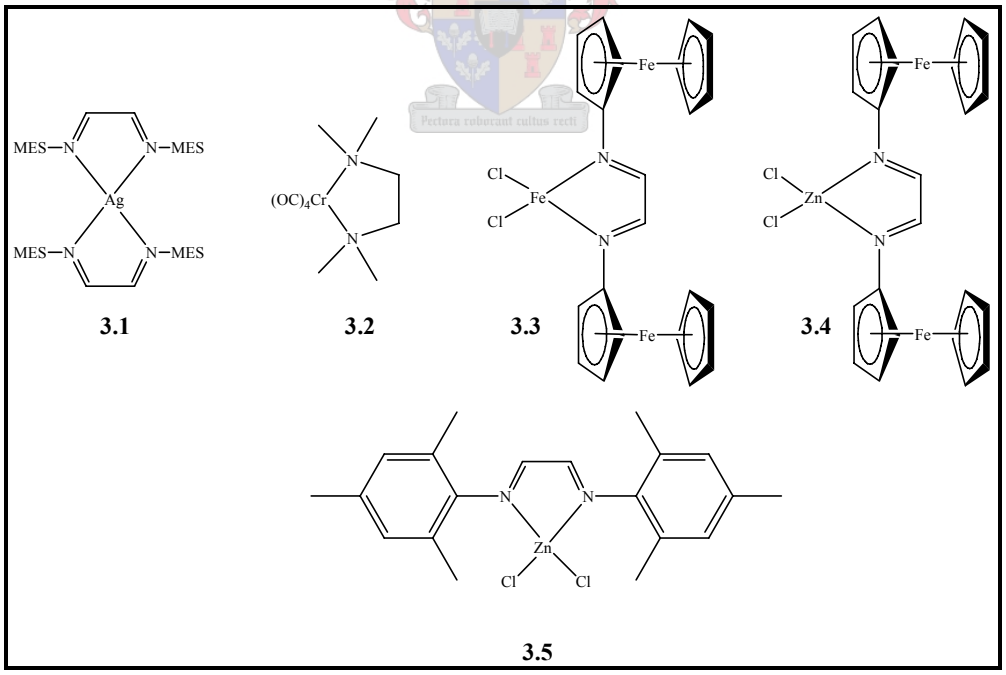

Scheme 4.1

The most effective α-diimine transition metal catalysts, such as the Brookhart-type catalysts, are still in the development stage and their application is still not suitable for the commercial production of polyolefins. Some of these α-diimine transition metal catalysts are difficult to synthesise, sensitive towards the atmosphere and moisture and expensive to manufacture. Such catalysts are, therefore, not used yet in industrial application even though they are comparatively active and yield polymers products with high molar mass and narrow polydispersities.

The objective for this polymerisation study was to investigate the activity of the complexes described in the previous chapter. Only the homopolymerisation of ethylene and 1-pentene were investigated. Polymerisation of these olefins was attempted with the complexes illustrated in Scheme 4.1.

Methyl aluminoxane (MAO) was chosen as the co-catalyst for the polymerisation reactions for the reason that it is readily available. MAO is added in large excesses to neutralise any impurities so the catalytic system is not compromised. A typical ratio of the co-catalyst (MAO) to catalyst is 400:1. Polymerisation reactions were carried out in a stainless steel Parr reactor equipped with an inlet valve and a pressure gauge. The reactor was fitted with a glass liner and stirrer bar. Characterisation methods of polyethylene included Differential Scanning Calorimetry (DSC), ^{13}C NMR and high temperature Gel Permeation Chromatography (GPC) also known as Size Exclusion Chromatography (SEC). The two polymerisation characterisation techniques (Differential Scanning Calorimetry and Size Exclusion Chromatography) will be discussed in brief prior to the results of the polymerisation study.

Differential Scanning Calorimetry (DSC):

The operation of a Differential Scanning Calorimeter is based on measurement of the thermal response of an unknown specimen as compared with a standard when the two are heated uniformly at a constant rate. Any difference in temperature of the two specimens is caused by differences in mass, specific heat, heats of reaction or phase transitions. On

the first cycle of heating, at a certain temperature, the polymers will have gained enough energy to move into very ordered crystalline arrangements. This temperature is known as the crystallisation temperature (T_c) as illustrated in Figure 4.1.[1]

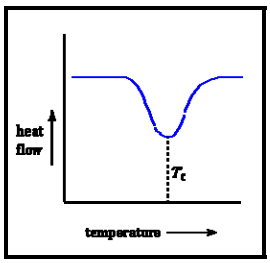

Fig. 4.1: Illustration of T_c

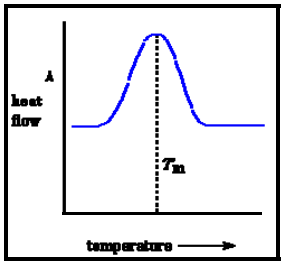

Fig. 4.2: Illustration of T_m

On the second heating cycle, the polymers are heated to the melting temperature (T_m). The melting process is a first order transition, thus the temperature will not rise until all the crystals have melted. The temperature will, therefore, stay constant for an instant while the heating pan still increases in temperature, explaining the large peak on the DSC plot as illustrated in Figure 4.2.

<u>Size Exclusion Chromatography (SEC):</u>

Size Exclusion Chromatography is a powerful technique for the separation of high molar mass species. In SEC, a steel column is packed with porous material (typically silica or cross linked polystyrene) and solvent is forced through the column at a flow rate of 1 mL/min and pressures between 50 to 200 bar. A sample is dissolved (in the same solvent that is running through the column) and then introduced into the solvent stream going through the column. A detector monitors the concentration of sample exiting the end of the column. Inside the column, molecules are separated based on their hydrodynamic volume (the volume the sample molecule occupies in a dilute solution). The molecules are separated by whether they can fit within the pore size of the packing material. As a molecule flows through the column it passes by a number of the porous beads of the packing material. If the molecule can fit inside the pore then it is drawn in by the force of diffusion. There it stays a short while and then moves on, thus impeding its progress

through the column. The larger molecules just flow past these pores and are rapidly eluted from the column. The size of the larger molecules then dictates their flow rate from the column and causes a molecular mass distribution. By calibrating the sample polymer to a standard sample, *e.g.* polystyrene, a relative distribution of molar mass can be determined and from this data the average molar mass (M_w), number average molar mass (M_n) and polydispersity index (PDI) are calculated. The main objective for most polymerisation reactions is to synthesise a polymer product with high molar mass coupled with a narrow polydispersity (PDI).

4.1 Polymerisation of ethylene:

The polymerisation of ethylene with the metaldichloride catalyst pre-cursors depicted in Scheme 4.1 (complexes **3.3**, **3.4** and **3.5**) proceeds *via* a cationic pathway. A catalyst solution of known concentration was prepared under inert conditions (argon) in a Schlenk tube. The co-catalyst was added to yield a ratio of 400:1 (co-catalyst:catalyst). The pre-mix was injected into the reactor followed by ethylene gas with a ratio of 10000:1 (monomer:catalyst). The reaction run took 60 minutes after which the reaction was terminated using methanolic HCl. The polyethylene was precipitated using methanol and dried under reduced pressure at 60°C.

Pectora roborant cultus recti

Here follows a brief explanation of the mechanism followed during the polymerisation of ethylene. The metaldichloride catalysts are activated by the co-catalyst, MAO, to form a cationic species (Step 1, Scheme 4.1); from here on alkene insertion occurs into an M-H bond. A single monomer coordinates *in situ* with the cationic species to form a methyl(olefin) complex (Step 2). The propagation by olefin insertion proceeds without branching of the polymer chain to yield high density polyethylene (Step 3). Termination proceeds *via* the standard β-hydride elimination mechanism (Step 4).

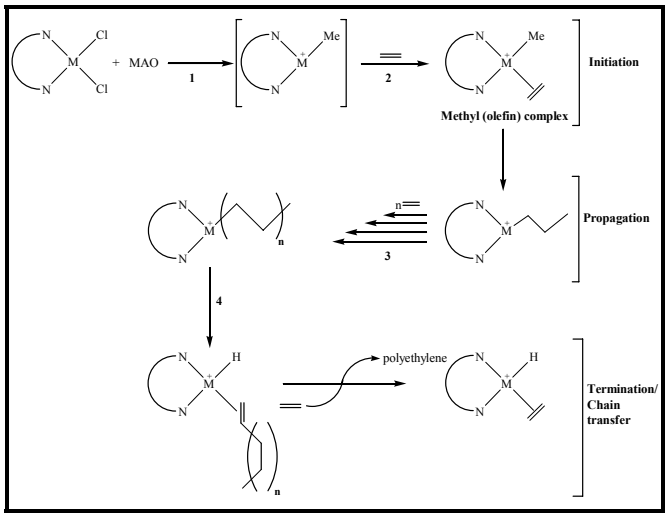

Scheme 4.2

Characterisation of polyethylene

Table 4.1 lists the analytical data that include DSC, NMR (^{13}C) and high temperature GPC of polyethylene.

Table 4.1: Analytical data of polyethylene

Catalyst	3.1	3.2	3.3	3.4	3.5
^{13}C NMR (ppm)	29.78	29.76	29.78	29.77	29.77
M_w (SEC)	396 000	1 067 000	725 000	588 000	518 000
M_n (SEC)	158 000	303 000	289 000	162 000	199 000
PDI (SEC)	2.5	3.5	2.5	3.6	2.6
T_c (°C) [DSC]	117.07	116.53	118.73	117.31	117.61
T_m (°C) [DSC]	132.45	131.48	133.16	132.85	132.89
TOF[a] ($x10^{-3}$)	26.1	16.0	66.0	14.1	1.0
%Yield	5.30	5.00	36.70	4.13	0.37

[a] In units of mass PE produced per mol catalyst consumed per hour.

NMR data were collected at 120°C by dissolving the polyethylene in trichlorobenzene (TCB) with benzene (C_6D_6) as an internal standard. Singlet ^{13}C signals were observed at approximately δ 29.8 for all the polyethylene products obtained with various metal catalysts. This is characteristic of linear PE. The molar mass was determined by GPC relative to polystyrene (PS) calibration at 160°C. The average molar mass (M_w) suggests that the products are of high density. Differential Scanning Calorimetry (DSC) was performed between 0 and 220°C and displayed an average crystalisation temperature (T_c) of 117.5°C on the first heating cycle. The second heating cycle (220 to 0°C) displayed an average melting temperature (T_m) of 132.6°C. These results confirm that the polymer products are high density PE.

The turn over frequency (TOF) for complexes **3.1** to **3.5** is in general much smaller than for the best known catalysts (see Table 4.2). Only pre-catalyst **3.3** ([diferrocenyldiazabutadiene]iron dichloride) outperforms the published complexes containing iron as metal centre. It is, true to expectation, apparent that the metal centre plays an important role in the activity of the catalyst. Metal centres such as Ni and Pd exhibited very high activity, but the compound of interest in Table 4.2 is the iron complex (**B**) bearing 2,6-bis(imino)pyridyl ligands. This catalyst is one of very few useful iron-based catalysts. The low activity, high molar mass and broad polydispersity seem to be characteristic of the most of these pre-catalysts. The iron(II)-[diferrocenyldiazabutadiene] compound (compound **3.3**) exhibits similar activity and product molar mass, but a much better polydispersity. In general, however, the catalysts tested in the present study exhibit low activity towards the polymerisation of ethylene. The iron-(DFDAB)dichloride complex exhibits the highest yield of 36.7% of all the pre-catalysts tested in the present study. Low yields are characteristic of α-diimine complexes, another reason why these types of catalysts are not used in the industry. Unexpectedly, the bis(dimesityldiazabutadiene)silver(I) compound produced a polyethylene yield of 5.3%, the second highest of all the pre-catalysts investigated. This is unusual since no chloride atom which can easily be displaced by the MAO is present. A completely different mechanism has to be applicable here.

While the catalysts exhibited low activity, the products resulting from their polymerisation activity are of exceptionally high molar masses coupled with relatively narrow polydispersities (PDI). The iron pre-catalyst (complex **3.4**) displays reasonable activity, but exceptionally high polyethylene molar mass and a polydispersity of 2.5.

The zinc-based pre-catalysts (complexes **3.4** and **3.5**) exhibits low polymerisation activity, but the narrow polydispersities and high molar mass, are significant redeeming features. Even the silver-based pre-catalyst (complex **3.1**), displays catalytic activity and produces polyethylene of high molar mass coupled with a relatively narrow polydispersity. Very few silver-based pre-catalysts have been mentioned in literature. The surprise of the study has to be the chromium based pre-catalyst (compound **3.2**). While exhibiting a low turn-over-rate (16.0 units PE produced per mol catalyst consumed) and moderate yield (5%), the molar mass PE produced exceptionally high. The M_w = 1 067 000 g/mol borders on the ultra-high molar mass region from which fibers such as Kevlar® are made.

Pectora roborant cultus recti

Table 4.2: Comparative polymerisation data from literature

Complex	$P(C_2H_2)$	Co-cat	T (°C)	Time $_{(min)}$	TOF[a]	M_w	M_n	PDI
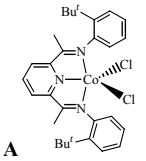 A	10 bar[4]	MAO	25	60	53.40	234 000	54 000	2.3
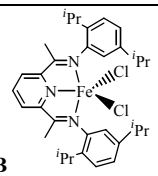 B	10 bar[4]	MAO	25	60	17.40	611 000	64 000	9.5
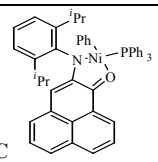 C	200 psig[1]	none	40	30	11.20	256 500	171 000	1.5
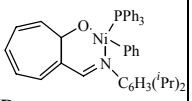 D	400 psig[2]	none	60	60	890	575 240	292 200	1.97
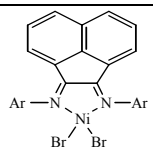 Ar = C_6H_3-2,6-(^{i}Pr)$_2$ E	1 atm[3]	MMAO	23	60	3000	273 600	190 000	1.44
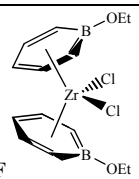 F	1 atm[26]	MAO	60	30	3200	109 000	53 500	2.04
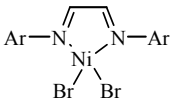 Ar = C_6H_3-2,6-(^{i}Pr)$_2$ G	1 atm[27]	MAO	0	15	662.7	160 000	65 000	2.4
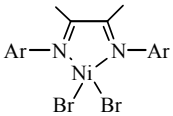 Ar = C_6H_3-2,6-(^{i}Pr)$_2$ H	1 atm[27]	MAO	0	15	187.5	81 000	52 000	1.6

[a] TOF in g(PE) produced per mol catalyst consumed per hour in x10^3

4.2 Polymerisation of 1-pentene:

Complex 3.3 was chosen for the polymerisation of 1-pentene considering the high activity it exhibited in the polymerisation of ethylene. A pre-catalyst solution, of a specific concentration, was prepared before hand in a Schlenk tube and saturated with argon gas. The polymerisation of 1-pentene was carried out in a Schlenk tube equipped with a screw cap to ensure that pentene vapour did not escape the reaction vessel. The pre-catalyst and monomer were stirred at room temperature for 24 hours. The mixture was quenched with acidified methanol (hydrochloric acid) and extracted with toluene to yield a brown oil containing poly-1-pentene. Table 4.3 summarises the ^{13}C NMR and SEC data. The analytical data confirmed that oligo-1-pentene was the product from the oligomerisation of 1-pentene.

Table 4.3: ^{13}C NMR and SEC data for oligopentene

Polypentene	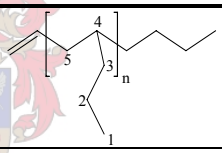
^{13}C NMR (75 MHz)	
Solvent	$CDCl_3$
Temperature (K)	273
C1	42.1
C2	28.7
C3	29.5
C4	21.2
C5	13.9
M_w	856
M_n	548
PDI	1.56
TOF	105
%Yield	3.60

As a result of the low polydispersity index (PDI) of the products, Gas Chromatography (GC) analysis was not done to detect lower oligomers. The pre-catalyst displays very low activity in the polymerisation of 1-pentene with a turn-over-frequency of only 105 g poly-1-pentene produced per mol catalyst consumed per hour. This is not worthwhile to

elaborate forth. The result is in line with the low activity shown by other α-diimine pre-catalysts in the literature towards the polymerisation of 1-pentene. Metallocene-based catalysts remain the preferred pre-catalysts of choice for the polymerisation of α-olefins with more than three carbon atoms.

Conclusions

To conclude this study, α-diimine ligands with varied degree of bulkiness were synthesised. The ligands synthesised were N,N,N',N'-tetramethyl ethylenediamine (TMEDA), N,N'-dimesityldiazabutadiene (DMDAB) and N,N'-diferrocenyldiazabutadiene (DFDAB). The latter two ligands were characterised fully by means of ^{1}H and ^{13}C NMR, FT-IR, UV/Vis spectrophotometry, mass spectrometry and X-ray diffraction. These ligands were then coordinated to various metal ions residing in the middle- to late transition metal region of the periodic table.

These complexes were characterised fully where possible. A number of these metal-α-diimine ligand complexes [$Ag(DMDAB)_2(BF_4)$, $Fe(DFDAB)Cl_2$, $Zn(DFDAB)Cl_2$, $Zn(DMDAB)Cl_2$ and $(CO)_4Cr(TMEDA)$] were then employed for the polymerisation of ethylene. The polymerisation results showed clearly that these complexes exhibited low turn-over-frequency rates, but produced high-density, high molar mass polyethylene with narrow polydispersities. The $Fe(DFDAB)Cl_2$ and $(CO)_4Cr(TMEDA)$ pre-catalyst complexes yielded polyethylene with the highest molar mass. The $Fe(DFDAB)Cl_2$ complex also exhibited the higher turn-over frequency and it was decided to utilise this pre-catalyst complex for the polymerisation of 1-pentene. The success with this monomer was much lower compared to that of the ethylene monomers. Only oligomers were obtained. No additional effort was made to elucidate the structure of the oligopentene. The conclusion can be made that the complexes synthesised are first-rate pre-catalysts for the polymerisation of lower α-olefins.

Future work could involve the clarification of the reaction mechanism when using pre-catalysts bearing carbonyl groups and in the case of the $Ag(DMDAB)_2$ complex, the role

that the ligands play in the activation step by Lewis acids such as MAO or MMAO. An investigation into the tacticity of polymer products can be accomplished when using monomers such as propene.

Reference:

1. *Differential Scanning Calorimetry,* http://www.pslc.ws/mactest/dsc.htm.
2. G.J.P. Britovsek, M. Bruce, V.C. Gibson, B.S. Kimberley, P.J. Maddox, S. Mastroianni, S.J. MacTavish, J. Redshaw, G.A. Solan, S. Strömberg, A.J.P. White and D.J. Williams, *J. Am. Chem. Soc.,* **1999**, *121*, 8728.
3. J.C. Jenkins and M. Brookhart, *Organometallics,* **2003**, *22*, 250.
4. C.M. Killian, D.J. Temple, L.K. Johnson and M. Brookhart, *J. Am. Chem. Soc.,* **1996**, *118*, 11665.
5. R.W. Barnhart and G.C. Bazan, *J. Am. Chem. Soc.,* **1998**, *120*, 1082.
6. L.K. Johnson, C.M. Killian and M. Brookhart, *J. Am. Chem. Soc.,* **1995**, *117*, 6414.

Pectora roborant cultus recti

Chapter 5: Experimental Procedure

General Procedures:

Air-sensitive materials were handled under dry argon using standard Schlenk techniques and vacuum-line manipulations. All solvents were purified, dried and deoxygenated prior to use, except where stated otherwise. Tetrahydrofuran (THF) and diethyl ether were distilled under N_2 from benzophenone, *n*-pentane and *n*-hexane from sodium and dichloromethane (methylene chloride) and methanol from CaH_2. Chemicals were purchased from Sigma-Aldich or Merck Chemicals and used without further purification.

Melting points were determined on a Stuart Scientific Melting Point Apparatus SMP3 and are uncorrected. Electron Spray Mass Spectra were collected on a VG Quattro 70eV and Electron Ionisation Mass Spectra on an AMD 604 70eV apparatus.

Matrix Assisted Laser Desorption Ionisation Time-of-Flight (MALDI-TOF) mass data were collected on a Perseptive Biosystems Voyager DE-PRO Biospectrometry Workstation equipped with Delayed Extraction Technology. A saturated solution of 2,5-dihydroxybenzoic acid (DHB) in deuterated water was used as the matrix for data collection which is ideally suited for small organic and inorganic molecules. A mixture of the matrix solution (1 μl) and sample (1 μl) was applied to a MALDI P100 gold sample plate and allowed to dry completely under a gentle stream of argon. The drying process allowed crystallisation of the matrix in which the sample was trapped. After confirming crystal formation by light microscopy, the plate was inserted into the instrument. The sample was analysed using the method HCD1001 in the positive ion mode, which has an accelerated voltage of 20kV (94.5% grid voltage). Guide Wire Voltage of 0.05% delayed extraction at 250 ns and laser intensity of ~ 3000. The spectrum were captured using "Perseptive Grams/32® version 4.14 Level II" software.

Nuclear Magnetic Resonance spectra were determined either on a Varian 300FT or an INOVA 600 MHz spectrometer (δ reported in ppm relative to the solvent resonance).
Infrared spectra were recorded on a Nicolet Avatar 330 FT-IR apparatus. Crystal X-Ray structure determinations were carried out on a Bruker Smart Apex® apparatus. A single

crystal of suitable quality was mounted on a glass fibre and transferred to the X-ray diffractometer. The crystals were radiated with a monochromatic Mo- K_α X-ray source at a wavelength of 0.71073Å and were corrected for Lorentz- and polarisation effects.

A Perkin-Elmer Lambda 20 spectrophotometer was used to determine the UV/Vis spectra with THF as solvent.

High-temperature Gel Permeation Chromatography (GPC) also known as Size Exclusion Chromatography (SEC) was used to determine molar mass. A flow-rate of 1 ml/min was maintained and measurements were performed at 160°C. The column dimensions are 300 mm (length) and 7.5 mm (diameter). A packing particle size of 10 μm was used and the sample concentration was 2 mg/ml in 1,2,4-trichlorobenzene with 0.0125% 2,6-di-tert-butyl-4-methylphenol (BHT) as stabiliser and flow rate marker. The instrument was calibrated with monodisperse polystyrene standards (EasiCal) from Polymer Laboratories.

Crystallinity and melting points were determined by Differential Scanning Calorimetry (DSC) on a TA Instruments Q100 DSC system. The instrument was calibrated with indium metal according to standard procedures. Heating and cooling rates were maintained at a standard 10 °C/min. The polymer samples were first subjected to a heating ramp of up to 220°C and kept at this temperature for 5 minutes to remove thermal history. The cooling cycle followed the isothermal stage, with the subsequent second heating scan being recorded for analysis.

The number between brackets indicates the discussion of the corresponding complex number from the above mentioned chapter.

[Lithiated ferrocene] ^{t}BuOK (6.94 g, 0.062 mol) was dissolved in 50 mL deoxygenated THF and added dropwise to BuLi (1.37 M, 0.062 mol, 45.12 mL) in 100 mL hexane at -100°C in a dry-ice/acetone bath over a period of 10 minutes. The reaction mixture was stirred for an additional 10 minutes. Ferrocene (10.0 g, 0.054 mol) was added to the base in one portion and stirred at this temperature for 20 minutes. The cooling bath was removed and the reaction mixture was allowed to reach room temperature. *n*-Hexane

(300 mL) was then added to precipitate the pyrophoric powder. The lithioferrocene was transferred *via* canula to a Schlenk filter (Por. 4). The unreacted ferrocene was filtered and the product washed with five 30 mL portions of hexane. The dark orange-brown powder was dried under vacuum. Yield 9.45 g (92%).

[Iodoferrocene] (2.1) Lithiated ferrocene (9.45 g, 0.049 mol) was suspended in 100 mL THF and cooled to a temperature of -80°C (dry-ice/*n*-propanol bath). Iodine (12.49 g, 0.049 mol) was added in one portion under efficient stirring. The cooling bath was removed and the reaction mixture was allowed to reach room temperature. Diethyl ether, 400 mL, was added and the organic layer was washed with an aqueous, saturated $Na_2S_2O_3$ solution and water. The product was extracted form the aqueous phase with diethyl ether and dried over $MgSO_4$. The drying agent was filtered off and the solvent removed under vacuum yielding an orange-brown oil. Yield 7.62 g (50%), mp 43-46°C (lit. 44-45°C), agreeing with literature values.[1,3]

[N-ferrocene phthalimide] (2.2) Iodoferrocene (7.62 g, 0.024 mol), Cu_2O (1.75 g, 0.012 mol) and phthalimide (5.86 g, 0.040 mol) were refluxed in 80 mL pyridine for 48 hours. The solvent was removed under vacuum and the dark brown precipitate chromatographed through a short Al_2O column using *n*-hexane to elute the unreacted ferrocene and iodoferrocene. Diethyl ether was used to elute the dark red N-ferrocene phthalimide. Recrystalisation from ethanol afforded, red crystalline N-Ferrocenyl phthalamide. Yield 6.82 g (84%), mp 155.2 - 157.9°C (lit. 156 – 157°C).[1]

[Aminoferrocene] (2.3) N-Ferrocene phthalimide (6.82 g, 0.021 mol) and 40 mL of hydrazine hydrate were refluxed in 80 mL argon-saturated ethanol for 2 hours. The mixture was cooled to ambient temperature, water was added and the product was extracted with diethyl ether. The yellow organic layer was dried over Na_2SO_4 (anhydrous), transferred to a Schlenk tube and stripped of solvent, yielding 4.05 g (64%) of bright, yellow, aminoferrocene, mp 147.3 – 149.2°C.

[N,N'-Diferrocenyldiazabutadiene] (2.4) Aminoferrocene (3.51 g, 0.017 mol) and 1.012 g of a 40% aqueous solution of glyoxal (corresponding to 0.087 mol of glyoxal) were

stirred in 150 mL acetone for 12 hours at room temperature. Upon addition of 200 mL of water, a deep purple precipitate formed which was collected by filtration and washed repeatedly with water. The product was dried in a vacuum oven yielding 1.94 g (88%) of N,N'-Diferrocenyldiazabutadiene, mp 198.1 - 203.1°C (lit. 200°C).[1]

[N,N'-dimesityldiazabutadiene] (2.5) 2,4,6-Trimethylaniline (10.0 g, 0.074 mol) was stirred with a 40% aqueous solution of glyoxal (2.15 g, 0.037 mol) in 50 mL *n*-propanol and 30 mL water for 16 hours at room temperature and then at 60°C for an additional 4 hours. Upon addition of 100 mL water, a precipitate formed which was filtered off and washed with copious amounts of water and the yellow precipitate dried under vacuum. Yield 8.33 g (77%), mp = 155.2 – 160.2°C (lit 157 – 8°C).[5]

[Bis(dimesityldiazabutadiene)silver(I) tetrafluoroborate] (3.1) $AgBF_4$ (1.40 g, 0.0072 mol) was dissolved in 30 mL THF and the pre-dissolved ligand [N,N'-dimesityl-diazabutadiene] (4.20 g, 0.014 mol) in 30 mL THF was added in one portion at room temperature. A deep, red color formed almost instantly. The reaction mixture was stirred for an additional 60 minutes. The deep red precipitate was filtered and washed with several portions of THF to remove all unreacted ligand and the precipitate dried under vacuum. Yield 4.1 g (82 %), mp = 212.9°C. A portion was dissolved in dichloromethane and layered with toluene and slowly cooled to 0°C. Deep red crystals formed in seven days.

[Tetracarbonylchromium(0)(N,N,N',N'-tetramethylethylenediamine)] (3.2) This product was obtained from an unsuccessful attempt to synthesise bis[pentacarbonyl-(methoxy)methylchromium(0)carbene]bis(benzene)chromium, thus the method described by Kruger and co-workers[11] are reported here for the synthesis of $Cr(CO)_4$(TMEDA). $Cr(CO)_6$ [0.584 g, 0.0027 mol] was suspended in THF. A mixture of N,N,N',N'-tetramethylethylenediamine (TMEDA) [0.67 g, 0.0058 mol, 0.87 mL] and BuLi (3.82 mL, 0.0058 mol, 1.51 M in hexane) in THF was added dropwise to the chromium solution over a period of 30 minutes at -78°C (a dry ice/*n*-propanol bath). The mixture was stirred for an additional 2 hours. The solvent was removed under vacuum and the yellow residue was dissolved in the minimum of methylene chloride and absorbed onto

silica gel at -15°C. The absorbed residue was then placed on a silica gel column (approximately 15 cm in length) and the yellow product eluted with diethylether/hexane (3:1) as eluent. The yellow fraction (R_f = 0.78) was collected and the solvent was removed under vacuum and the yellow product dried. Yield 260 mg (35%). A portion of the product was dissolved in diethylether and layered with pentane. Yellow crystals suitable for X-Ray diffraction analysis formed after 60 days.

[Dichloro(N,N'-diferrocenyldiazabutadiene)iron(II)] (3.3) Anhydrous iron(II)chloride was prepared by refluxing $FeCl_2$ in chlorobenzene for 12 hours. The reaction mixture was cooled to room temperature and the rust-colored anhydrous $FeCl_2$ was filtered off and washed with several portions of diethyl ether. The compound was dried under vacuum for 5 hours and stored under argon.

N,N'-diferrocenyldiazabutadiene (500 mg, 0.0012 mol) was dissolved in THF and $FeCl_2$ was added and the reaction mixture stirred for 20 hours. The reaction mixture changed from a deep purple to a dark, emerald green color. Diethyl ether was added and the dark green precipitate was filtered off and washed with several portions of diethyl ether. Yield 412 mg (64%). The product decomposed at temperatures exceeding 250°C.

[Dichloro(N,N'-diferrocenyldiazabutadiene)zinc(II)] (3.4) Anhydrous $ZnCl_2$ (80.32 mg, 0.59 mmol) was dissolved in THF at room temperature. N,N'-diferrocenyldiazabutadiene (250 mg, 0.59 mmol) was added in a single portion, and the reaction mixture was consequently stirred for 7 hours. During this time the product precipitated from solution as it formed. Diethyl ether (100 mL) was added and the light green precipitate was filtered off and washed with several portions of ether. Yield 250 mg (76%). The product decomposes at temperatures exceeding 234°C.

{Dichloro[N,N'-dimesityldiazabutadiene]zinc(II)} (3.5) Anhydrous zinc(II)chloride (1.0 g, 0.0073 mol) was dissolved in dry anhydrous diethyl ether. The mesityl ligand (2.146 g, 0.0073 mol) was added and the reaction was stirred for two hours. During this time the complex was precipitated from solution as it formed. Additional diethyl ether (100 mL) was added to precipitate the remainder of product left in solution. The bright,

orange product was filtered off and washed with copious amounts of ether and dried under vacuum. Yield 1.41 g (45%), mp = 320.0 – 327.6°C. $ZnCl_2$(dimesityldiazabutadiene) was dissolved in chloroform in a small Schlenk tube equipped with a bubbler to allow slow evaporation of the solvent. Single crystals fit for crystallographic data collection formed after a couple of weeks.

[Tricarbonyl(N,N'-diferrocenyldiazabutadiene)iron] (3.6) N,N'-diferrocenyldiazabutadiene (600 mg, 0.0014 mol) was dissolved in 30 mL THF and added dropwise to an equimolar solution of $Fe_2(CO)_9$ (515 mg) in THF at -70°C (a dry ice/*n*-propanol bath) over a period of 20 minutes. The reaction mixture was allowed to reach room temperature and stirred for an additional 20 hours. The solvent was removed under vacuum and the product redissolved in the minimum of methylene chloride and absorbed unto silica gel at -15°C and placed unto a silica gel column (approximately 15 cm in length). The product was chromatographed using ether/hexane = 1:4 as eluent. The dark blue fraction (R_f = 0.60) was collected and the solvent evaporated. Yield 500 mg (63%). The product decomposed at temperatures exceeding 215°C. The product was dissolved in methylene chloride and layered with *n*-pentane and stored at 0°C for crystals to form. Unfortunately the crystals that formed were not suitable for X-Ray diffraction analysis.

[Ferrocenyl(methoxy)-carbene}pentacarbonylchromium(0)] (3.7) A solution of ^{t}BuOK (1.23 g, 0.011 mol) in 50 mL THF was added dropwise to a solution of BuLi (0.011 mol, 7.28 mL, 1.51 M in hexane) in 50 mL hexane over a period of 10 to 15 minutes at -78°C (a dry-ice/*n*-propanol bath). The resulting mixture was stirred for an additional 5 minutes.

Ferrocene (2.0 g, 0.011 mol) was added in a single portion and stirred for 2 hours at this temperature. The solvent was removed under vacuum and the lithiated ferrocene was suspended in 100 mL diethyl ether and cooled to -80°C using a propanol-dry ice bath. $Cr(CO)_6$ (1.89 g, 0.009 mol) was added in small portions to the suspension over a period of 90 minutes and the resulting mixture was stirred for 2 hours. The solvent was removed and the brown powder was dissolved in 100 mL of an argon-saturated

water/dichloromethane (H_2O/DCM = 1:1) mixture. Trimethyl oxoniumtetrafluoroborate (1.27 g, 0.009 mol) was added and the resulting mixture stirred for 15 minutes. The purple methylene chloride layer was extracted and dried over $MgSO_4$.

The $MgSO_4$ was filtered off and the purple product was dissolved in dichloromethane and absorbed onto silica gel (approximately 3.0 g) at -15°C. The absorbed product was then placed unto a cold silica gel column (approximately 15 cm in length) and eluted with hexane. The second fraction (R_f = 0.40 in hexane) was collected and the solvent removed under vacuum. Yield 2.24 g (62%), mp = 123-130°C.

[Polymerisation of ethylene] Polymerisation reactions were carried out in a stainless steel Parr reactor equipped with an inlet valve and a pressure gauge. The reactor was fitted with a glass liner and stirrer bar. The catalyst was transferred *via* syringe to a 50 mL Schlenk tube under argon. The co-catalyst (MAO) was added to this Schlenk tube in the pre-calculated ratio (~ 1:400) and the mixture diluted with 20 mL toluene.

Catalyst	Monomer	Ratio Cat:MAO	Ratio Cat:Mono	Time (min)
$Ag(DMDAB)_2(BF_4)$	C_2H_4	1:400	$1:10^4$	60
$Cr(CO)_4(TMEDA)$	C_2H_4	1:400	$1:10^4$	60
$Fe(DFDAB)Cl_2$	C_2H_4	1:400	$1:10^4$	60
$Fe(DFDAB)Cl_2$	C_2H_4	1:400	$1:10^4$	360
$Zn(DFDAB)Cl_2$	C_2H_4	1:400	$1:10^4$	60
$Zn(DMDAB)Cl_2$	C_2H_4	1:400	$1:10^4$	60
$Zn(DMDAB)Cl_2$	C_2H_4	1:400	$1:10^4$	120

The catalyst mixture was transferred *via* syringe to the Parr reactor and diluted with an additional 10 mL toluene and flushed with argon. Ethylene gas was pumped into the reactor to constitute a ratio of 1:10 000 catalyst to monomer (approximately 4.0 g). The reaction mixture was stirred for an hour at room temperature. The reactor was opened and the catalyst destroyed with 30 mL of a 10% HCl-methanol solution. The polyethylene was filtered and washed with copious amounts of methanol. The product was dried under

vacuum at 60 ºC for 6 hours. Table 5.10.1 gives the experimental detail of the respective catalysts.

[Polymerisation of 1-pentene] 1-Pentene (10 mL, 0.092 mol) was diluted with 50 mL toluene and MAO (6.06 mL, 0.0012 mol) added. The stock solution of the catalyst was prepared (0.0138 M) and 6.63 mL (91.4 μmol) added to constitute a 1:1000 monomer:catalyst ratio. The mixture was stirred at room temperature in a screw-top Schlenk tube for 24 hours. A 10% HCl/methanol (50 mL) solution was added to quench the polymer. The polymer was extracted with toluene and dried over $MgSO_4$. The solvent was removed under vacuum yielding 0.230 g (3.6%) polypentene.

References:

1. B. Bildstein, M. Malaum, H. Kopacka, K. Wurst, M. Mitterböck, K. Ongania, G. Opromolla and P. Zanello, *Organometallics*, **1999**, *18*, 4325.
2. L. Brandsma and H.H. Verkruijsse, *Preparative Polar Organometallic Chemistry,* **Vol. 1**, Springer-Verlag, Berlin, 18.
3. D. Guillaneux and H.B. Kagan, *J. Org. Chem*, **1995**, *60*, 2502
4. M. Herberhold, M. Ellinger and W. Kremnitz, *J. Organomet. Chem.*, **1983**, *241*, 227.
5. A.J. Arduengo III, R. Krafczyk and R. Schmutzler, *Tetrahedron*, **1999**, *55*, 14523.
6. M. Zora, B. Yucel and B. Peynircioglu, *J. Organomet. Chem.,* **2002**, *656*, 11.
7. G.J. Kruger, G. Gafner, J.P.R. de Villiers, H.G. Raubenheimer and H. Swanepoel, *J. Organomet. Chem.*, **1980**, *187*, 333.
8. B. Bildstein, M. Malaum, H. Kopacka, M. Fontani and P. Zanello, *Inorg. Chim. Acta.*, **2000**, *300*, 16.
9. H. tom Dieck and J. Dietrich, *Chem. Ber.*, **1984**, *117***,** 694.
10. H. tom Dieck, R. Diecks, L. Stamp, H. Bruder and T. Schuld, *Chem. Ber.*, **1987**, *120***,** 1943.
11. G.J. Kruger, G. Gafner, J.P.R de Villiers, H.G. Raubenheimer and H. Swanepoel, *J. Organomet. Chem.,* **1980**, *187*, 333.